2002

Characterization and analysis of the localized deformation of 6xxx aluminum alloy extrudates

Steven R. Claves
Lehigh University

Claves, Steven R.

Characterization and Analysis of the Localized Deformation of 6xxx Aluminum Alloy Extrudates

June 2002

Characterization and Analysis of the Localized Deformation of 6xxx Aluminum Alloy Extrudates

by

Steven R. Claves

A Thesis

Presented to the Graduate and Research Committee

of Lehigh University

in Candidacy for the Degree of

Master of Science

in

Materials Science and Engineering

Lehigh University

January 10, 2002

CERTIFICATE OF APPROVAL

This thesis is accepted and approved in partial fulfillment of the requirements for the Master of Science.

04/25/02

Date

Wojciech Z. Misiolek
Thesis Advisor

David B. Williams
Co-Advisor

G. Slade Cargill
Department Chairperson

ACKNOWLEDGEMENTS

I would like to express my gratitude to the following individuals and organizations for their guidance and assistance during the formulation of this thesis. This research would not have been possible without the support of the Aluminum Association and Werner Co. These organizations have provided valuable ideas and suggestions that contributed to the success of this research. In particular, I would like to thank Richard Kelly of Werner. I would like to thank Peter Rossin for his generous contribution to Lehigh that supported me through my first year of study as a PC Rossin Fellow. I would also like to thank the American Society for Engineering Education (ASEE) for the National Defense Science and Engineering Graduate (NDSEG) Fellowship, which I was awarded starting in September 2001.

I am grateful for the assistance of many individuals. First, my advisor, Dr. Wojciech Misiolek, has been extremely helpful in formulating and polishing the various ideas into a coherent research agenda. I would also like to thank my co-advisor Dr. David Williams, who has made time to offer important guidance. Arlan Benscoter is irreplaceable and provided assistance and instructions with metallography and light microscopy techniques. David Ackland has been a great help with the electron microscopy facilities. Fellow graduate students William Van Geertruyden and Alexander Bandar helped with their research of aluminum extrusion simulation and modeling of localized deformation. Kelly Eaton has helped immensely with sample preparation and other metallographic tasks. Most importantly, I would like to thank my family who have supported me throughout my education and have made all of this possible.

TABLE OF CONTENTS

LIST OF TABLES

LIST OF FIGURES

ABSTRACT

Heterogeneous deformation is present in most of the metal forming processes, especially those which involve high amounts of plastic strain. This strain localization is responsible for the formation of microstructural gradients. These gradients are manifested in terms of variations in grains' size, shape, mechanical properties, and orientation. These characteristics are measured by light optical microscopy (LOM), microhardness tests, and electron backscatter diffraction (EBSD).

The microstructural characterization and evaluation was performed on three different samples. The first shape was a solid extrudate with a non-uniform cross sectional profile. This piece has a heavy section attached to two thin legs. Geometrical variations are a source of localized deformation. Structural variations were observed from the outside surface to the center of the heavy section. Observations were also made of areas from the legs, which underwent high localized strain. Two extrusion-welded samples were examined to investigate the localized deformation in the vicinity of the longitudinal weld. One sample was a simple rectangular profile, which was extruded with a very low extrusion ratio using controlled, test parameters. The other extrudate was a complex shape that was deformed under typical industrial conditions.

The propensity of the grains to recrystallize was heavily dependent upon the localized strain. Recrystallization occurred at very high localized deformation whereas grain growth occurred for low deformations. Areas that had an intermediate level of deformation possessed the deformed microstructure. This behavior is due to the complex interaction of the thermal and mechanical processes.

1.0 INTRODUCTION

1.1 Aluminum Extrusion Background

1.1.1 Extrusion Process Fundamentals

Forming processes are necessary to convert cast ingots into basic forms that have typical wrought microstructures. The shape of the metal piece is changed by plastic deformation. This deformation must be induced by an external stress, the magnitude of which must exceed the yield strength of the material. Ductile metals have the ability to flow plastically in the solid state. The force required to deform a material is dependent on the amount of deformation required and also the geometry of the workpiece.[1-2]

Extrusion is the forming process whereby a block of material (usually called a billet) is reduced in cross section by forcing it to flow, under high pressure, through an opening in a die. The billet is continuously deformed into a long length of material with a uniform cross section. The extruded piece that emerges has the desired shape, which is defined by the die orifice. The reduced cross sectional area leads to a large increase in the length of the part in relation to the starting billet. Depending on the material, cross sections of varying complexity can be extruded. The products of the extrusion process, known as extrudates, are long straight pieces that may take the form of strips, wires, bars, solid shapes, tubes, or hollow profiles. These products require minimal finishing; therefore, extrusion is a "near net shape" process with little waste.[2-6]

In extrusion, an imposed hydrostatic compression stress is developed by the reaction of the workpiece (billet) with the container and die. Unequal compressive stresses are used to create shear stresses. The combined compressive stresses are effective in reducing the cracking of the billet during the deformation process. Thus large plastic deformations are possible without failure.[1]

When deformation is achieved at a temperature above that at which recrystallization occurs, the process is termed hot working; otherwise it is cold working. Most metals are extruded hot to facilitate plastic deformation. With increasing temperature there is a decrease in flow stress or deformation resistance. The deformation energy requirements are less than for cold working and large strains are possible. Because of the extensive deformation produced in extrusion, considerable internal heating of the metal also results.[3]

The two main types of extrusion processes are indirect (also called back or inverted) and direct (forward) extrusion; they are both illustrated in Figure 1. For indirect extrusion, there is no relative displacement between the billet and the container. Thus the process is relatively time independent. Typically, for most indirect extrusion processes, the die is at the ram end of the stock and the product travels in the direction opposite that of the ram, either around the ram or up through the center of a hollow ram. However, there are novel approaches where the container *and* billet move into a fixed die. This is still considered an indirect process because friction is eliminated at the billet-container interface.

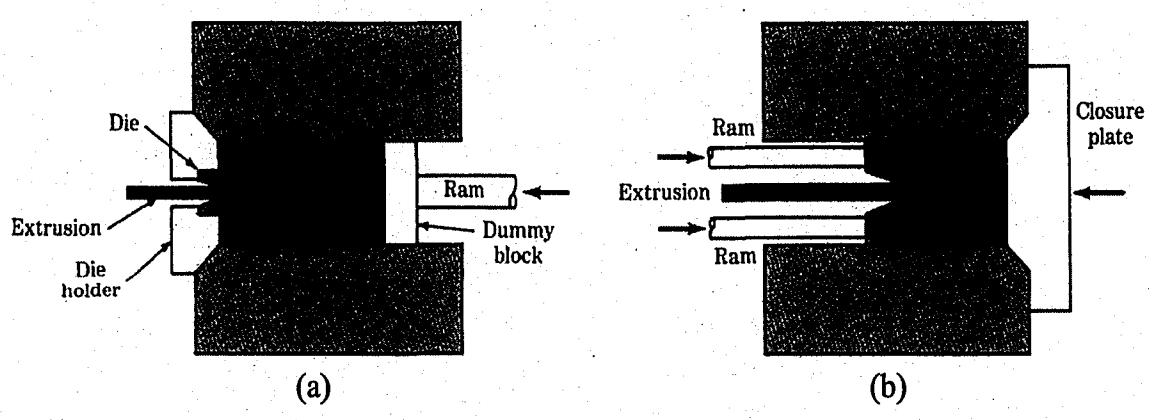

Figure 1: Diagrams of the (a) direct and (b) indirect extrusion processes.[4]

For direct extrusion, the metal billet is placed in a container of an extrusion press and forced directly through the die by the ram. The die and ram are at opposite ends of the extrusion stock, and the direction of final product's metal flow is in the same direction as ram travel. During this process, the billet slides relative to the walls of the container. The friction decreases as time increases thus making this a time dependent process.[3,5]

The actual application of extruded sections depends upon the mechanical properties of the material employed. With modern technology, a wide variety of materials can be extruded, from the very soft and ductile plastics to hard and strong refractory ceramics. Whether any metal or alloy can be extruded depends upon its malleability at the working temperature. This material spectrum, which covers the full range of metals, is classified on the basis of working temperature.

Room temperature and low temperature extrusion (0-300 °C) is performed on low melting point metals and alloys including: lead, tin, bismuth and their alloys, as well as some aluminum alloys, and the soft solders. The use of these very ductile metals is often

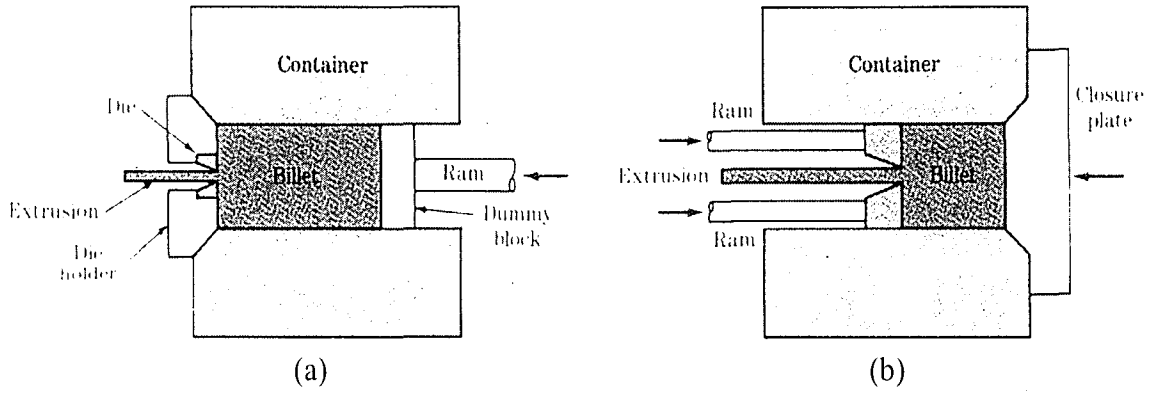

Figure 1: Diagrams of the (a) direct and (b) indirect extrusion processes.[4]

For direct extrusion, the metal billet is placed in a container of an extrusion press and forced directly through the die by the ram. The die and ram are at opposite ends of the extrusion stock, and the direction of final product's metal flow is in the same direction as ram travel. During this process, the billet slides relative to the walls of the container. The friction decreases as time increases thus making this a time dependent process.[3,5]

The actual application of extruded sections depends upon the mechanical properties of the material employed. With modern technology, a wide variety of materials can be extruded, from the very soft and ductile plastics to hard and strong refractory ceramics. Whether any metal or alloy can be extruded depends upon its malleability at the working temperature. This material spectrum, which covers the full range of metals, is classified on the basis of working temperature.

Room temperature and low temperature extrusion (0-300 °C) is performed on low melting point metals and alloys including: lead, tin, bismuth and their alloys, as well as some aluminum alloys, and the soft solders. The use of these very ductile metals is often

limited because they cannot satisfy the desired mechanical properties for engineering structures. Low deformation temperatures (300-600 °C) are used for most aluminum, magnesium, zinc, and solder alloys. Copper, titanium, and zirconium alloys, as well as precious metals, can be extruded with moderate deformation temperatures (600-1000 °C). High deformation temperatures (1000-1800 °C) are required to extrude nickel alloys, steels, cast irons, cobalt alloys, and high melting point metals (chromium, molybdenum, tungsten, niobium, and tantalum). Due to the intense temperature and pressure requirements, these high deformation temperature extrusions are very rare.[6]

1.1.2 Aluminum Alloy Extrusions

The extrusion of aluminum sections represents advanced extrusion technology in terms of alloy making, press design, tooling, and die design. All commercially available aluminum wrought alloys can be extruded. However, dilute aluminum alloys are the most suitable for extrusion, while high strength alloys are difficult to process.

To extrude aluminum alloys, the starting material, known as billets, are cut from round, and occasionally flat, cast logs. The cast billets are usually homogenized before extrusion because the as-cast condition gives a product of unsatisfactory quality and has a lower workability. The billet chemistry determines the type of alloy and its applications. The type and amounts of the elements added to the aluminum, either as alloying elements or as additions, are the first criterion in recognizing the specific alloy. The effects of the alloying elements on the properties of aluminum do not depend only on the nature and the quantity of the alloying element, but also on the way in which it combines with the

aluminum and interacts with it in the microstructure. Increasing percentages by weight increases the hardening capacity of the alloy.[7]

The alloys covered by standards can be divided and considered in two main groups, namely those used for casting and those to be fabricated into wrought forms. The introduction of an International Alloy Designation System (IADS) was developed in 1970 and has been accepted by most countries for the designation and naming of aluminum alloy systems. The IADS gives each wrought alloy a four-digit number, of which, the first digit is assigned on the basis of major alloying element(s), as listed in Figure 2. The major additions are used for strengthening, however, other elements are used to obtain specific structural states. These conditions include: finer grains, higher critical recrystallization temperature, or blocking the effects of certain impurities, etc.

For 1xxx, the third and fourth digits indicate the degree of purity of aluminum. In all other series, these two numerical indices are a serial number identifying the individual alloys within the group. The second digit indicates a close relationship or modification of the original alloy (which is given the index zero).[8] For example, 6105 and 6005 are aluminum-silicon-magnesium alloys that differ only slightly in composition from each other. This is shown later in Table I.

In order to specify the mechanical properties of an alloy and the way these properties were achieved, a system of temper nomenclature has also been adopted as part of the IADS. This takes the form of letters and digits that are added as suffixes to the alloy number. The system deals separately with the strain hardening alloys and heat treatable alloys. These essential features are also outlined in Figure 2. Alloys supplied in the as-fabricated or annealed conditions are designated with the suffixes F and O

respectively. Strain hardened alloys are designated with the letter H. For heat treatable alloys, tempers other than O are denoted by the letter T followed by one or more digits.[8]

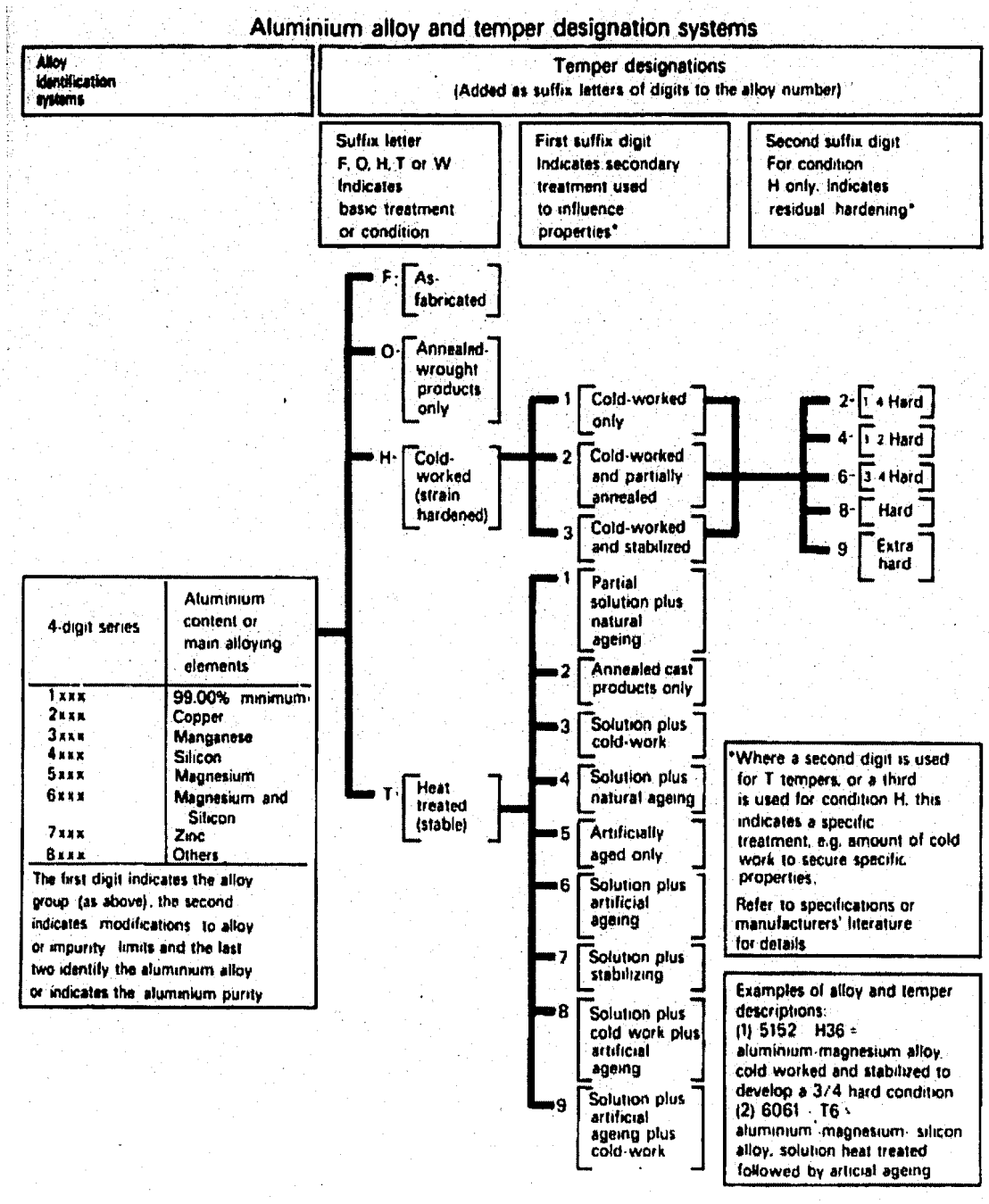

Figure 2: Diagram of aluminum alloys and temper designations.[8]

1.1.3 6xxx Aluminum Alloys

The most widely used series of commercial aluminum extrusion alloys is the 6xxx series: alloys based on the aluminum-magnesium-silicon (Al-Mg-Si) system. Several million tons of 6xxx alloys are produced every year and are used for metal fabrication and architectural purposes. The wide variety of possible applications include anything from simple bars and rods, to intricate shapes such as door and window frames, automobile trim, building structures, electrical bus bars, heat exchangers and so on.

Al-Mg-Si alloys have good extrudability, yielding possible high extrusion speeds as well as the ability to form hollow and complex shapes. These alloys have medium strength, with a decorative appearance (potential anodizing abilities) and good surface quality, while meeting narrow dimensional tolerances. Additional advantages include good electrical conductivity, weldability, corrosion resistance, an immunity to stress corrosion cracking, and simplicity in heat treatment.[6-10]

Equilibrium diagrams represent the relationships between temperature and composition of the phases in an alloy system in equilibrium; i.e. which phases are stable. Although most alloys in practice are not at equilibrium conditions, the diagrams provide valuable guidance to their behavior. The aluminum-rich region of the ternary Al-Mg-Si phase diagram is shown in the Figure 3. This is the solvus phase diagram, which reports the solid solubilities of the major alloying elements at various temperatures. The solvus diagram is extremely important for age hardening alloys because it lists the temperature above which an alloy of certain composition must be held at before quenching to form a supersaturated solid solution.

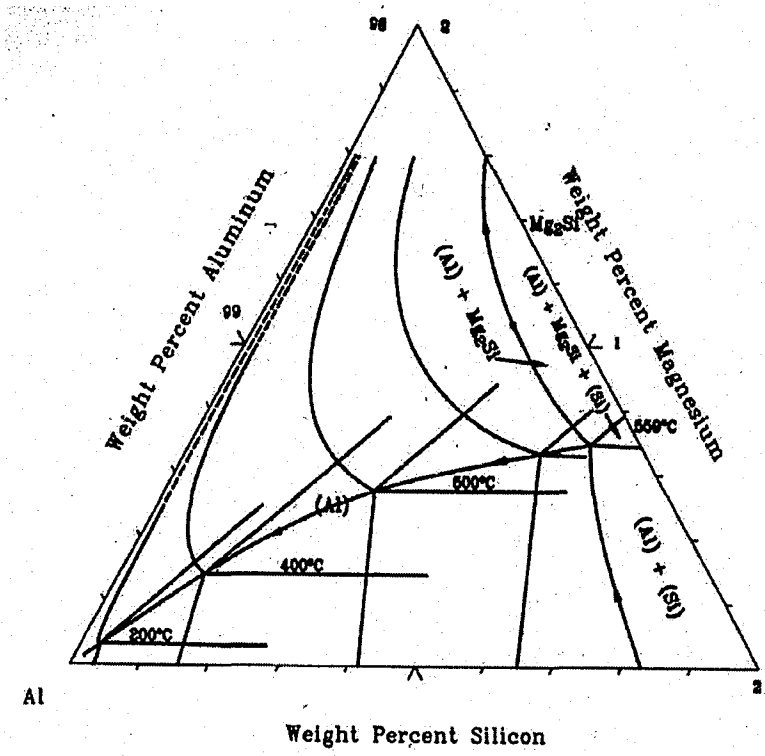

Figure 3: Al-Mg-Si solvus phase diagram.[11]

The properties of an alloy are determined by its microstructure, which depends on temperature and may include a number of phases differing in composition. For 6xxx aluminum alloys, the controlling phase for the age hardening process is magnesium silicide, Mg_2Si. Aluminum and the constituent Mg_2Si form a quasi-binary system, at magnesium to silicon ratios of 1.73:1.00 wt % (2 atoms of Mg [2x24.32] to 1 atom Si [28.06]). A line at this ratio divides the ternary system into two parts, where there is either excess magnesium or excess silicon. The binary Al-Mg_2Si phase diagram, shown in Figure 4 is very useful because it predicts the approximate solubility of the precipitate in the aluminum matrix at various temperatures.

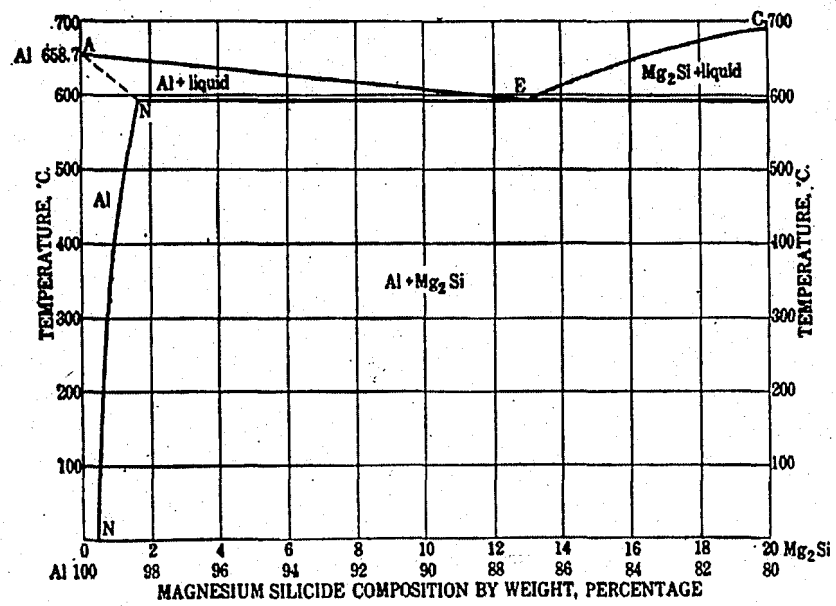

Figure 4: Pseudobinary Al-Mg_2Si phase diagram.[12]

Aluminum-magnesium-silicon alloys are formulated to make use of the solubility of Mg_2Si and thereby utilize precipitation hardening. As noted in Figure 4, the solubility of Mg_2Si in α-aluminum decreases as the temperature is lowered. Quenching Al-Mg-Si commercial alloys from high temperatures produces a supersaturated solid solution of magnesium and silicon in α-aluminum. The aluminum is solid solution strengthened by the excess silicon or magnesium compared with the stoichiometric ratio. However, the major contribution to hardening and the improvements in mechanical properties is due to the dispersion of Mg_2Si precipitates. These particles may be coherent with the matrix or produce hardening by partial coherency stressing, and by dispersion.[13] An example of an Mg_2Si precipitate is shown in Figure 5. These particles tend to align with the matrix <100> directions.

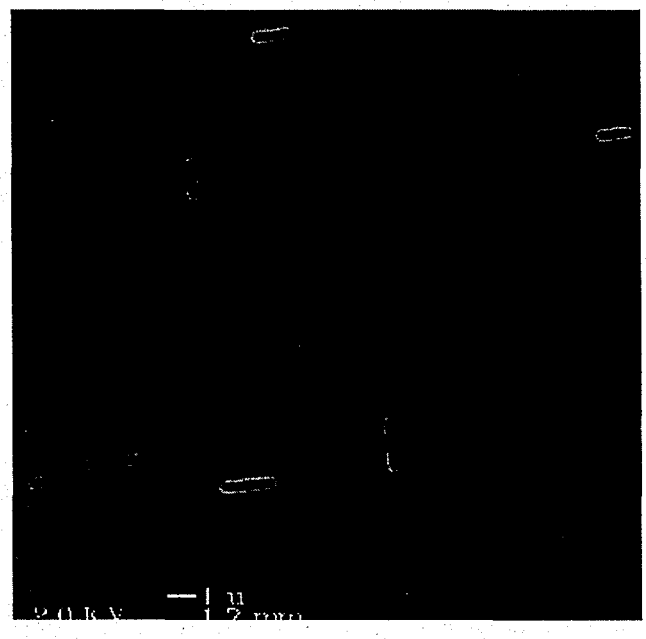

Figure 5: SEM image of Mg_2Si precipitates in 6xxx alloy.

Heat treatments are designed to promote a very high density of precipitates that strongly interact with dislocations and thereby increase the yield strength of the alloy. A typical heat treatment program for precipitation hardened alloy systems consists of an initial solution heat treatment that dissolves the particular alloying elements. The single-phase is quenched to form a supersaturated solid solution. The supersaturated state is non-equilibrium, and possesses a high level of alloying elements in solution; this concentration exceeds the amount allowed for the particular temperature. Over time, the solution seeks to attain the equilibrium, multi-phase state. Excess alloying additions form precipitates, which strengthen the material. This process may be accelerated by giving the alloy an artificial heat treatment to achieve the required temper and mechanical properties. Significant improvements in the properties may also occur through natural or room temperature aging. For normal precipitation hardening of 6xxx Al alloys , the following sequence takes place:

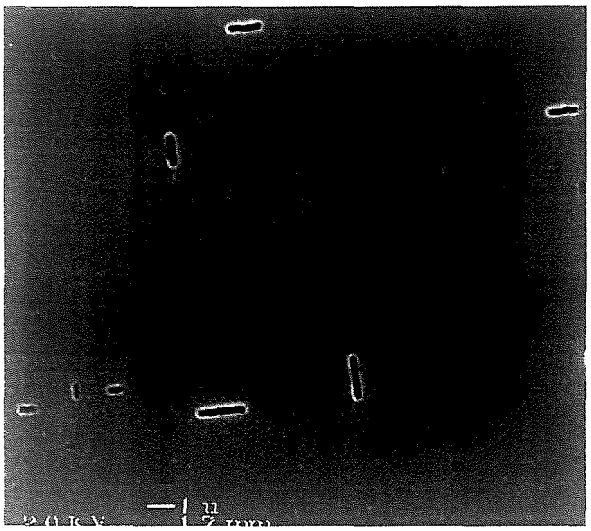

Figure 5: SEM image of Mg_2Si precipitates in 6xxx alloy.

Heat treatments are designed to promote a very high density of precipitates that strongly interact with dislocations and thereby increase the yield strength of the alloy. A typical heat treatment program for precipitation hardened alloy systems consists of an initial solution heat treatment that dissolves the particular alloying elements. The single-phase is quenched to form a supersaturated solid solution. The supersaturated state is non-equilibrium, and possesses a high level of alloying elements in solution; this concentration exceeds the amount allowed for the particular temperature. Over time, the solution seeks to attain the equilibrium, multi-phase state. Excess alloying additions form precipitates, which strengthen the material. This process may be accelerated by giving the alloy an artificial heat treatment to achieve the required temper and mechanical properties. Significant improvements in the properties may also occur through natural or room temperature aging. For normal precipitation hardening of 6xxx Al alloys , the following sequence takes place:

supersaturated α-aluminum solid solution → semicoherent β" rods →
semicoherent β' needles → semicoherent β plates → noncoherent β-Mg_2Si [10]

Although, the reaction between magnesium and silicon is a balanced one, it requires an excess of either magnesium or silicon for its completion. Excess magnesium causes a rapid lowering of the solubility of Mg_2Si at high temperatures, while excess silicon, on the other hand, has little effect on the solubility of Mg_2Si. Therefore, extra silicon is added and will appear as a micro-constituent in the alloys. Silicon promotes an additional response to age hardening by both refining the size of the Mg_2Si particles and precipitating as silicon. 0.2% excess Si increases strength significantly but greater amounts are less beneficial. However, silicon may also reduce the ductility and cause intergranular embrittlement, as it segregates to the grain boundary.[6,12-14]

By including additional elements, it is possible to improve the mechanical properties of Al-Mg-Si alloys. Additions of manganese, chromium, and zirconium counteract the effect of silicon embrittling the grain boundaries by inhibiting recrystallization during solution treatment. Manganese reduces the preferential precipitation on grain boundaries, thus promoting a fine grain size. Chromium does the same but is twice as effective by weight. Copper increases the stress hardening effect and also increases the strength in the T6 temper. Lead and bismuth can be added to improve machining characteristics.[8,13-14] Iron often appears in Al-Fe-Si intermetallics at the grain boundaries. It originates from the process of mining aluminum from the ore. Parts requiring a good surface finish must have low iron contents.

Because it is relatively easy to work with 6xxx alloys, development of many derivatives of 6xxx alloys continues in order to fulfill the requirements of different customer applications throughout the world. Some 6xxx alloys have a higher level of alloying elements to achieve higher strength for structural and semistructural applications. Other alloys are more dilute for increased extrudability

Commercial Al-Mg-Si alloys can be divided into 3 groups. The first group contains balanced amounts of magnesium and silicon adding up to less than 1.2 wt. %. Because ease of extrusion is a prime requirement for many shapes, 6063 was introduced for the applications where mechanical strength requirements were less stringent. These alloys have low quench sensitivity; the critical cooling speed is such that thin sections need not be quenched in water, but can be air-cooled. Alloys within the second group contain additions of Mg and Si exceeding 1.2 wt. % and may contain other additions such as 0.3% Cu. These alloys, such as 6061, require a higher solution treating temperature than the first group and are quench sensitive. Higher alloy contents necessitate a faster rate of cooling to obtain maximum hardenability. The importance of a good quench is increased with thicker wall sections. The third group of alloys contains an amount of Mg_2Si overlapping the first two, but contains substantial excess silicon. 6005 is an example of an excess silicon alloy.[6,8]

There are hundreds of aluminum wrought alloys, however, the majority of extrusions produced involve just a few Al-Mg-Si alloy compositions. These alloys are among the most promising to meet ever increasing demands, and are widely used based on their having the best technical and economic characteristics. Among the most common are 6005, 6061, and 6063. The composition limits of these 3 alloys are listed in

Table I along with 6105, a variation of 6005. Aluminum constitutes the remainder of the composition.

Table I: Composition Limits of Four Aluminum Alloys: 6005, 6061, 6063, and 6105 [15]

Alloy	Si	Fe	Cu	Mn	Mg	Cr	Zn	Ti
6005	0.6–0.9	0.35	0.10	0.10	0.40–0.6	0.10	0.10	0.10
6061	0.40–0.8	0.7	0.15–0.40	0.15	0.8–1.2	0.04–0.35	0.25	0.15
6063	0.2–0.6	0.35	0.10	0.10	0.45–0.9	0.10	0.10	0.10
6105	0.6–1.0	0.35	0.10	0.15	0.45–0.8	0.10	0.10	0.10

Extrusion technology has been furthered by continuing demands for new shapes and improved product quality. The main areas of application, including architecture, vehicle construction, and small machined components, concentrate on selected alloys that are suitable for the final application and can be produced and worked at a reasonable cost. Many complex shapes are extruded that would either be impossible or difficult to produce by rolling or drawing. This fact, together with the ease at which profiles can be produced by extruding, accounts for the increased popularity of the process.[12]

The most important aluminum extrudates are standardized according to product group: tubes, bar, and shapes. Heat treatable alloys are more important for extrusion because of their ability to form complex shapes before they are precipitation strengthened. They are then age hardened to achieve the desired mechanical properties. Diverse sections are naturally associated with varying degrees of difficulty in extrusion and die manufacture. Aluminum extruded profiles have been systematically classified according to their shape and difficulty to produce, as seen in Figure 6. Actual billet temperatures and extrusion speeds vary with product complexity.[6]

Section category	Section type	Examples
A	Simple bar	
B	Shaped bar	
C	Standard sections	
D	Simple solid sections	
E	Semihollow sections	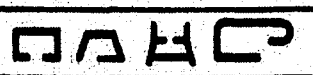
F	Sections with abrupt section transitions and thin walls; wide sections	
G	Sections with difficult tongues and very narrow inlets	
H	Tubes	
J	Simple hollow sections	
K	Difficult hollow sections; hollow sections with two or more cavities	
L	Tube sections with external projections	
M	Tube shapes with internal projections or K + L	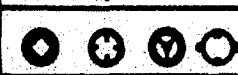
N	Large or wide hollow sections	

Figure 6: Classification of aluminum extruded sections according to their production degree of difficulty.[6]

1.2 Extrusion Die Design

1.2.1 Die Fundamentals

Forming processes all involve the interaction of a workpiece (the starting material) with some form of tooling to produce a change in shape.[1] To meet quality requirements, the performance of the extrusion die is critical; it is the heart of the extrusion process. Even the most sophisticated press will not be capable of making acceptable products without proper dies. Die performance impacts product design,

quality, productivity, and recovery. The three basic goals of extrusion die design are: to provide for relative ease of metal flow, dimensional stability, and desirable surface finish.[9]

A die is a complex mechanical piece. The extrusion tool assembly package is illustrated in Figure 7. It consists of a die, die ring, backer, and bolsters.

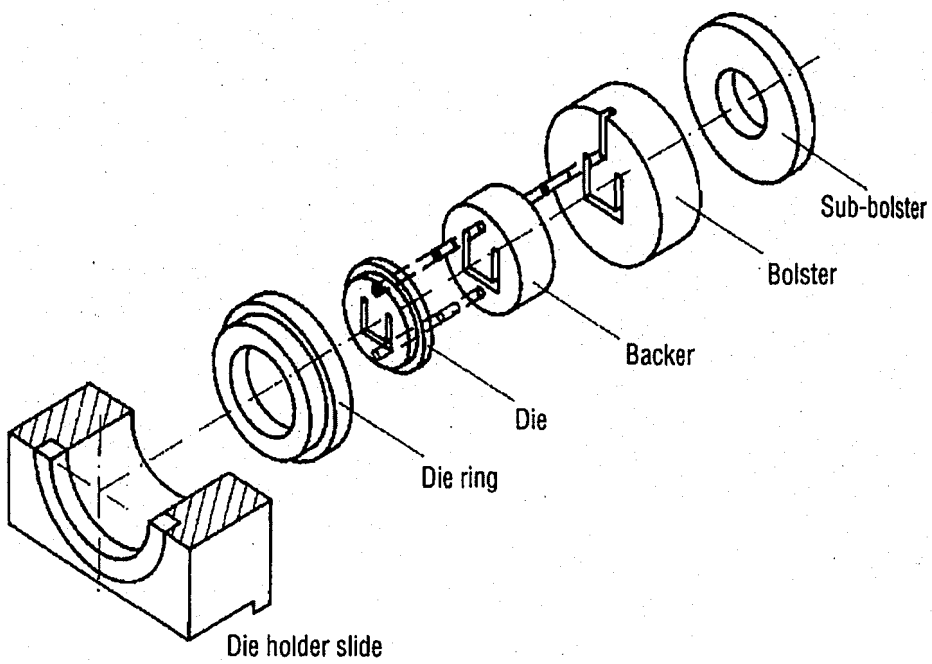

Figure 7: Parts of an extrusion die.[7]

Extrusion dies are made of particularly hard and expensive material. The die is subjected to elevated temperatures and high stresses, which it must be able to endure without fracturing under the thrust of the press. For aluminum extrusions, the most frequently used die-material worldwide is the well-established hot die steel AISI H13.[7,9]

1.2.2 Die Classifications

Extrusion dies may be divided into simple ones used for open, solid sections and those with welding chambers (porthole, spider, and bridge dies) for semihollow and hollow shapes. Extrusion dies can be categorized into three fundamental classes, shown in Figure 8. They are classified based upon the die semi-angle, α, which is the angle between the die face and the direction of metal flow. The majority of dies used for the extrusion of aluminum are flat faced (a), meaning the die face is perpendicular ($\alpha = 90°$) to the direction of the metal flow. Conical or concave dies (b) make an acute angle ($\alpha < 90°$) and novel convex dies (c) have an obtuse angle ($\alpha > 90°$).

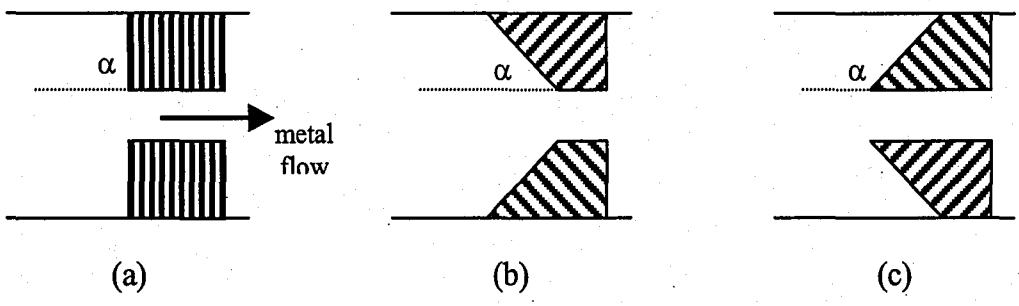

Figure 8: Extrusion dies: (a) flat-faced, (b) conical, (c) convex.

1.2.2 Die Bearing Lands

The most important element of the die is the bearing land. These are the surfaces that are either parallel, or near parallel to the direction of metal flow. The function of the bearing land is to control the size, shape, finish, and speed of the extrusion. To manufacture a sound extrudate with certain physical properties, the whole product needs to undergo similar process conditions such as strain rate and temperature. Die design can

correct the differences in these conditions caused by localized strain. The velocity distribution of the extruded metal should be balanced both within the die orifice and in front of it. Ideally, there should be laminar flow of the metal through the die. Proper die design will manipulate the shape of the die bearing lands by changing their length and/or angle to produce uniform conditions. Friction at the bearing land is the dominant factor for controlling the metal flow.

Three different die bearing lands are shown in Figure 9. Typically, parallel bearing lands are used. These working surfaces are flat, square with the die face, and are parallel to the metal flow. If die correction is needed, different land lengths may be used. Shorter bearing lands will decrease frictional forces whereas longer lands will slow the metal down. Relief bearing lands widen in the direction of the metal flow allowing slow metal volumes to "catch up" to faster moving material. Choke bearing lands have the opposite effect, becoming narrower in the flow direction; they are comparable to a wire drawing die. The added surface friction increases the drag force, retarding the metal flow and thus slowing a faster moving volume of the metal.[16]

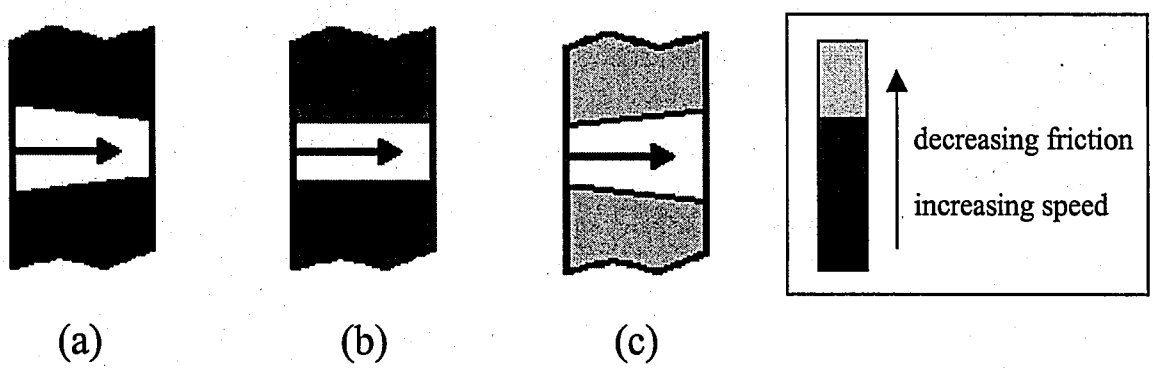

Figure 9: Bearing lands: (a) choke, (b) parallel, (c) relief.

Proper die design is necessary to produce sound flow properties and ultimately a quality product. Geometrical differences inherent to the shape of a part (for example, a thick section adjacent to a thin area) result in metal flow variations. The resistance to metal flow is greatest in the narrow parts of the die, and therefore small, thin sections naturally flow with slower velocities. These regions of a part, with a high surface area to volume ratio (S/V), are often extruded through relief bearing lands or shortened parallel bearing lands. This approach allows these slow-flowing profile sections to catch up to the faster moving material that forms the other regions of the part. Large cross sectional areas (those with low S/V) extrude relatively more quickly. These sections are often checked by extruding them through a choke bearing land. Therefore, a die used to extrude one profile may have several variations in the die bearing lands.

The extrusion ratio of a profile also affects the metal flow and speed. The extrusion ratio, R, is defined as the cross sectional area of the billet divided by the cross sectional area of the extrudate.[3,5] A large R defines high deformation, which requires a larger forming pressure, and results in a slower extrudate exit-velocity than a lower ratio.

In front of a flat-faced die, a feeder plate or straight cavity (welding pocket) may exist to help control the metal flow, often assisting in the extrusion of difficult profiles. Also known as a minicontainer[17] or piastrina[18], these pockets are used to reduce the heat generation that a longer bearing land would create. They can also have a significant effect on the extrusion pressure and exit speed.[19] The feeder plates can be considered as an extension of the bearing or an auxiliary pocket that surrounds the profile shape partially or totally. Depending on the desired effect, it must be located at a certain distance from the bearing edge and have a certain height.

1.3 Extrusion Welds

1.3.1 Longitudinal Welds

There are various methods to extrude tubes and hollow shapes in the industry, based on the requirements of the product and the limitations of the alloy being extruded. Two different methods to produce hollow shapes are seamless extrusion and extrusions with welding joints. Seamless profiles are produced from ingot by extrusion over a central mandrel. The ingots may be cast as solid cylinders and then bored to take a mandrel; or they may be pierced at the extrusion press by forcing a short cylindrical plug, slightly larger than the mandrel diameter, ahead of the mandrel.[13]

Thin walled hollow sections may also be extruded from solid ingots through specially designed hollow dies. These dies make use of longitudinal welds to form the final profile shape. This method is often used for aluminum and some of its alloys since these materials can be easily deformed and welded at typical extrusion temperatures. At high temperatures, plastic deformation of the metal under high pressure in the welding chamber allows solid bonding of the extruded aluminum.[20] Flow through a hollow die is much more complex than that through a solid die. Typically, when tubes and hollow sections are extruded, a die determines the outer shape while a mandrel, located in the aperture of the die, determines the inside shape. Together, the gap determines the section thickness. There are many variations of hollow die designs in the aluminum extrusion industry, such as porthole, spider, and bridge dies. These dies are shown in Figure 10.

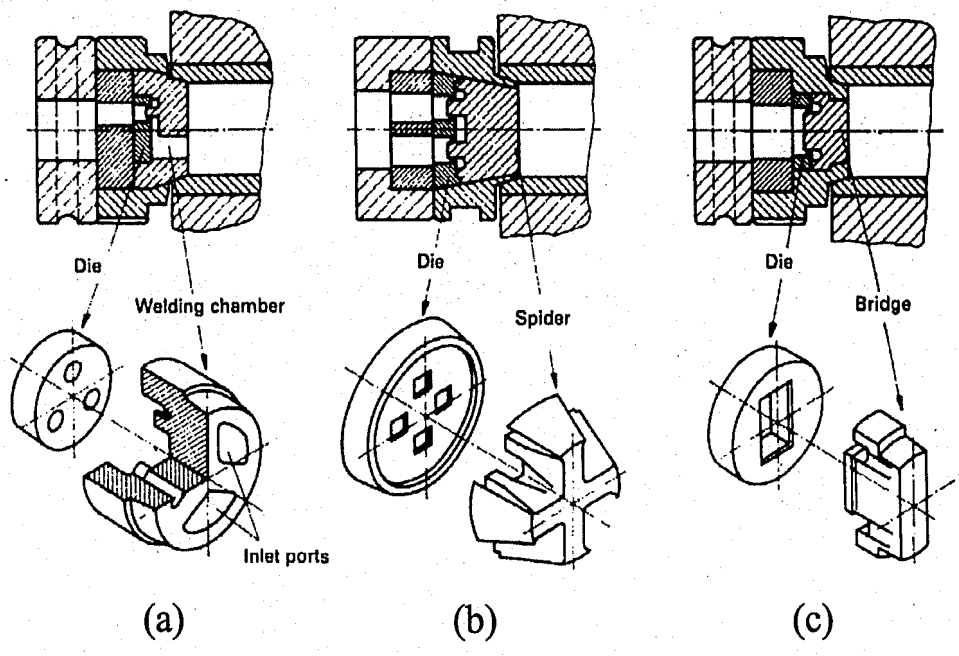

Figure 10: Hollow dies: (a) porthole, (b) spider, (c) bridge.[6]

Metal flow through a porthole die is shown in Figure 11. For hollow extrusions, the formation of the final profile shape may be divided into four stages. Initially, the billet material fills in the ports located at back of the die face. Secondly, the metal streams are split by the bridges of the die, and flow tangentially around the mandrel supports. Upon entering the weld chamber, the surfaces of two or more plastic streams slide together, then stick, and ultimately weld. Finally, the material is extruded through the gap between the mandrel and the die orifice.[21] The mandrel and the die form the inside and the outside dimensions of the extruded hollow shape respectively. The metal that exits from the die as a hollow shape has one or more seams that lie along the product length, which are referred to as longitudinal welds. Welding occurs because clean oxide-free metal is brought together at elevated temperatures under high pressure.[3,22-23]

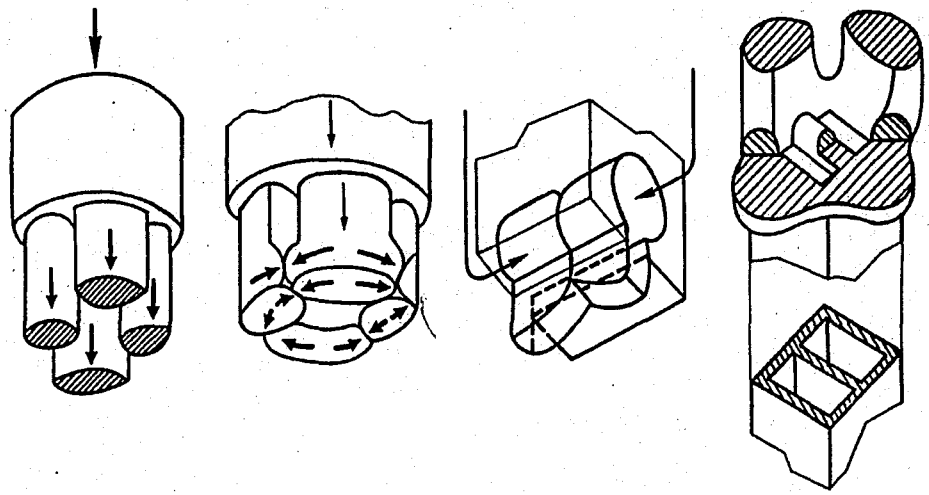

Figure 11: Complex porthole die displays the four stages in producing a longitudinal weld seam.[21]

Akeret describes the longitudinal welding process as a joining of two separate extrusions, consisting of the less-worked core and much more heavily worked peripheral zone.[21] Figure 12 illustrates this concept in the formation of seam welds. The microstructural characteristics of the welded material may include the absence of a proper grain structure and the random distribution of the intermetallic particles. Even macroscopically, the "unstructured" weld zones in the etched section of hollow shapes contrast with the more fibrous material in the core of each part of the shape.[21]

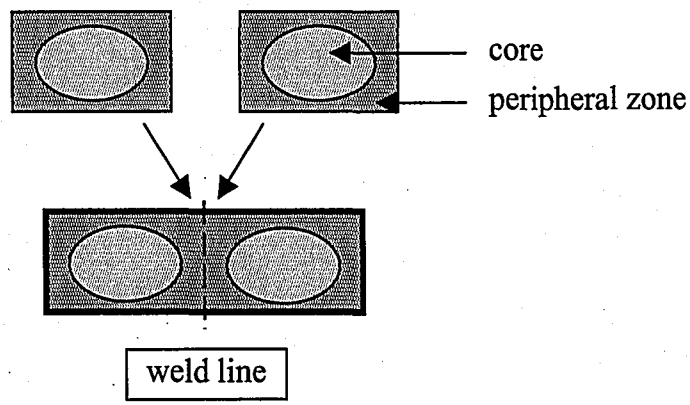

Figure 12: Two simple rectangular shapes flow through the pockets of a porthole die and form an extrusion weld.

The strength of the extrusion weld depends on several factors, among which the most critical are temperature, pressure, metal cleanness, roughness of the welded interfaces, and the velocity of the metal flowing through the welding chamber. In practice, the selection of process parameters, such as billet temperature and extrusion ratio, is critical to assure a good, quality bond. The mechanical properties of the extrusion welds and of the neighboring material can differ from those of the metal at greater distances from the weld. These differences may be in terms of grain size, local strain, or orientation of subgrains and grains.[21]

1.3.2 Transverse Welds

The other type of extrusion welding is transverse or billet-to-billet welds. Billet-to-billet extrusion is a special method for alloys that easily weld together at the extrusion temperature. Welding can occur with a feeder plate (weld pocket) or not. Using this process, shown in Figure 13, continuous lengths can be produced by discontinuous extrusion. Typically, the welded region possesses inferior mechanical properties and is discarded.[6]

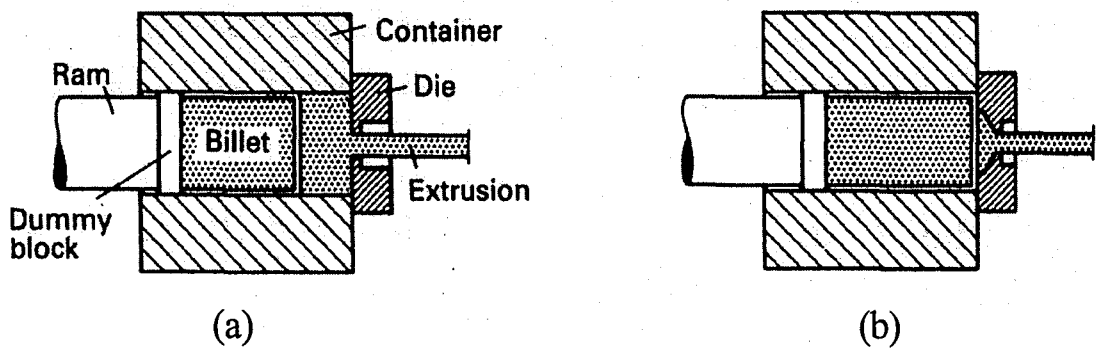

Figure 13: Transverse welding: (a) without and (b) with a weld pocket.[6]

1.4 Localized Deformation

1.4.1 Heterogeneous Strain

Localized deformation is present in most of the metal forming processes. Industrial practices involve large-scale plastic deformation that becomes heterogeneous at high plastic strain.[24] The change in mechanism from a dominantly homogeneous one to a localized form of deformation, increases with increasing strain. Therefore, larger extrusion ratios produce a higher amount of heterogeneous localized deformation. The generation and development of localized deformation from metal forming process exist on different scales. Shear bands, Luder bands, and microcracking all form at the micro level and can also be combined to form meso-defects. Macro shear localization is exhibited in mechanical property gradients.

During the extrusion process, large plastic strain is needed to form the part into its final shape. The deformation is non-uniform and varies as a function of position. Material towards the perimeter of the extruded part undergoes significant shearing; whereas, billet material at the centerline of the die orifice travels in a straight line relatively undisturbed. The shear deformation at the centerline of the extrudate is zero and increases as one moves outwards. Therefore, strain localization and the amount of redundant deformation increases for grains located further from the center of the profile.[25] Figure 14 presents an image from a visioplastic modeling experiment. Alternate layers of different colored plasticine were extruded in order to analyze the material's flow. The flow lines are easily extrapolated from the interfaces of the different colors. The path length of the outer material is longer and has a slower speed as illustrated in Figure 15. In this diagram, the thickness of the lines is proportional to the relative extrusion speeds.

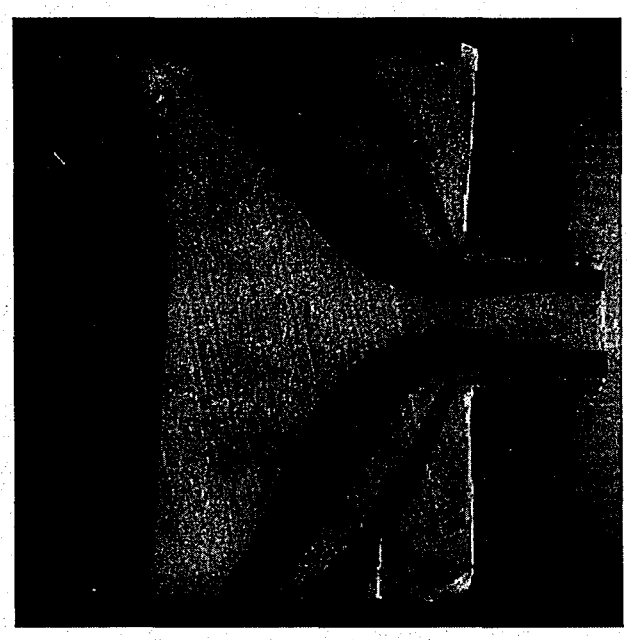

Figure 14: Visioplastic model of the metal flow in the extrusion process.

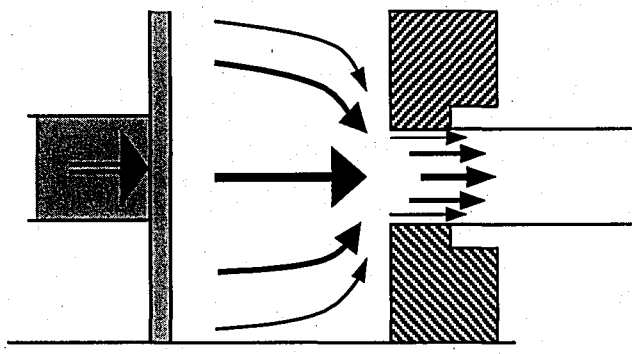

Figure 15: Paths of metal flow from the billet through the die.[26]

Figure 16 summarizes that material from the outside of the billet forms the exterior of the profile. Closer to the billet surface, the material has a longer path to travel and is heavily deformed. Metal from the shear zone flows through the die and forms the outer layers of the profile. The extrudate surface grains experience higher strain than material towards the center of the part. The visioplastic model and deformation presumptions are verified by examining the photograph of the partially extruded billet

that is found in Figure 17. Material near the edge of the billet flows along the outside, then past the dead metal zone and into the intensive shear metal zone.

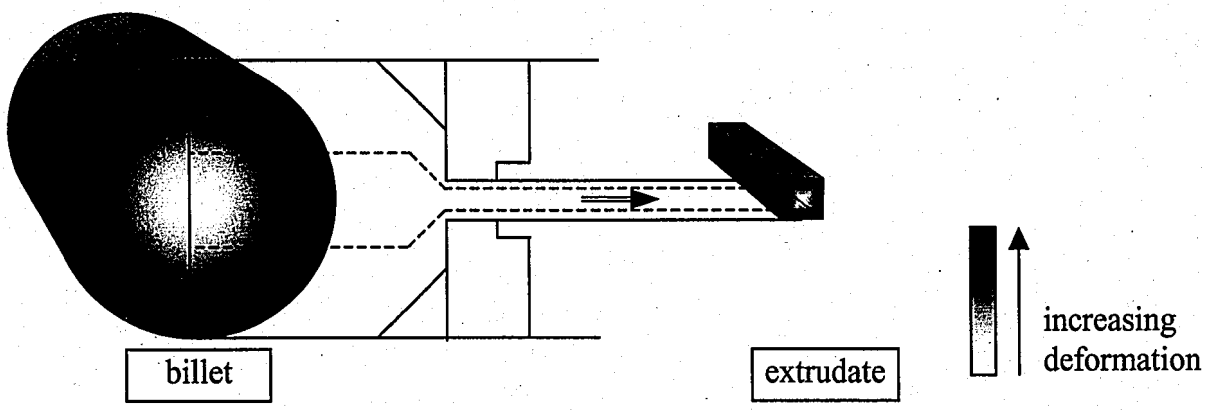

Figure 16: Illustration displaying that material towards the exterior of the billet will form the surface layers, which are heavily deformed.[27]

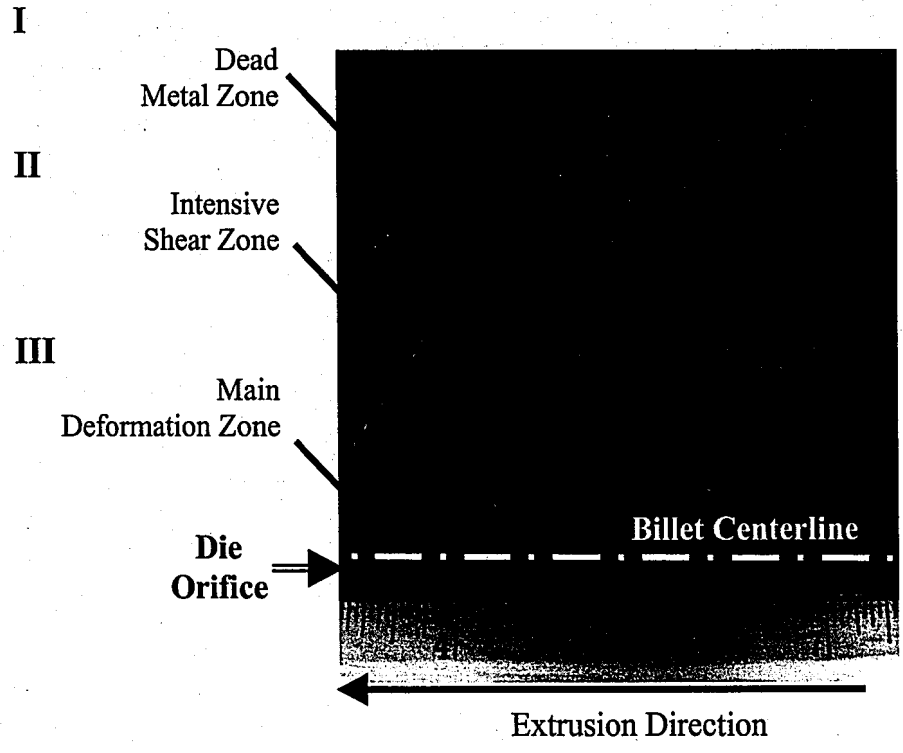

Figure 17: Macroetched half of a partially extruded 6105 billet displaying metal flow patterns.[28]

Heterogeneous deformation also occurs due to differences in geometrical dimensions. Complex parts with varying section sizes develop regions of highly localized strain. Consequently, structural differences often appear across the profile of a finished product.

1.4.2 Surface Defects

The large local deformation near the surface can also be attributed to another factor. Extreme tensile forces are formed at the surface due to the materials' interaction with the die bearing land. The surface material travels alongside the quick moving central metal volumes. However, at the surface, this material is restrained by the frictional forces from its interaction with the die.[29]

The surface quality of the extrudate is one of the limiting factors of the extrusion process. This is shown in the extrusion forming limit diagram in Figure 18. At elevated temperatures, large extrusion ratios or high speeds will cause surface cracking, incipient melting, or recrystallization, which will all limit the possible extrusion speed and the formability.

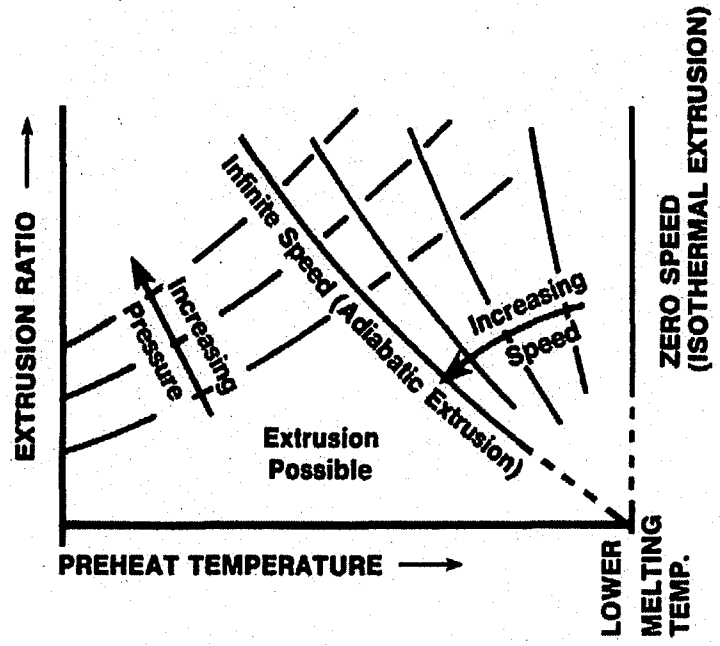

Figure 18: Forming limit diagram for extrusion.[30]

The crystal orientation and surface roughness control the surface appearance. If grain structure or orientations vary significantly, constant surface properties are no longer obtained. The quality of finishing processes, such as anodizing or painting, depends heavily on the surface texture. Upon anodizing, the etching response depends on texture, grain structure, and particle distribution. Local variations in these parameters, caused by complex dies, can therefore lead to inconsistent surface appearances.[31-32]

The term "surface texture" is primarily used to describe the variation in surface roughness of the part. However, here, in this research, surface texture is used to indicate the orientation of the grains at the surface and just beneath to a depth of approximately 250 μm.

1.4.3 Microstructural Gradients

The final extrudates' microstructure is the result of the metal flow, which is controlled by extrusion parameters and die design. In these experiments, multiple regions from the same profile were examined to eliminate variations in process conditions. This will also discard deviations that exist in multiple extrusion runs, or even from the front to the back of an extrudate. By doing this, for each extrudate studied, the extrusion process parameters, such as temperature and extrusion speed, were held constant. Therefore, the microstructural response to these parameters are neglected, and the effective changes to the microstructure can be isolated. The response of the material is evaluated as being a function of either geometrical differences or die design.

Localized deformation contributes to the development of material anisotropy by creating structural differences that appear across the profile of finished complex parts. The microstructure within the localized zone is usually distinctively different from the other sections of the product. Therefore microstructural gradients are created and are manifested in terms of differences in grain sizes, shapes, mechanical properties, and crystallographic orientations. Characterization of these physical qualities was performed using light optical microscopy (LOM), microhardness tests, and electron backscatter diffraction (EBSD). LOM was used to measure grain size/shape variations while the microhardness tests were used to evaluate the relative strength of the individual grains. EBSD was used for microtextural determination and can also be used for grain size/shape measurements.

During the hot extrusion of aluminum, the cast microstructure is changed. Some regions of the new microstructure may consist of recrystallized grains, whereas in others

the recrystallization may be suppressed or partly suppressed. Therefore, microstructural discrepancies can result from differences in metallurgical states that may exist: as-deformed, recovered, and recrystallized. In heat treatable aluminum alloys, a non-recrystallized grain structure possesses higher mechanical properties in the extrusion direction than recrystallized material.[32]

The analysis of the size and shape of the grains, in conjunction with microhardness measurements, were used to study the recrystallization behavior of the grains, as well as Kikuchi pattern quality indices from EBSD. The pattern quality and confidence index used by the EBSD system indicates the amount of strain present in the grain. A higher strain will be the result of a higher dislocation density resulting in low pattern quality. For deformed microstructures, a higher index may designate grains that have recovered and decreased their strain. Lastly, the microtexture of specific small regions may indicate a preferred recrystallization texture. Significant amounts of the cube texture may be retained during the hot deformation of aluminum alloys. Aluminum alloys, which possess high stacking fault energy, often possess a cube component of texture upon recrystallization.[33-34] The size and shape of the grains are a good indication of whether or not grain growth had occurred.

1.5 Material Anisotropy

1.5.1 Texture

The texture is the preferred grain orientation – one or more specific orientations which appear with a higher than average probability in a sample population of orientations.[34] Texture determinations examine the direction dependence of the

material's anisotropy, a result of its structure. The actual orientation distribution in a polycrystal is the result of the manufacturing process and thus texture contains detailed information about the production history of a workpiece.

In general, casting and solidification processes produce a randomly oriented or weakly textured material. As a result of deformation, the grains are not randomly oriented. The crystallographic orientation distributions of the grains exhibit a tendency for alignment with a specific, dominant direction in the bulk material, commonly related to the direction of working. The texture is a function of the metal forming process and therefore the orientations of the deformed grains depend on the die design and process parameters, such as state of stress, temperature, strain, and strain rate.[28]

On the other hand, texture is important for the physical behavior of the material, and has a strong effect on physical properties. Therefore, the texture contains easily accessible information on the interrelation between processing parameters and materials' performance. The microstructural elements responsible for anisotropy are not so much scale as morphology; the size of the grains in a polycrystalline aggregate is much less important than their shape and orientation. In polycrystals, many macroscopic physical properties are anisotropic. They depend on the orientation of the grains relative to the load direction. Such properties include: Young's modulus, strength, and ductility.

The recrystallization texture is strongly dependent on the pre-existing deformation texture, as nucleation and growth are influenced by the orientations of adjacent regions of the microstructure.[35] The combined effect of deformation and recrystallization on the microstructure of a workpiece is due to complex interplay between the thermal and mechanical processes.

Several theories on the relationship between texture and plasticity have been developed. The most recognized full constraints model by Taylor, predicts a rotation towards the <111> or <100> orientation for FCC metals. A <100> fiber deformation texture has been reported after axisymmetric compression, while a mixture of <111> and <100> are seen in extruded rods.[36]

Microtexture is a population of orientations measured on a grain-by-grain basis.[37] This is in contrast to an average texture measured from a bulk sample, obtained via techniques such as traditional x-ray diffraction (XRD). The microtexture can be measured by electron backscatter diffraction (EBSD) in the scanning electron microscope (SEM) or by either selected area diffraction (SAD) or convergent beam electron diffraction (CBED) in the transmission electron microscope (TEM).

1.5.1 Texture Measurement Using Electron Backscatter Diffraction (EBSD)

EBSD, also known as backscatter Kikuchi diffraction (BKD), is a diffraction technique for obtaining microtextural information from thin (near-surface) layers of bulk samples in the SEM. The microtexture is obtained by summing the orientations of the individual grains and is important for the analysis of localized deformation. EBSD is able to generate important information about the size, shape, and orientation of the grains with accuracy and speed. This diffraction technique, combined with the imaging capabilities of the SEM, enables the user to directly relate the crystallography to deformed microstructure.

EBSD is a powerful tool used for the characterization of deformed microstructures. For this research, EBSD has been used to follow, in detail, the

orientation aspects of the deformed grains and the metal flow in several aluminum extrudates. The extrudates' microstructures provide insight into the materials' responses to the intricate dies.

The EBSD patterns (EBSP) are produced when high-energy electrons are elastically scattered by atomic planes in a crystalline sample. The incident electrons are scattered by the crystal lattice according to Bragg reflection. Because this technique is based upon crystallography and not visual observations, such as LOM, the grain measurements are very accurate and even low angle grain boundaries can be identified. The ability to measure microtexture is a major advantage over XRD, which reports an average texture.

An additional benefit is that EBSD combines the important crystallographic information with the powerful imaging capabilities of the SEM. This combination is possible in the TEM, however, the volume of material studied is severely limited. Also, thin TEM foils require arduous sample preparation. Traditional metallographic sample preparation is all that is required for EBSD. The samples are polished flat with a minimum of mechanical deformation on the surface layer.

The EBSD system hardware can be retrofitted to nearly any SEM, which, until recently has not been well suited for performing diffraction experiments. A diagram of the hardware setup is illustrated in Figure 19. The components of an EBSD system are: the sample at a 70° tilt angle, a phosphor screen, lead glass window, camera, and a computer equipped with orientation imaging microscopy (OIM). A 70° tilt is used to increase the intensity of the backscattered signal. After diffracting within the sample, the

electrons impinge on a phosphor screen within the sample chamber. The patterns are captured by a charge-coupled device (CCD) or low-light-level video camera.[38]

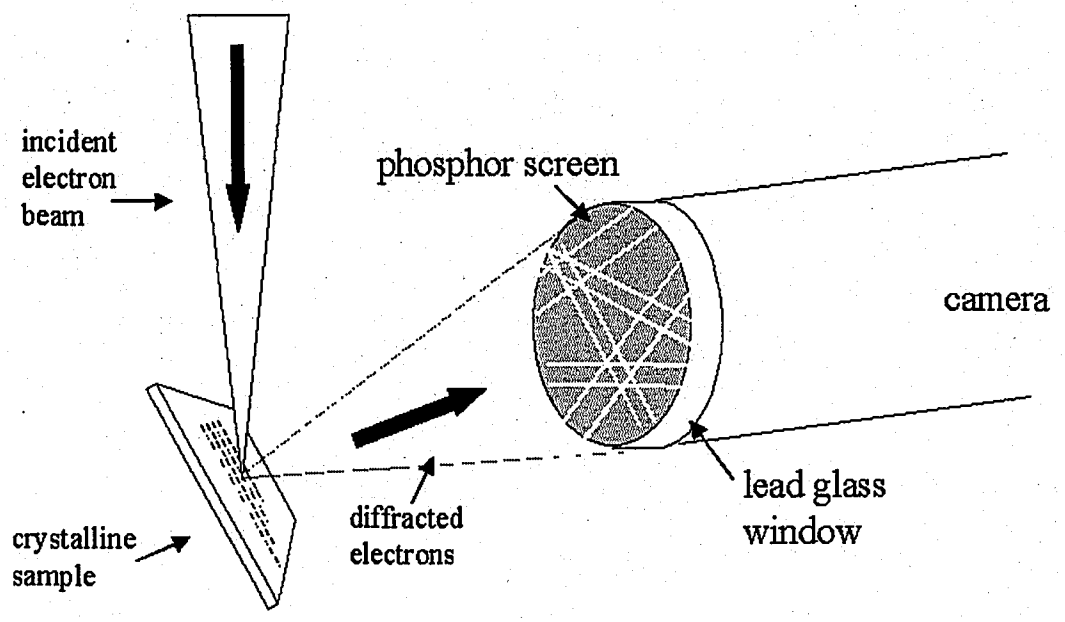

Figure 19: Illustration of the EBSD technique.

The acquired patterns resemble those produced by electron channeling experiments, and thus are often referred to as backscattered Kikuchi diffraction patterns (BKP). These patterns contain information regarding the symmetry and alignment of the probed crystal. The patterns are a "map" of the angular relationships between the atomic planes. The patterns are readily indexed by the computer, which simply notes the major symmetry elements of the patterns as well as the positions of the intersecting Kikuchi lines forming poles.

An example of a diffracted pattern and how the computer indexes the poles is shown in Figure 20. The index determines the crystallographic orientation of the individual grain and, in turn, its relationship to neighboring grains. Using a high quality

CCD camera, phase identification can be determined by the precise location of major poles as well as the thickness of Kikuchi bands. These band widths are inversely proportional to the planar lattice spacing.

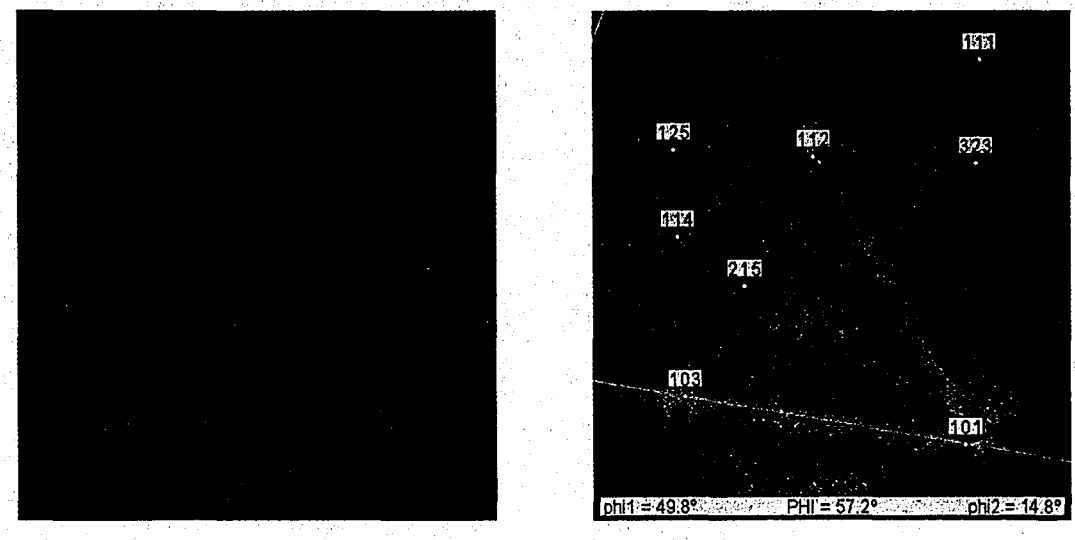

Figure 20: EBSD pattern and the identifying index by the computer.

The orientation of large areas can be determined. Many grains can be characterized by scanning the electron beam continuously across the sample in straight lines.[39] Instantaneous patterns are analyzed at each point illuminated by the incident electron beam. The computer records the three calculated Euler angles, which describe the orientation of the particular grain with respect to fixed reference axes. In addition, pattern quality and confidence index parameters are listed. These two indices are related to the quality of the lattice from where the diffraction pattern originated. Highly strained regions will have low quality and a low confidence index. In addition to orientation measurements, observation of the sample yields information on microstructure including

phase information, grain size, grain boundaries, precipitates, and impurity elements. The good spatial resolution of the SEM allows grains smaller than 1 μm to be examined.[35]

The diffraction data and texture information can be summarized in several different output forms: pole figures (PF), inverse pole figures (IPF), and orientation distribution functions (ODF). These figures are plots of the frequency with which a specific direction coincides with one of the specimen axes.[35] The strength of the texture is determined by examining the peaks (high intensity areas) and by noting the maximum values found in the scale.

The pole figure represents the distribution of a specific family of lattice planes in the stereographic projection, a two-dimensional image of the three-dimensional orientation space. The specified crystal axes are given with respect to a sample reference frame. Pole figures are viewed as one would view a globe at the equator level. The north and south poles correspond to the + and – direction. The texture is determined by analyzing these figures. Grain orientations are indicated by the positions of the plane normals, also called poles, on the projection. By calculating the angles between these directions and the origin of the coordinate system, which is placed at the center, the orientation is determined.[40]

Additional texture information and grain structure (size/shape) are given by inverse pole figure grain maps. This is a simulated microstructure generated by the computer, which assigns different colors to grains based upon their orientation according to a color coded inverse pole figure key (shown in Figure 21). Similarly orientated grains have like colors. Definitive texture determinations are found by analyzing the pole figures and confirming the information with the orientations shown in the grain maps.

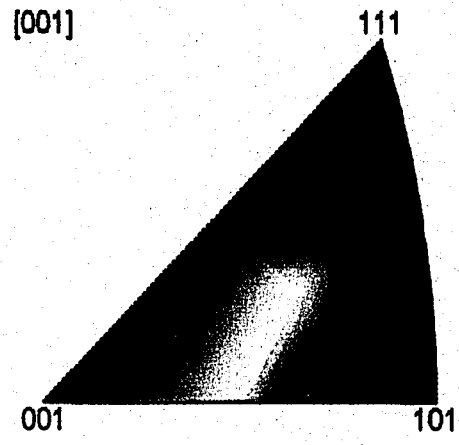

Figure 21: Inverse pole figure color key used to identify orientations of grains in an IPF grain map.

The texture information is correctly analyzed when the orientation of the grains are understood relative to known axes. The relationship between the crystallographic directions, e_x^c, and the sample directions, e_x^s, is very important and is illustrated in Figure 22.

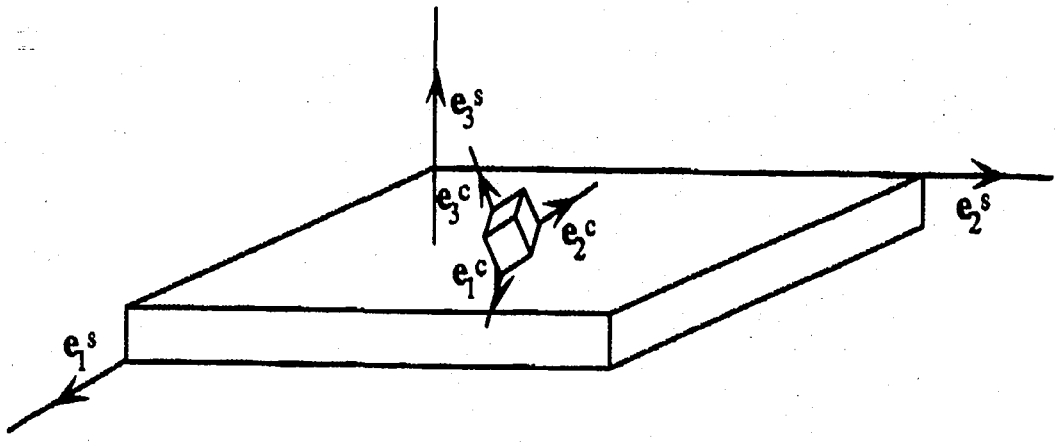

Figure 22: Relationship between the crystal orientation, e_x^c, and sample axes, e_x^s.[41]

The sample directions (e_1^s, e_2^s, e_3^s) are perpendicular to each other and are fixed by the sample's position in the SEM. This is shown in Figure 23. The normal direction (ND) is perpendicular to the sample, whereas the reference direction (RD) and transverse direction (TD) lie in the plane of the sample surface. The RD points down the sample and the TD (coming out of the page in the diagram) is parallel to the sample tilt axis. Because these directions are fixed, it is useful to position the sample in such a way that these directions coincide with the directions of the metal forming process. For instance, when examining the cross section of an extrudate, the normal direction will coincide with the extrusion direction. For longitudinal sections, to make the analysis simple, the extrusion direction should be aligned parallel to the TD or RD.

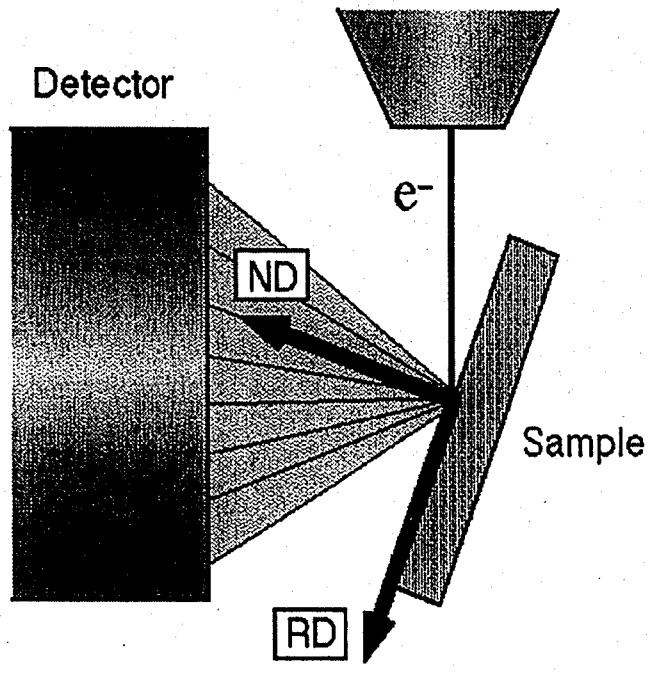

Figure 23: Sample orientation in the microscope. Definition of sample axes: ND, RD, and TD (coming out of the page).[41]

1.5.2 EBSD Limitations

EBSD samples must be crystalline; i.e. they must have a regular lattice that diffracts the incident electron beam. Samples must also be free of high dislocation densities (large amounts of plastic strain), since Kikuchi patterns are washed out at high local deformation. The pattern quality is dictated by the conditions at the surface. Crystallographic imperfections, either inherent to the sample or caused by preparation techniques, degrade the quality of the patterns.

Careful sample preparation is therefore essential for good results. Thorough final polishing using a fine (0.05 μm or less) non-diamond medium and a final etch yield good results.[42] This etchant partially removes the surface deformation layer created by mechanical polishing. Without it, the large amount of dislocations will diffuse the backscattered pattern and deteriorate its quality. Electropolishing or lapping will improve sample preparation and the resulting pattern signal.

Pattern quality is further marred by the strain already present in a deformed sample. Although the aluminum samples that were analyzed are hot deformed, extrusion involves a heavy amount of deformation that can not be totally alleviated due to the speed of the process. With careful selection of temperature and time, the material could be recovered without recrystallizing. This would preserve the grain orientation, but lower the dislocation density.

The extrudates tested were made of aluminum, a low atomic number element. Pattern quality is improved for heavier atomic elements, which have a higher backscattered electron yield.[43] Because the sample is at a 70 degree tilt, some diffraction

patterns are partially shaded as a consequence of surface relief. Thus, it is important that the surface be completely flat.[24]

Grain boundaries, which separate two grains, are a stack of misfit dislocations and are regions of highly-concentrated strain. At the boundary, two EBSD patterns may exist at the same time (one for each grain) or a diffuse pattern will appear because of the high dislocation density. OIM may have difficulty indexing the boundaries and these points will appear darker or in different colors to the surrounding areas. Figure 24 shows two overlapping patterns from adjacent grains. A large beam should be used to provide adequate current needed to produce good contrast EBSP's. However, a small beam is desired to avoid overlapping patterns at the grain boundaries.

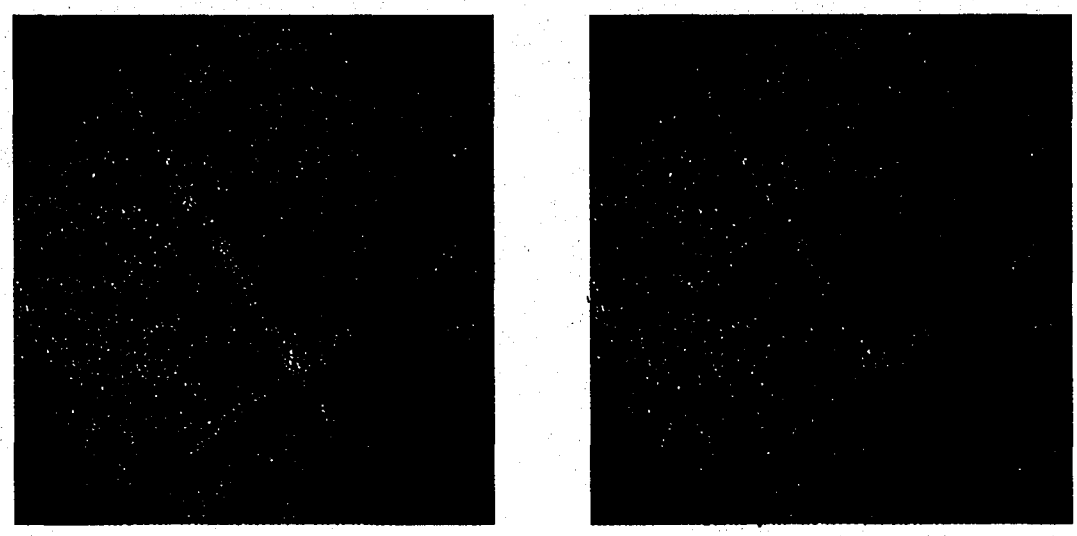

Figure 24: EBSD image showing two overlapping patterns that occur at a grain boundary.

2.0 EXPERIMENTAL PROCEDURE

2.1 Experimental Setup

2.1.1 Coordinate System

Initially, cross sectional samples, normal to the extrusion direction, were extracted from the extrudates and examined. Longitudinal sections were then cut to examine the sample from the transverse and/or reference direction. Planar samples from two perpendicular directions will yield a three dimensional representation of the grain shape and size.

Before beginning, it is important to establish a system of axes to remain consistent in all experiments. For all samples, the axes are setup such that the cross section of the extrudate lies in the yz plane normal to the x-axis (defined as [100]), which is the extrusion direction. For EBSD investigations (see Figure 23), when examining the cross section, the extrusion direction may also be classified as the normal direction (ND). When analyzing these pole figures, the z-direction [001] will be defined as the reference direction (RD); the y-axis [010] is known as the transverse direction (TD). Things get more complicated when inspecting the longitudinal sections. The ND is no longer coincident with the x-axis, [100] extrusion direction, but is rotated 90° depending on which direction (y or z) is normal to the specimen surface plane. Similarly, the pole figures of the longitudinal sections are also rotated from the cross section figures to account for the new specimen orientation in the microscope.

2.1.2 Experimental Specimens

The influence of localized deformation was studied for various types of samples, one solid extrudate and two different samples containing longitudinal welds. One of the welded samples was a simple rectangle profile extruded using controlled test conditions; whereas, the other was a complicated shape produced under typical industrial conditions. Geometrical variations concentrate deformation in certain areas, particularly where the surface area to volume ratio is the highest. For heavy extrusions, the shear localization will be at a maximum near the surface of the profile. For longitudinal extrusion seam-welding, the variation of localized deformation is similarly complex. Microstructural gradients occur due to geometrical differences and are also influenced by the weld zone.

2.1.3 Investigation Approach

The samples were initially examined under low magnifications (1-7X) using the stereomicroscope. When the capabilities of this instrument were exhausted, a light optical microscope with higher magnifications was used. This microscope had possible magnifications of 50, 100, 200, and 400X. All grains were easily distinguishable at 400X; therefore, a 1000X magnification was not needed. SEM imaging was similarly discarded as unnecessary. All images were digitally recorded using the Paxit image acquisition program. This program was used to add the micron bars to ensure accurate dimensional measurements. Most images were recorded at magnifications of 100X, a good compromise between field of view and magnification. The size and shape of the grains were observed from these images.

Microhardness tests were performed on all three extruded samples. This was done to investigate the relative variation in mechanical properties, which are derived from the microstructural gradients due to localized strain. A Knoop, elongated diamond, indenter was used with a dwell time of 15 seconds. For the solid extrudate a 50g load was used, whereas a 25g load was used for the welded specimens. A computer was used to measure the indent spacing that was then correlated to a Knoop microhardness (HK) value and a Rockwell A scale (HRA).

In general, tensile tests are used to evaluate the strength of a material. Microhardness tests are useful when tensile specimens are difficult to prepare due to section geometry.[44] In addition, tensile tests, record an average strength of the polycrystal, rather than of a specific region. Microhardness gives a good indication of the individual strength of the grains, neglecting the contributions to strengthening from the grain boundaries. Low hardness readings may indicate a low dislocation density specifying grains that have recrystallized.

Frequent microhardness tests were conducted in straight lines across the samples at regular intervals. This is to gain an accurate depiction of the gradients that occur from the surface of a part to its center or across a weld region. The average measurements are reported as well as the standard deviations.

2.1.4 Sample Preparation

After the samples were sectioned they were prepared using traditional metallographic techniques. Initially, the complete samples were ground up to 600-grit

silicon carbide paper and then macroetched in Tucker's Etchant (15% HF, 45% HCl, 15% HNO_3, and 25% H_2O). This revealed flow lines and some grain structure.

After examining these pieces under the stereomicroscope, the samples were reduced in size and mounted in epoxy to aid in future preparation work. The mounted samples were mechanically ground and polished. An alumina (Al_2O_3) intermediate polish was used to remove the heavy remnant surface damage from the silicon carbide grinding papers and the initial polishing using a diamond paste. A final polish of 0.05 μm Masterprep solution (colloidal silica [SiO_2] and alumina mixture) was used. For microstructural analysis, the samples were etched using a 5% solution of hydrofluoric acid (remainder H_2O). This etchant is effective in outlining the grain boundaries, useful for grain size/shape analysis. For several samples, this etchant was not effective enough and Barker's reagent (2.5% HB_4, 97.5% H_2O) was used instead. Using this etchant, grains contrast is achieved with polarized light. For microhardness tests, the delineation of grains is essential. Measurements should be taken within the grain to avoid the strengthening component of the boundaries.

EBSD is very sensitive to mechanical deformation and it was found that a thin deformation layer still exists on the surface even after the final polish. Prior to using the electron microscope, the samples were etched using 5% HF. In addition to outlining the grain boundaries, this etchant removes surface deformation induced by the mechanical polishing, and reduces the oxide layer thickness. One way to improve EBSD pattern quality would be to electropolish the sample or use a lapping machine; these are deformation-free preparation techniques. Electropolishing was not used because the chemical solution commonly used for aluminum involves perchloric acid, which is highly

explosive. A lapping machine was not available at the preparation facilities. A chemical polish was later used to avoid deformation, but it had a similar effect as the HF solution. The chemical polish consists of 25% H_2SO_4, 70 % H_3PO_4, and 5% of HNO_3. The samples were polished at 85 °C for 25 seconds.

2.1.5 Electron Backscatter Diffraction (EBSD)

The EBSD system used for this research was manufactured by TexSem Laboratories (TSL). Initial trials were performed using this hardware integrated with a Philips (FEI) Electroscan 2020 environmental scanning electron microscope (ESEM). This system, with a short objective lens, did not provide the optimum operating conditions and the EBSD system was transferred to a Philips XL30 ESEM.

In order to analyze a larger area, the experiments were performed at low magnifications (50-400X). The sample was aligned such that the scanned area was a thin rectangle with the larger dimension parallel to the TD, tilt axis of the stage (see Figure 25). The large sample tilt (70°) needed for EBSD investigations dictates that the electron beam will only be in focus for a limited range in height (z-direction, RD) unless the dynamical focus of the microscope is implemented.[45] For surface texture, actual EBSD measurements were taken between 0 and 250 μm from the surface, as shown in Figure 25. Large-area EBSD scans were recorded across the weld region, including the grains within the weld, as well as many grains on either side.

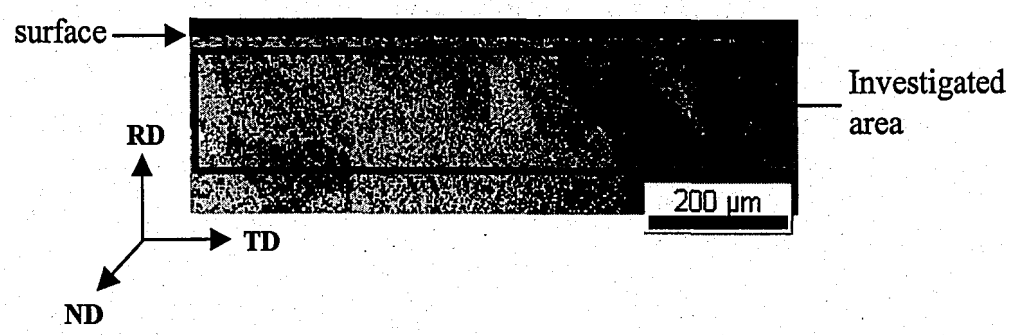

Figure 25: Typical area tested was a rectangle elongated in the transverse direction.

Initially, a focused image of the sample was obtained using the secondary electron detector. The specific areas of interest were identified, and a backscattered Kikuchi diffraction pattern was acquired on the phosphor screen. The automated crystallographic orientation measurement (ACOM) software was set up to scan a selected area. The data was analyzed with the OIM software. The intensity pole figures revealed the orientations of highest probability and were compared with the textures displayed in the IPF grain maps.

2.2 Solid Extrudate

2.2.1 Extrusion Process Parameters

The first sample analyzed for this research was the solid extrudate pictured in Figure 26. This 6105 aluminum alloy was manufactured under normal industrial process conditions. Typical composition limits of 6105 alloys were previously shown in Table I. The profile was extruded through a two-hole die with an extrusion ratio, R, equal to 52 For one orifice, the heavier portion of the profile is oriented toward the center (the sample used for this experiment), and the other orifice has the legs toward the center. The die is

laid out in such a manner to optimize handling, not die performance. The exit speed was approximately 355 mm per second.[46]

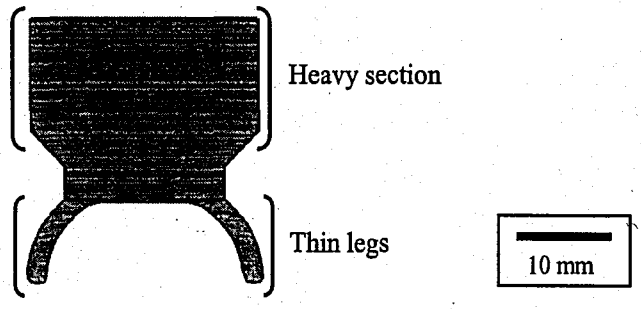

Figure 26: Solid extrudate used to study microstructural gradients due to geometrical differences.

This solid extrudate has a "heavy" section with a low S/V attached to two thin "legs" with a high S/V. To slow the metal flow in the heavy region, a choke bearing land with an angle of one degree over 25.4 mm was used. For the profile's legs, zero relief (parallel bearing land) was built into the die; however, under extrusion pressure some relief will occur as the die deflects. Bearing lengths for the legs are 3.56 mm and 2.16 mm at the tips of the legs. Starting stock was a cast, homogenized ingot, and the company reported that it did not have any strong texture.[46]

2.2.2 Profile Sectioning and Sample Definitions

The cross section of the thin legs was examined but little variation was found in the microstructure. Significant gradients due to localized deformation appeared at the "heavy" region, which includes the large upper rectangular section. This extrudate was initially sectioned into eight separate samples for LOM and microhardness analysis. The dashed lines in Figure 27 indicate where the cuts were made. This figure indicates the

surfaces that were being investigated, as well as defining the observation directions (normal to the sectioned plane). The sample was examined from all three orthogonal directions (x,y,z).

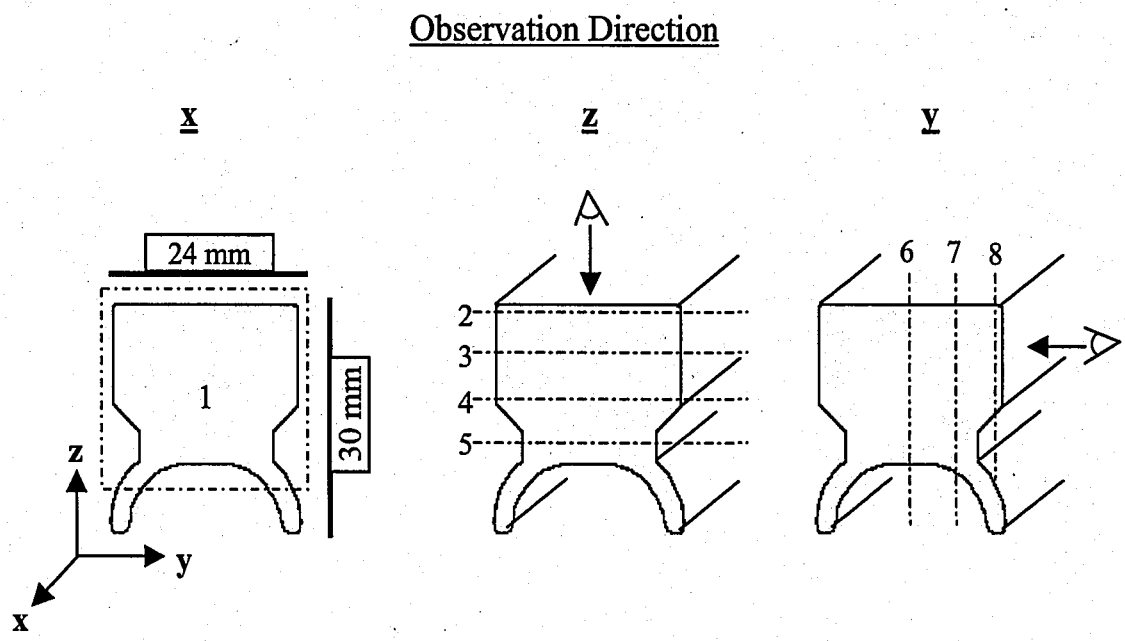

Figure 27: Profile of the solid extrudate indicating where the part was sectioned (dashed lines) and the observation directions (eye symbol).

The cross section (yz plane) was examined to understand the microstructural gradients occurring from the exterior to the center of the profile when looking down the extrusion direction (x-axis). Longitudinal pieces were cut (as shown) to examine the material from the top (z) and side (y). Samples 2, 3, 4 and 5 are from 1, 6, 12 and 20 mm beneath the top surface. Samples 6, 7, and 8 were sectioned parallel to the side 1, 6, and 12 mm from the edge. These measurements are summarized in Table II. Separate samples were cut for the legs; three in total, one for each of the orthogonal directions.

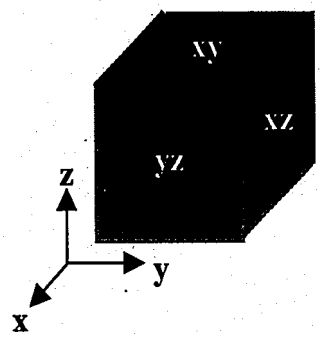

Table II: Summary of solid extrudate sample locations

Sample #	Sectioning Plane	Observation Direction	Distance from top surface (mm)	Distance from side edge (mm)
Heavy solid profile				
1	yz	x	-	-
2	xy	z	1	-
3	xy	z	6	-
4	xy	z	12	-
5	xy	z	20	-
6	xz	y	-	1
7	xz	y	-	6
8	xz	y	-	12

For the surface texture investigation smaller samples were sectioned and used so that they fit easily in the SEM chamber. These different samples studied with EBSD are illustrated in Figure 28. Longitudinal sections were prepared to examine the surface texture from additional directions. Once again, the heavy section and thin legs were the areas of interest. The influence of the two different die designs (choke and parallel bearing lands) was investigated.

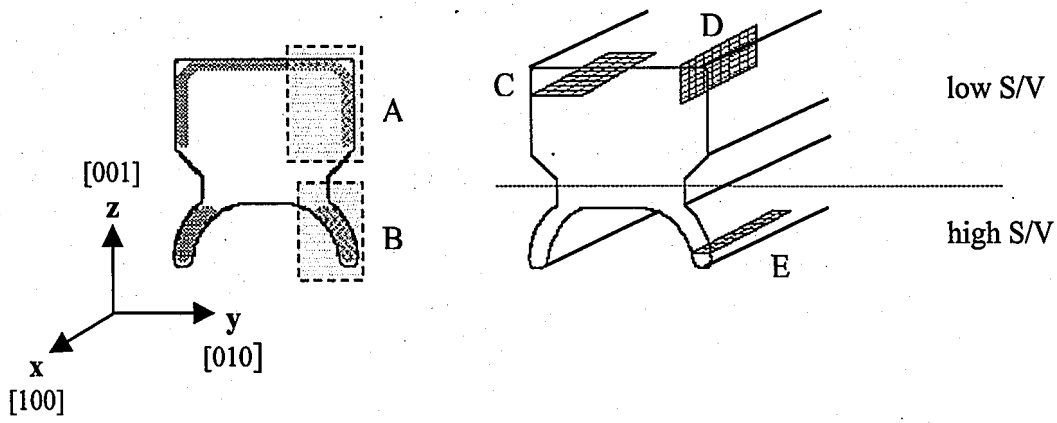

Figure 28: Indication of areas tested for surface texture analysis of the solid extrudate.

A total of five samples were prepared for EBSD investigation. Sample A indicated the microstructural variation that occurs from the side and top surface. Two different longitudinal sections (C&D) were needed to view those same variations. Two samples were prepared for the leg: B from the cross section and E was a longitudinal sample examined down the z-axis. Longitudinal samples were used to confirm the initial EBSD results from the cross section specimens. The grain maps from longitudinal samples give an indication of elongation of the grains in the extrusion direction that was also displayed by the LOM images.

2.3 Experimental Extrusion Weld

2.3.1 Extrusion Process Parameters

The objective of studying this extrudate is to assist in the understanding of extrusion-welding phenomena. The major difficulty during normal industrial processes is a lack of data related to pressure and temperature within the welding chamber. A special weld-integrity test-die, shown in Figure 29, was designed, built, and tested. The die allowed the investigation of weld integrity as a function of the die geometry and process parameters, such as extrusion temperature, pressure, and speed. The solid bonding taking place in the extrusion of hollow sections was adequately simulated by this die.[47]

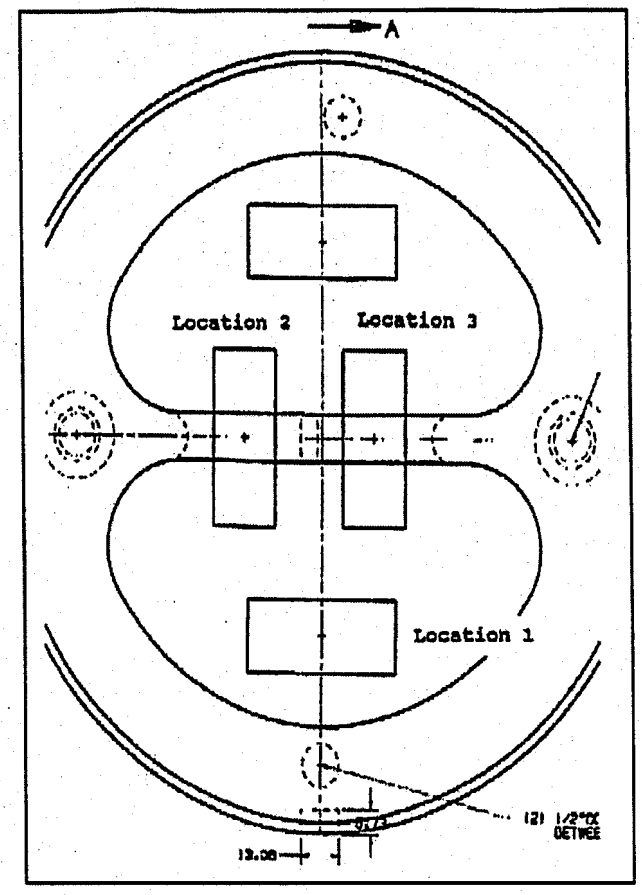

Figure 29: Test die used to form longitudinal welds in rectangular extrudates.[47]

These extrusion runs, used for testing, were performed under controlled conditions where the parameters were accurately recorded. The initial billet diameter was 229 mm defining an extrusion ratio of 9.2. The ram speed was 6.35 mm/s. The billet preheat temperature was 516 °C with an exit temperature of 520 °C for the front of the extrudate and 532 °C for the back end.

There are four orifices in the test die. Location 2 and 3 produce simple rectangular shapes that have the weld located in the center of the profile, as shown in Figure 30. Samples used for the analysis presented in this paper were extruded through the orifice at location 2. Location 1 and the corresponding location on the opposite side

of the die produce solid extrudates that do not contain welds. There are two such locations to maintain balance of the metal flow through the die. These extrudates were produced for a separate investigation. The mechanical properties of the welded and non-welded samples were compared to determine whether the extrusion weld is a source of weakness.

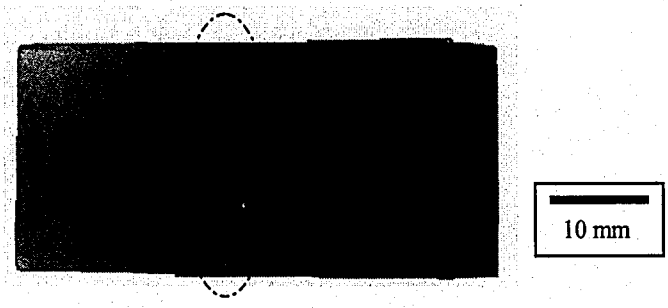

Figure 30: Experimental extrusion weld sample.

The extrudate, which is shown in Figure 30, is a 6061 alloy and has a rectangular cross section with dimensions 51 x 22 mm. Sample sectioning is shown in Figure 31; sample 9 was taken of the cross section. Because the profile was large, it was cut to a width of 28 mm (with the weld in the center) in order to fit into a standard 38 mm metallographic mount; the full height was unaltered. Longitudinal samples 10, 11, and 12 were sectioned parallel to the top surface at depths of 1, 6, and 11 mm. They were examined from above, along the z-axis. Because the weld is situated in the xz plane, the sample was not examined from the y-axis. To observe the weld from this direction, many successive polishing steps would be needed. A summary of the sample locations is listed in Table III.

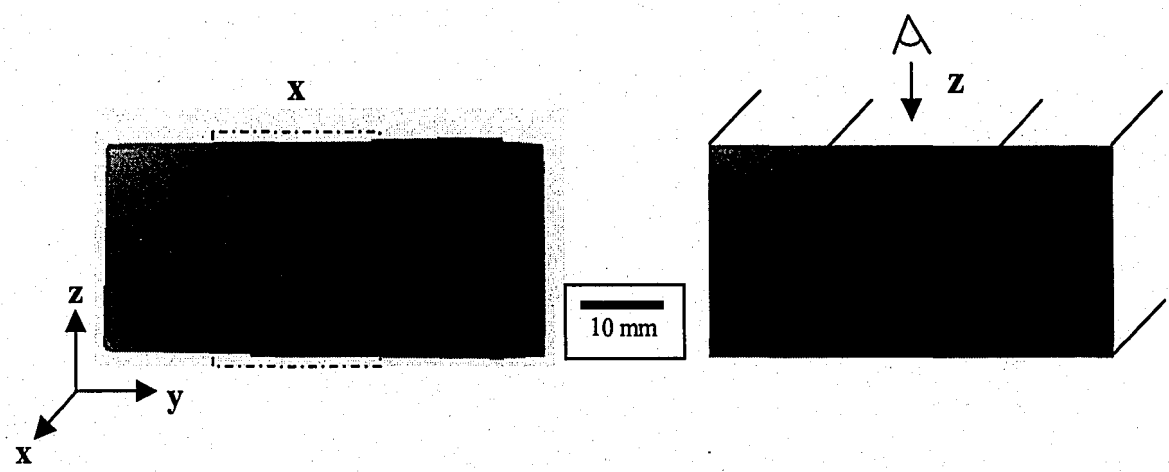

Figure 31: Samples used for die weld integrity studies.

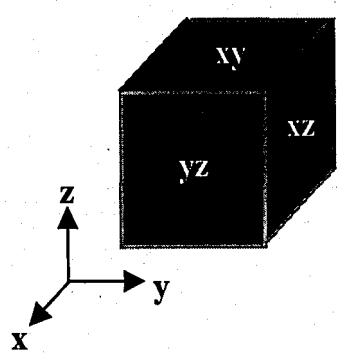

Table III: Summary of experimental weld sample locations

Sample #	Sectioning Plane	Observation Direction	Distance from top surface in. (mm)	Distance from side edge in. (mm)
Rectangular welded extrudate				
9	yz	x	-	-
10	xy	z	1	-
11	xy	z	6	-
12	xy	z	11	-

2.4 Industrial Extrusion Weld

2.4.1 Definition of Product Geometry

The other extrusion-welded sample being studied, shown in Figure 32, was part of an actual extrusion run, conducted with typical industrial parameters. The part shown is one quarter of the complete complex shape that uses a porthole die to produce the hollow sections. As revealed by the macroetch in Figure 33, the weld line is located along the entire length of the piece, from the top of the "arrow" to the edge of the hole at the bottom of the figure. EBSD was used to analyze the grain orientations across the weld.

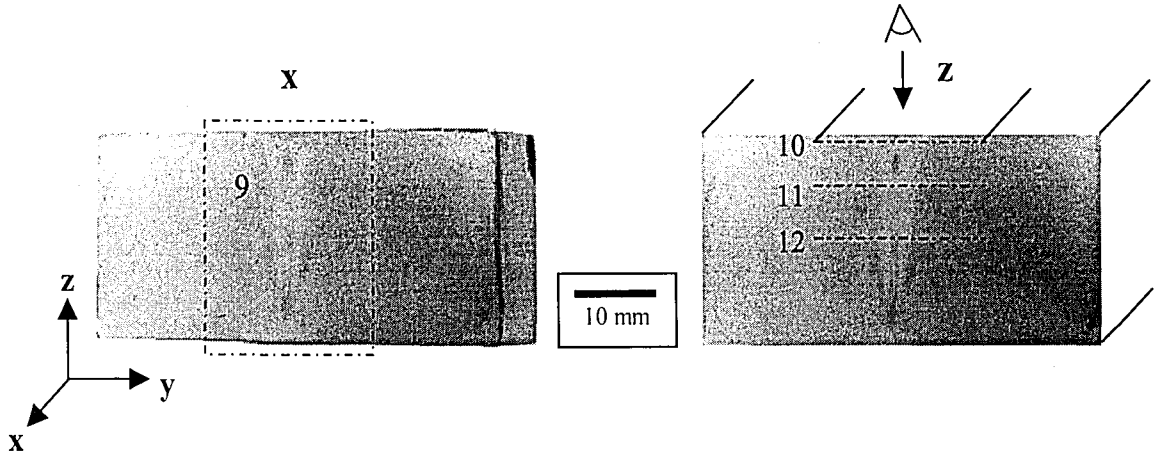

Figure 31: Samples used for die weld integrity studies.

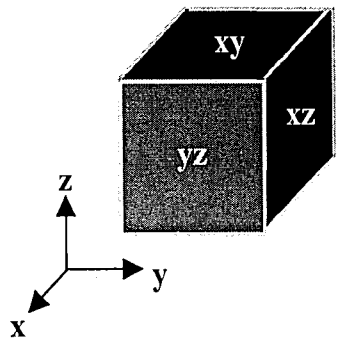

Table III: Summary of experimental weld sample locations

Sample #	Sectioning Plane	Observation Direction	Distance from top surface in. (mm)	Distance from side edge in. (mm)
Rectangular welded extrudate				
9	yz	x	-	-
10	xy	z	1	-
11	xy	z	6	-
12	xy	z	11	-

2.4 Industrial Extrusion Weld

2.4.1 Definition of Product Geometry

The other extrusion-welded sample being studied, shown in Figure 32, was part of an actual extrusion run, conducted with typical industrial parameters. The part shown is one quarter of the complete complex shape that uses a porthole die to produce the hollow sections. As revealed by the macroetch in Figure 33, the weld line is located along the entire length of the piece, from the top of the "arrow" to the edge of the hole at the bottom of the figure. EBSD was used to analyze the grain orientations across the weld.

The results were compared to the experimental weld to see if any discrepancies exist. The extrusion ratio was the critical variable that differed between these two profiles as well as the simple vs. complex geometries.

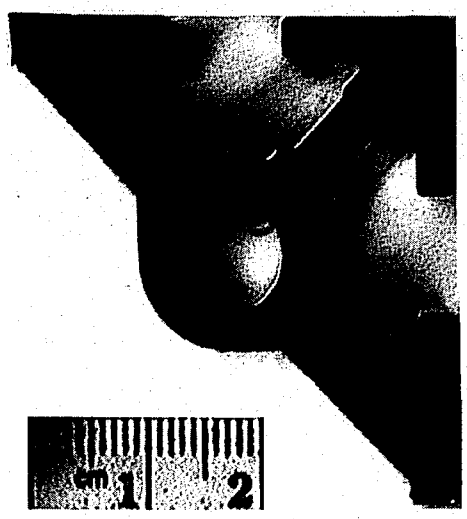

Figure 32: Section of a complex extrudate containing a longitudinal weld.

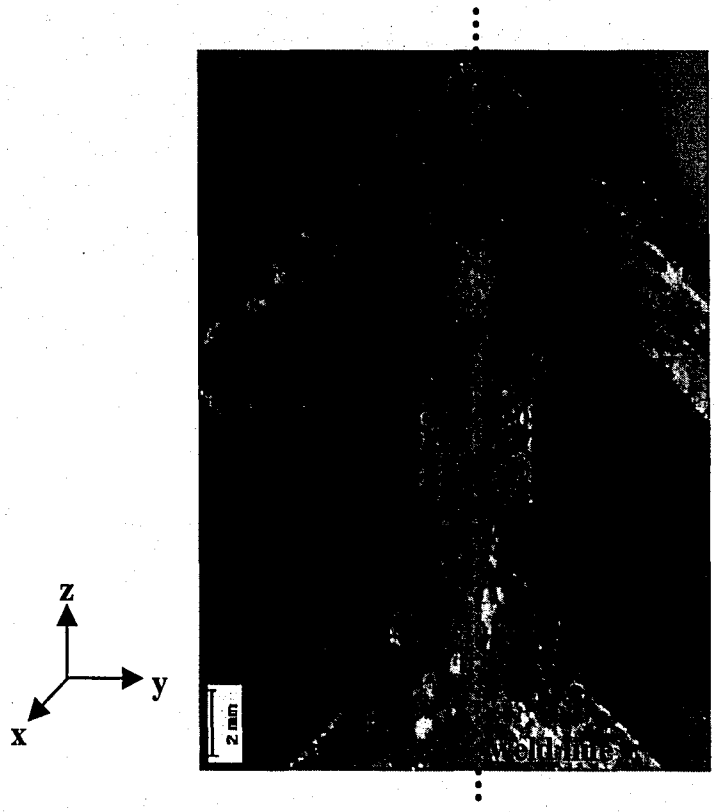

Figure 33: Section of industrial welded sample after macroetching.

The results were compared to the experimental weld to see if any discrepancies exist. The extrusion ratio was the critical variable that differed between these two profiles as well as the simple vs. complex geometries.

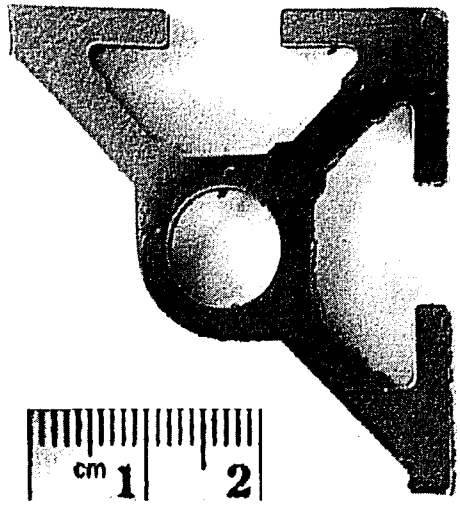

Figure 32: Section of a complex extrudate containing a longitudinal weld.

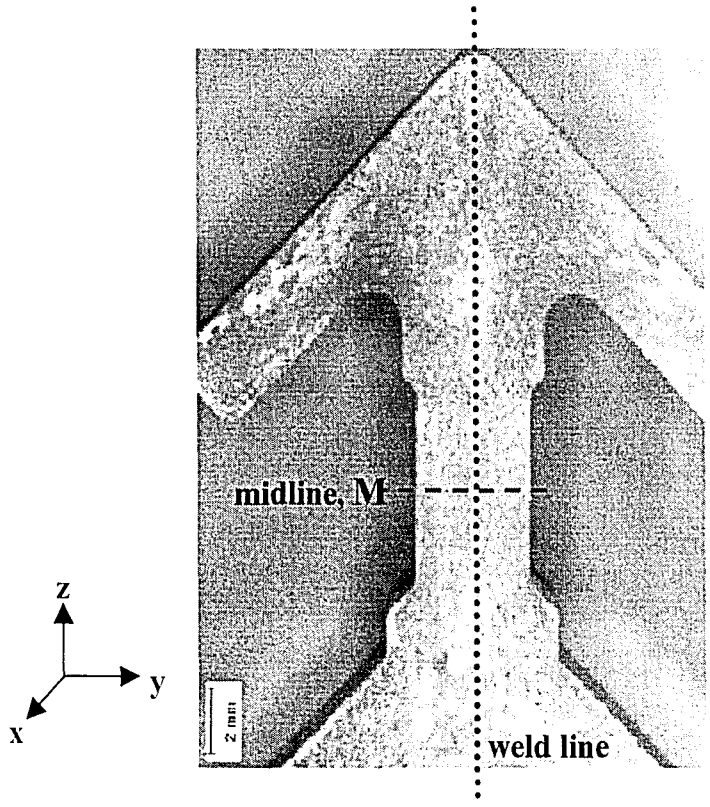

Figure 33: Section of industrial welded sample after macroetching.

The cross section of the sample was sectioned and is shown in Figure 33. In addition, a longitudinal sample was cut at the approximate mid section of the weld area, labeled M. LOM images were captured at three different locations of the cross section: the top near the arrow, the bottom near the hole, and across the mid section, M. Some pictures were taken of the longitudinal sample as well. Microhardness measurements were taken from the longitudinal section across the weld from one side of the part to the other. The grains of the longitudinal samples are slightly elongated, which made placement of the Knoop indenter easier. However, the primary focus of studying this part was to determine the orientation of the weld and the surrounding areas. Orientation (EBSD) scans were recorded across the entire width of the weld at the location M. The cross section was examined so that the ND was aligned with the extrusion axis.

3.0 RESULTS

3.1 Solid Extrudate

3.1.1 LOM Investigation

The solid extrudate sample contained a thick section that was coupled to two thin legs. For the heavy region, there was significant variation in size and microhardness from the surface of the part, with the highest amount of deformation, to the center region grains, which resemble those of the original, cast structure. Macrophotographs were taken using a stereomicroscope, and there appeared to be several distinct structural regions that were further revealed by the higher magnification LOM images.

Figure 34 presents an image of the macroetched solid extrudate upon inspection using the stereomicroscope capable of low magnifications (1-7X). Figure 35 presents higher magnification images of the two major areas studied: the heavy region and the thin legs. After etching, microstructural gradients are evident from the grain contrast.

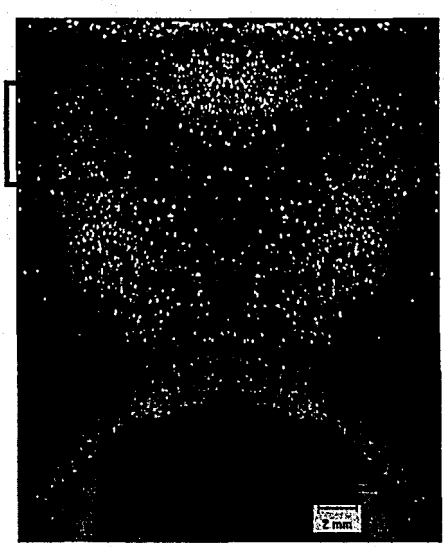

Figure 34: Macroetched sample of the solid extrudate.

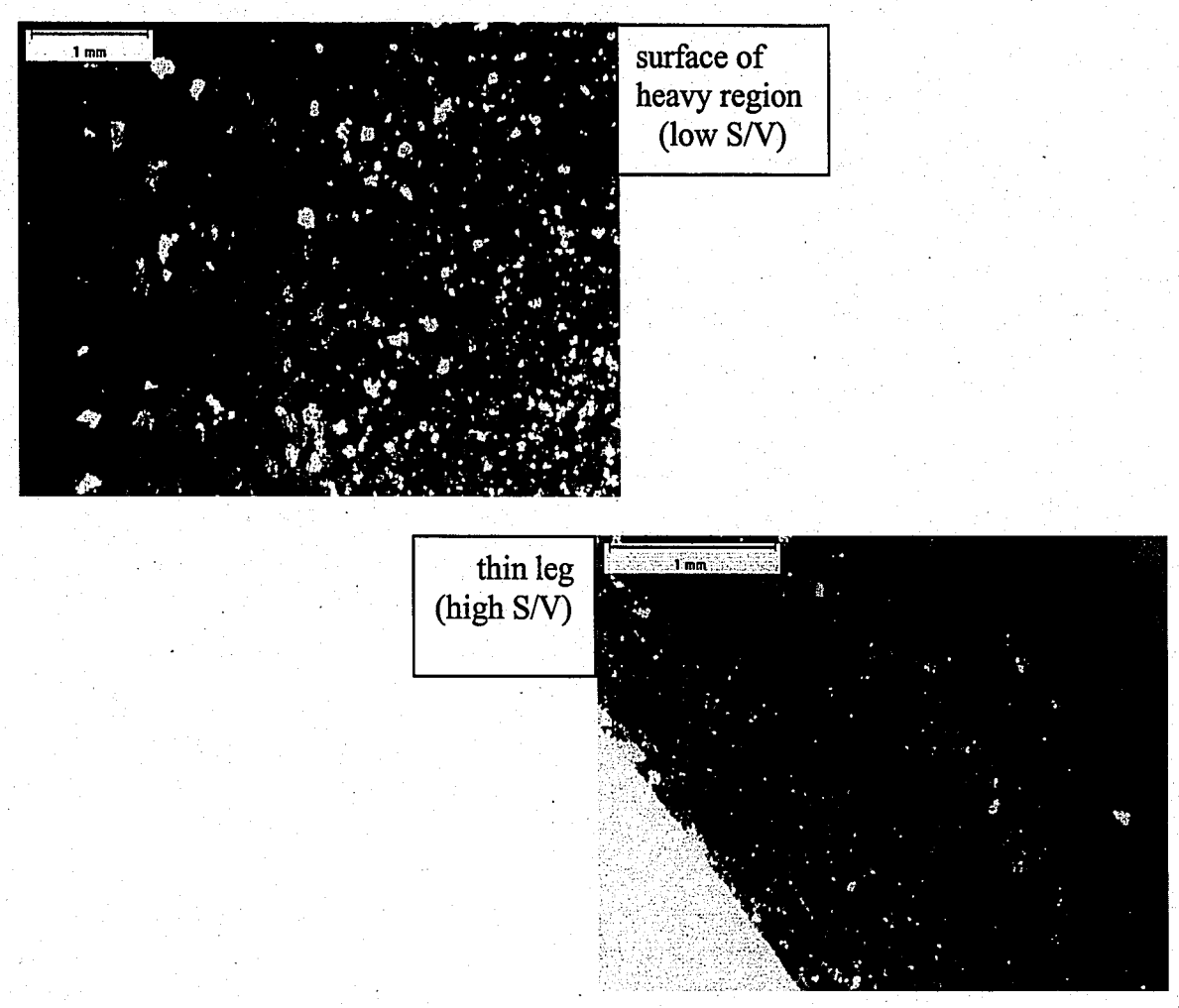

Figure 35: Higher magnifications of selected areas identified in Figure 34.

The same profile was etched in 5% HF acid for grain size/shape microanalysis. The cross section in Figure 36 displays a bright ring (labeled as region II) just beneath the outer surface that contrasts with the adjacent material. There appears to be five distinct regions of microstructural features. Figure 37 presents a longitudinal view of sample 2; this picture has the same grain-contrast variation that was previously shown. Even using this low magnification, some of the large grains can be resolved. To get a better understanding of the grain structure and gradients higher magnifications are needed.

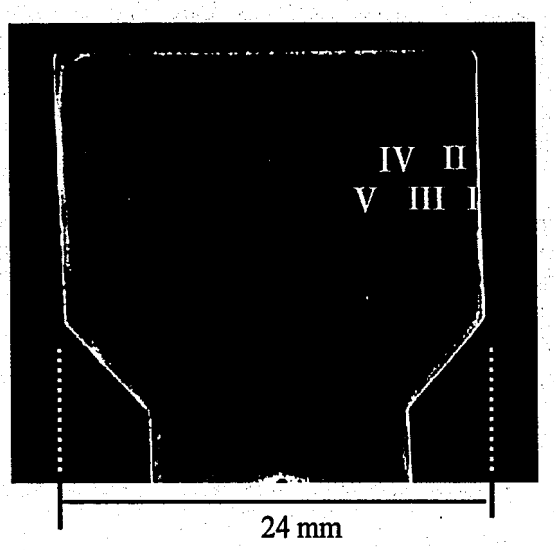

Figure 36: Etched cross section photograph of the heavy region from the solid extrudate.

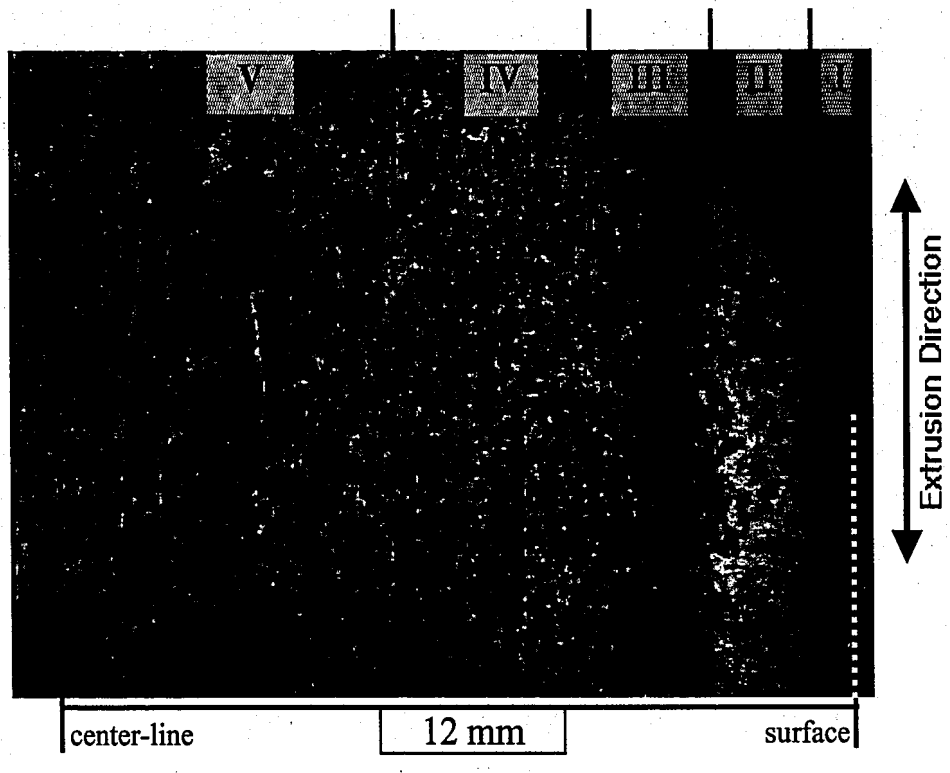

Figure 37: Longitudinal macro image of the sample 2 edge.

Figure 38 presents an image near the surface of sample 2 at higher magnification. The individual grains of the first three regions with varying contrast can now be discerned. There are small grains at the surface that are adjacent to large grains elongated in the extrusion direction (vertical for this picture). These grains decrease in size further away from the edge. Figure 39 displays a similar location at double the magnification. The grains just beneath the surface are very large relative to the surface microstructure.

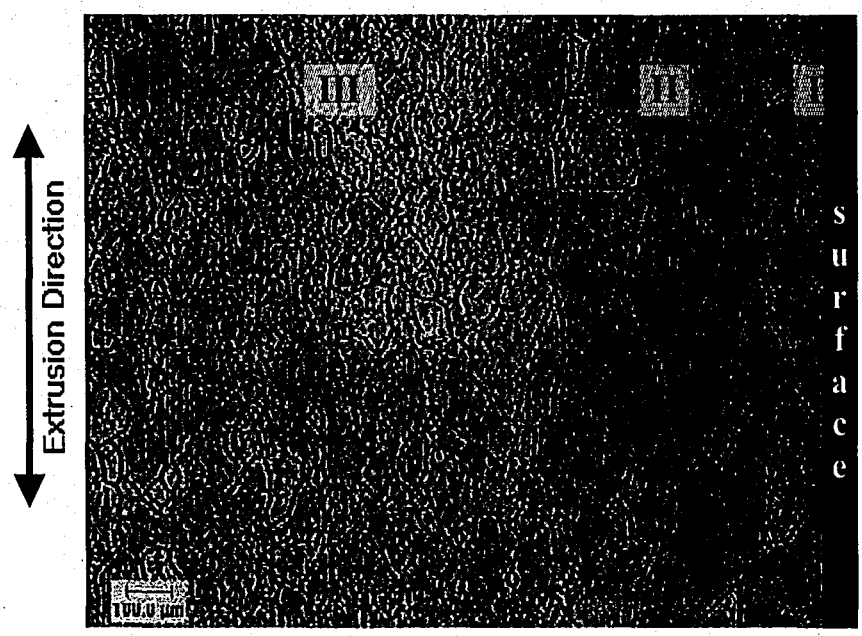

Figure 38: Edge of sample 2 displaying three different microstructural zones.

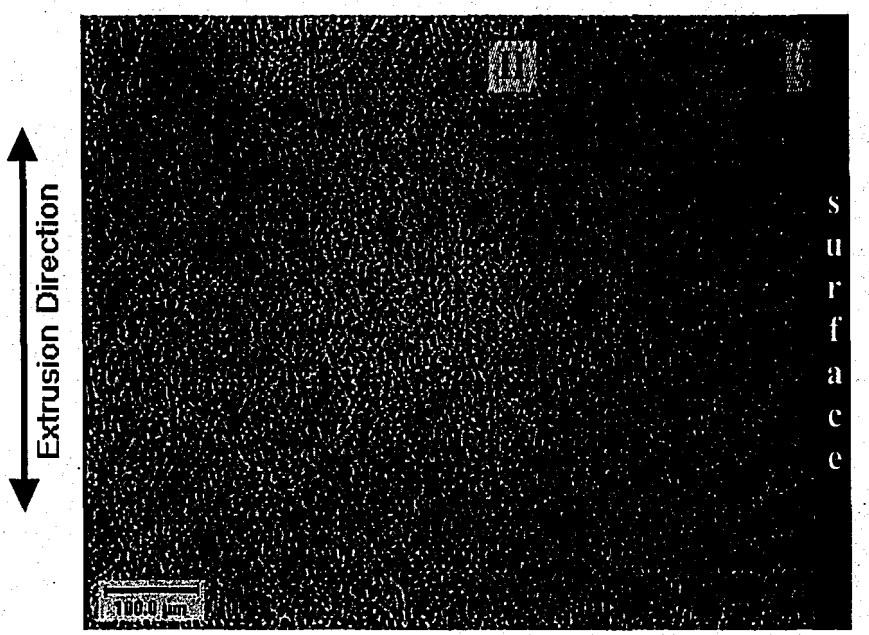

Figure 39: Edge of sample 2 at twice the magnification of Figure 38.

In these pictures, the extrusion direction is vertical and the surface appears to the right. Along the edge, there is a thin band, a row or two deep, of small grains (<50 μm) that penetrates less that 100 μm into the sample. These grains comprise the area previously described as Region I. Region II, adjacent to these grains, consists of very large grains; some of which were discernable in the macrophotographs. These grains average 150-250 μm wide, are elongated, and extend up to 500 μm in the extrusion direction. This region has a total thickness of up to 800 μm. As region II ends, the large grains decrease in size and are replaced completely by small, nearly equiaxed grains (III). Figure 38 and 39, both taken of sample 2, were included in this document because they accurately exemplify all of the samples and were the highest quality images as well. This structural variation existed for all of the heavy region samples.

Further into the sample, the small grains of region III grow gradually until they reach the center of the extrudate and attain their maximum size. Figure 40 shows an image closer to the center than those previously presented (about halfway between the edge and the vertical midplane of the sample), where the small grains being to grow. At the dashed line there is a subtle change in brightness. The grains to the right are smaller and appear somewhat brighter than those on the left half of the picture. This latter observation will be explained later in conjunction with the analysis of the microhardness measurements. Figure 41 was taken from the center of the profile where the grains achieve another maximum in size. The grains in this figure are slightly elongated in horizontal direction because this image was taken from sample 6 where the extrusion direction was oriented horizontally in the picture.

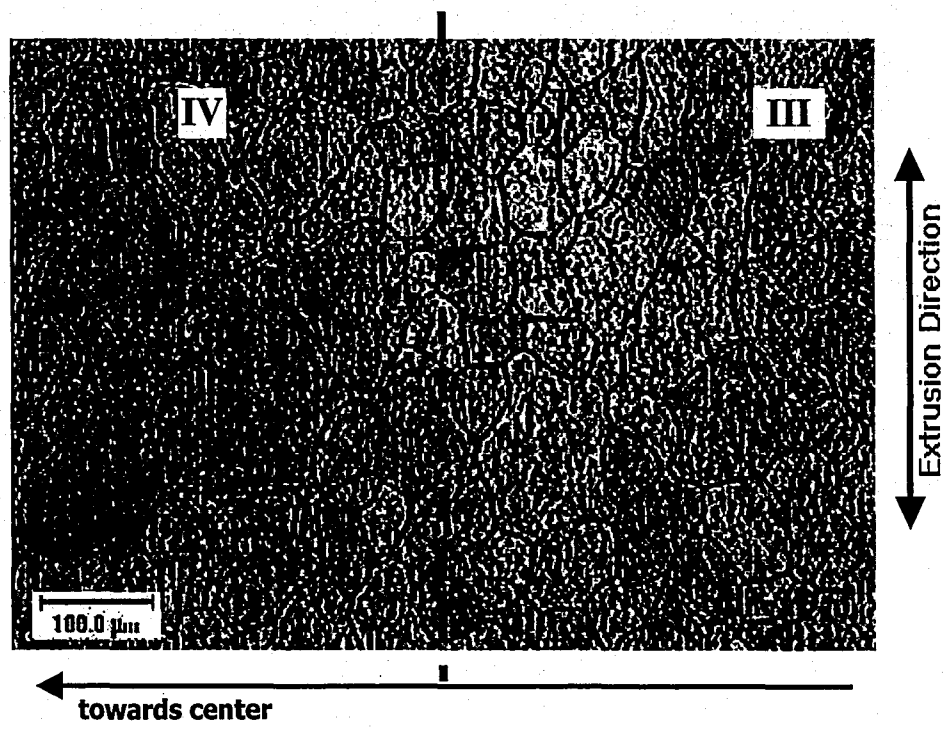

Figure 40: Transition from small to larger grains near the center of sample 3.

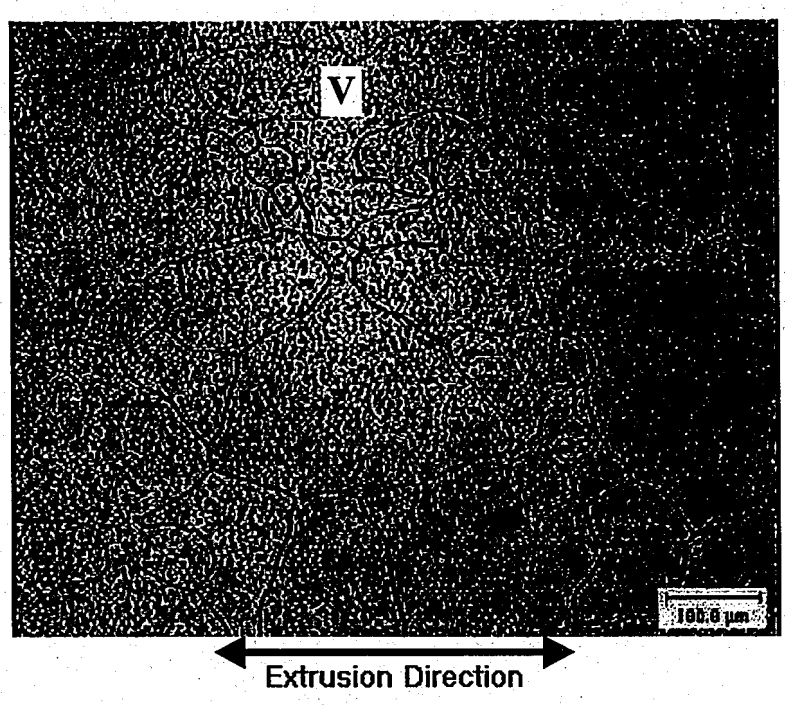

Figure 41: Maximum grain size found at the center of the profile.

The changes in grain size are not limited to those samples observed from the z-direction. Microstructural gradients occur due to the localized deformation near any surface: side or top. Figure 42 was taken from Sample 6 and displays the variation in grain size/shape from the top surface of the part towards the center. Therefore, the effect is combined when examining the cross section of the shape diagonally from the corner and moving towards the center. Figure 43 presents an image of the cross section and shows the microstructural variation from the side and top surfaces. The combined effect of both surfaces is also illustrated in Figure 36, the large macro image of the cross section.

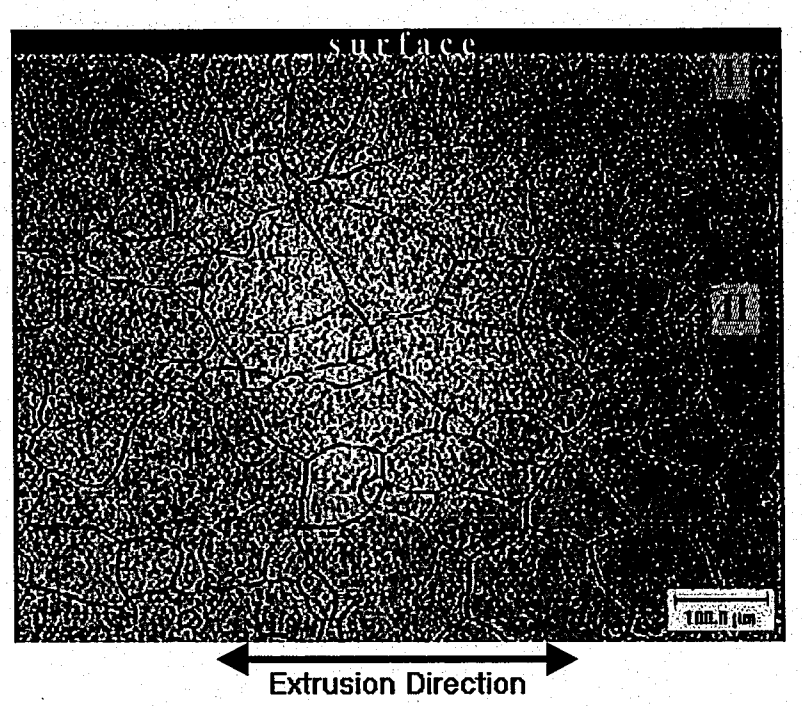

Figure 42: Microstructural gradients near the top surface.

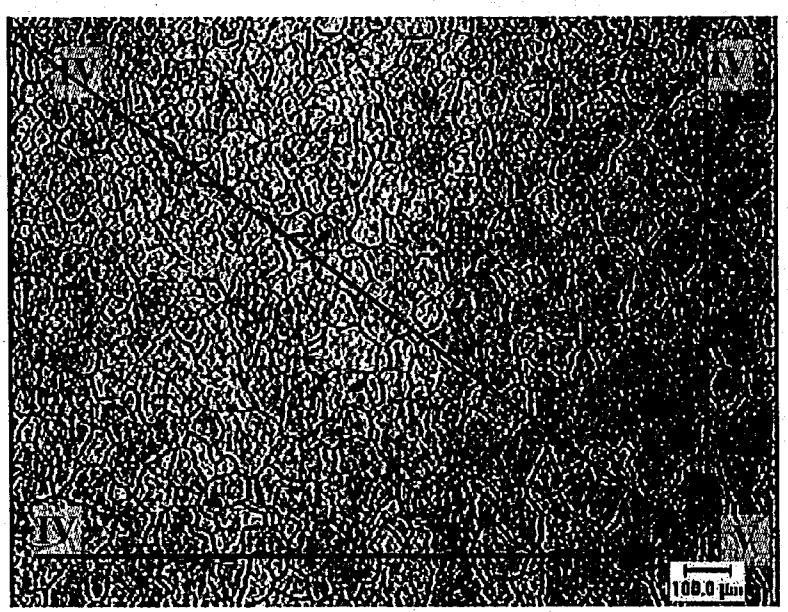

Figure 43: Grains grow in both the vertical and horizontal directions towards the center of the extrudate.

The microstructure of the legs was fairly consistent and did not display the strong gradients present in the larger, heavy section. Figure 44 presents an image from the cross

section of the legs. Small equiaxed grains dominate the microstructure. There are some relative variations that resemble regions I, II, and III from the heavy section. The deviation in grain size is much smaller relative to the extreme differences found in the heavy region microstructures.

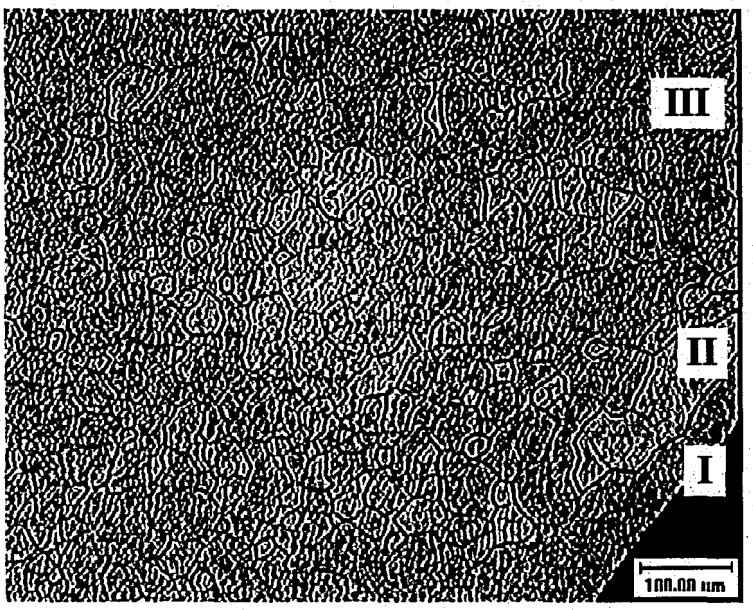

Figure 44: Typical microstructure of the thin legs.

3.1.2 Microhardness Measurements

As mentioned before, the strength of the individual grains was determined with microhardness measurements. A general pattern was established based upon data received from several tests of all samples. Qualifications from hardness measurements were based on relative values from the same part. Initially, the tested path was measured from one side edge completely across the sample to other edge. Subsequent tests were terminated at the center of the profile, because of its vertical symmetry. Microhardness as a function of distance from the surface for sample 2 is plotted in Figure 45.

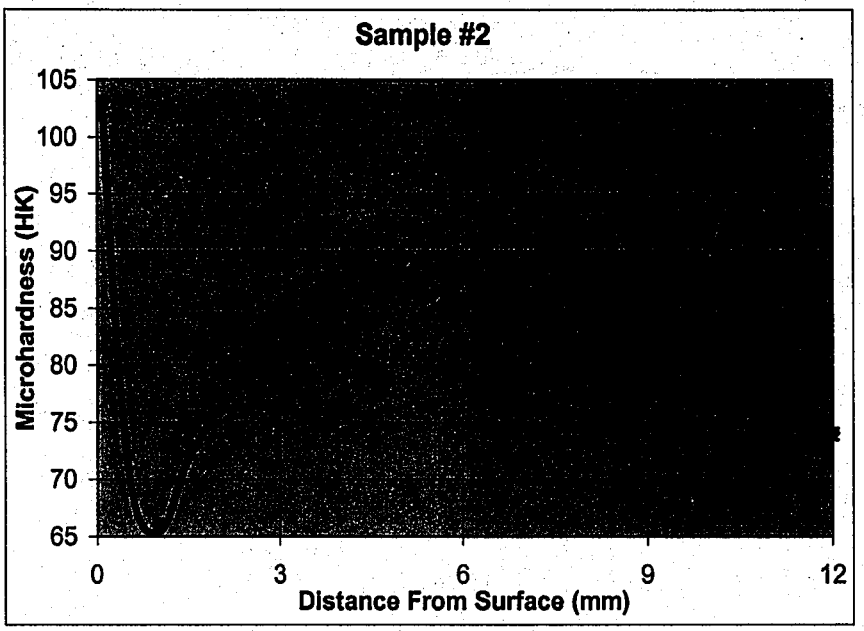

Figure 45: Microhardness traverse taken halfway across sample 2.

This microhardness trend also applies to the vertical direction where the same grain structure variation was present as that found in the horizontal traverse. Figure 46 displays a microhardness path tested from top surface of sample 7. When moving vertically greater care should be taken to know the distance from the top surface because the top and bottom of the part are asymmetrical unlike the two sides, which are equivalent.

Three microhardness traverses were conducted across the cross section of the legs. These measurements, along with the average, are shown in Figure 47. An average value of between 120 and 130 was obtained for most points. The test paths spanned the entire width of the legs, which should be relatively symmetric. No well-defined trend was observed.

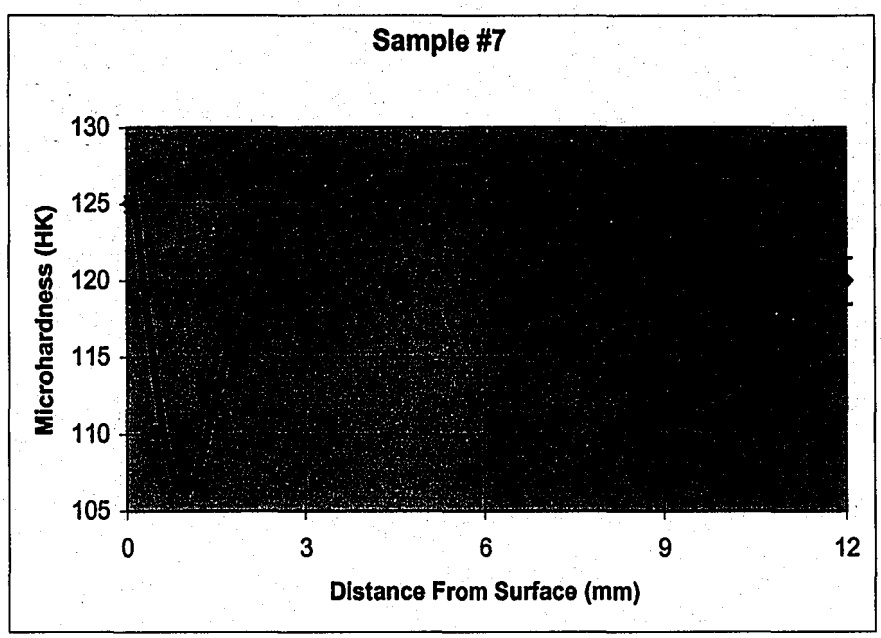

Figure 46: Microhardness traverse taken vertically down sample 7.

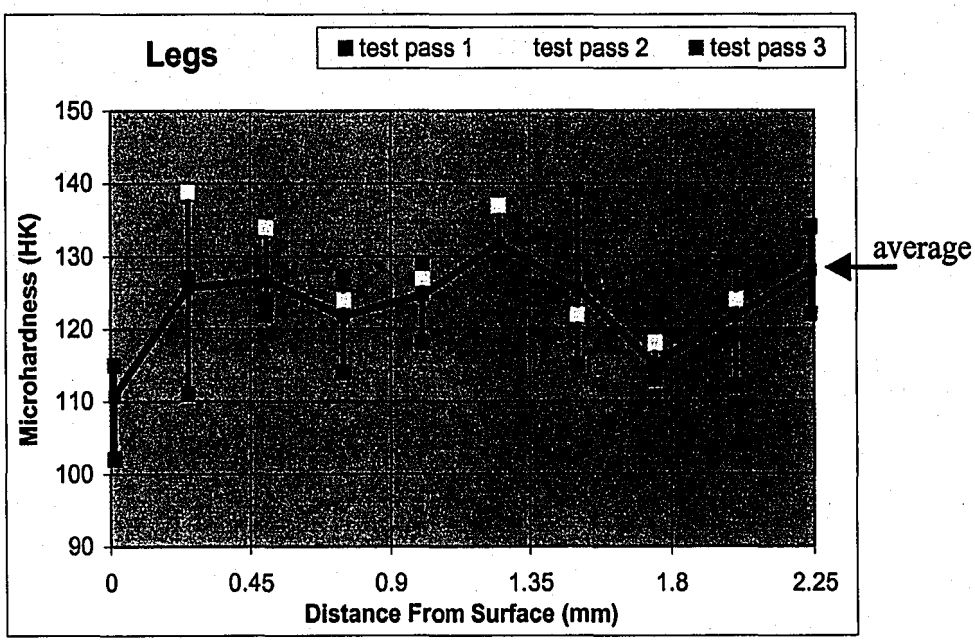

Figure 47: Microhardness traverses taken across a thin leg.

3.1.3 EBSD Analysis

The texture and grain structure at the surface layers of the extruded profile were also examined. The major objective was to investigate specific deformation regions (in terms of crystallographic structure) along the path of the metal flow. The principal areas of study involve the surface regions that have been previously defined in Figure 28. Surface regions from the heavy section and thin legs were examined to understand the differences between the textures created by choke and parallel bearing lands. Pole figures identified those orientations that occur regularly, i.e. texture. The results show strong texture for the thin leg areas, but a more random distribution for the heavy section.

The pole figures for the cross section of the legs (Sample B), are seen in Figure 48. Orientation scans were repeated in different areas of the thin regions and similar results were obtained. Figure 49 shows the secondary electron image of the leg where an orientation scan was performed. The pole figures demonstrate a strong maximum at the center and a weaker signal around the periphery. This is typical of the <100> fiber texture. Grains are oriented in multiple orientations about the extrusion axis, [100]. The most common plane-direction combination is the cube texture, (001)[100].

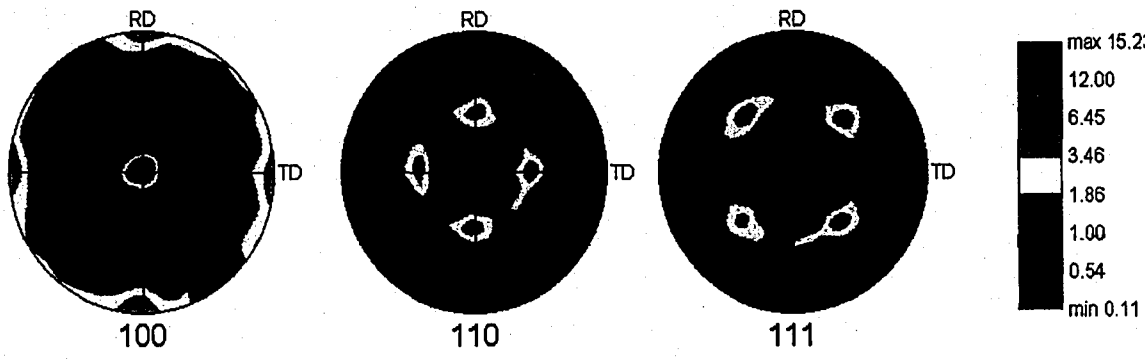

Figure 48: Typical pole figures for an area scan from the thin legs (high S/V).

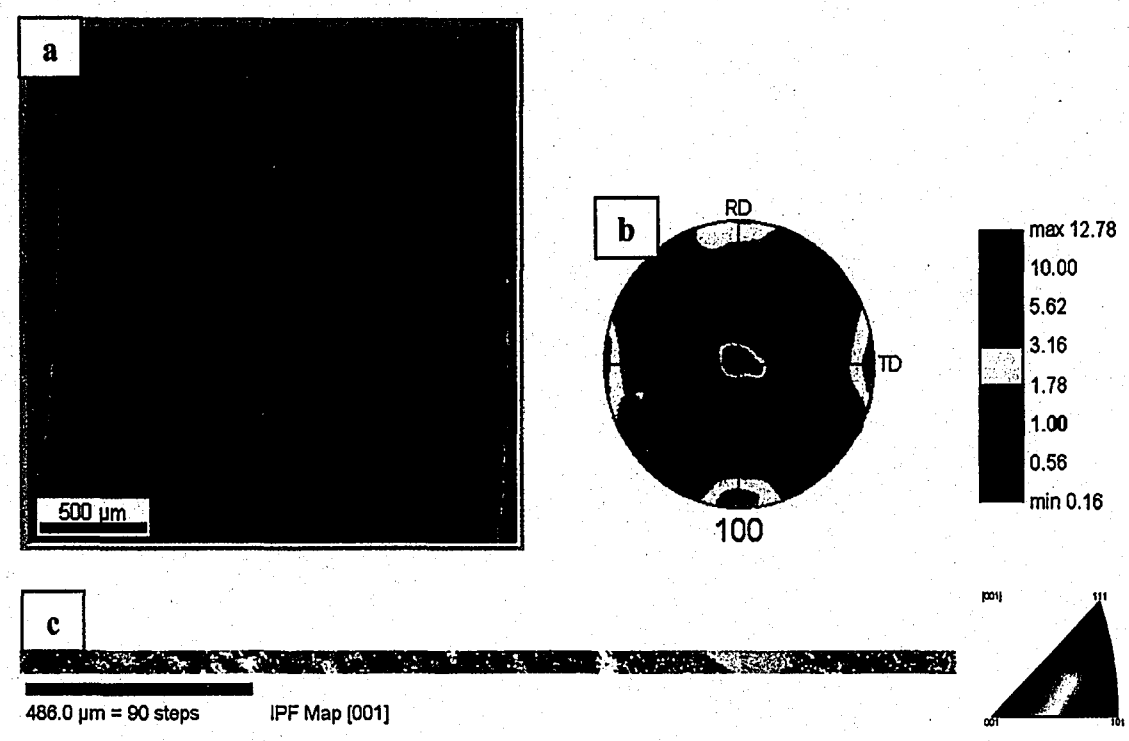

Figure 49: (a) Secondary electron image displays the scanned area
(b) 100 pole figure for the area shown in (a)
(c) inverse pole figure (IPF) grain map and the associated color key.

Figure 50 presents pole figures from a longitudinal section of the leg (sample E). The ND is no longer coincident with the extrusion direction, which was aligned with TD for this sample. Since ND (observation direction) is the z-axis, this is the 001 pole figure and RD is the y or [010] direction. The 001 pole figure displays a weaker intensity vertically through the center of the diagram and strong texture present to the east and west side of the "globe", representative of the [100] and [-100] directions, which correspond to the extrusion direction. Figure 48 and 50 display consistent results and show the rotations of the pole figures caused by the translation of the specimen in the microscope. Both figures describe the same <100> texture.

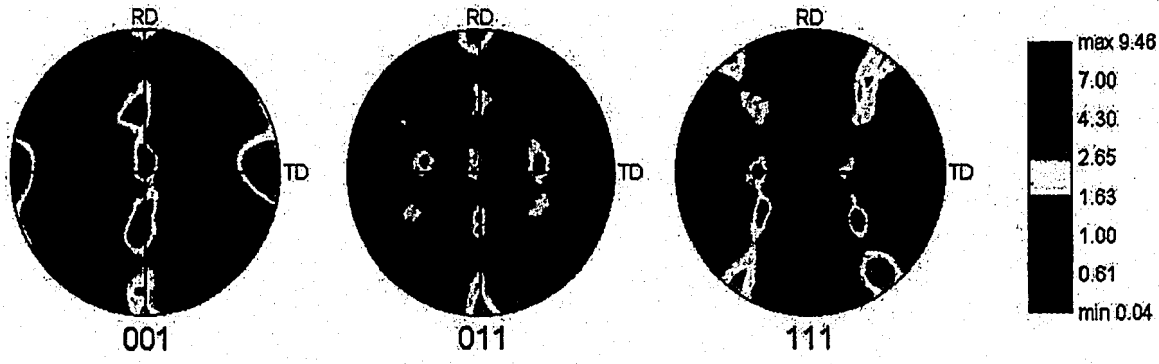

Figure 50: Pole figures from an EBSD scan from a longitudinal section of the legs (E).

To accommodate the change in the beam direction, the EBSD software allows a rotation of the data about the three orthogonal axes (ND, RD, and TD). To confirm that the two sets of figures are consistent, the pole figures from the longitudinal samples examined from the z-direction (Figure 50) can be rotated to match the pole figure recorded from the x-direction (Figure 48). Because the way the sample was set up in the microscope, the rotation must be accomplished by two separate 90° rotations. These may be performed in any of the following orders: 90° about ND followed by 90° about TD, TD followed by RD, or RD followed by ND. These rotations are summarized in Figure 51. The left hand pole figure represents the axes when the longitudinal legs (E) or side (C) of the part was examined (looking down the z-axis, from above) and the right hand side presents the original pole figure setup when looking along the extrusion axis at the cross section (samples A and B). The rotated data is presented in Figure 52; the pole figures accurately reproduce the previous experiments results given in Figure 48.

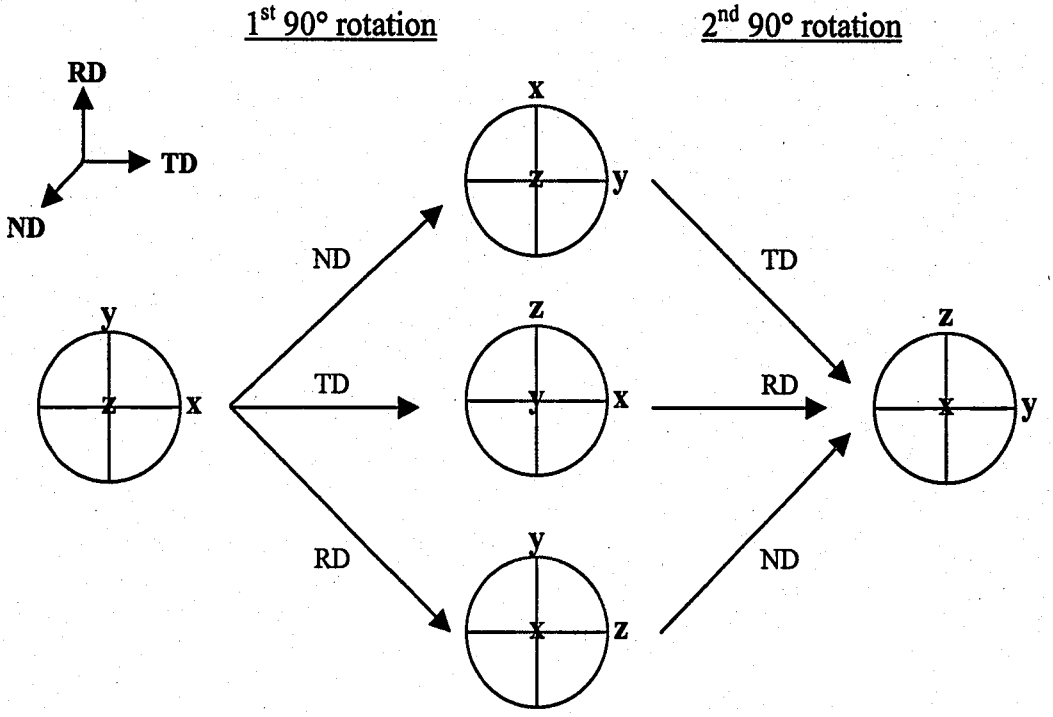

Figure 51: Two rotations are needed to return the longitudinal leg (E) and side (C) results to the original coordinate axes.

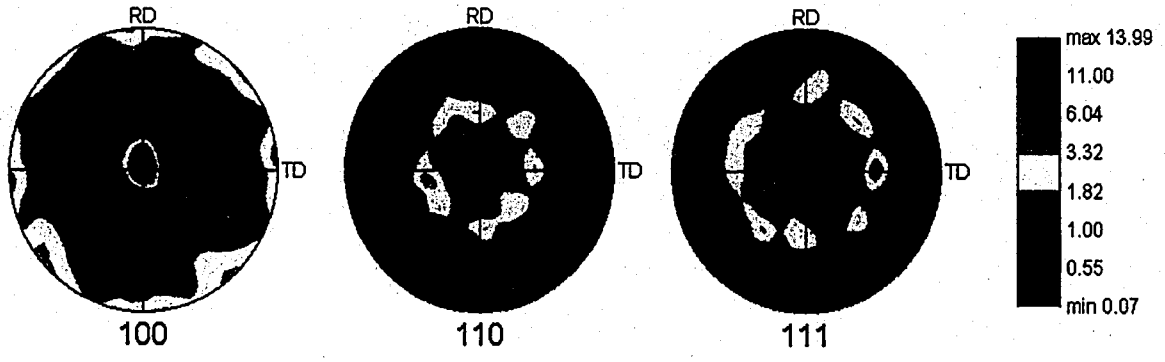

Figure 52: Orientation data from Figure 50 was given two 90° rotations to align the extrusion direction with ND. Results give good agreement to Figure 48.

One set of pole figures for the cross section sample (A) of the bulk (heavy) area is shown in Figure 53. The pole figures resemble those previously given, but rotated 45°

around the ND. This is known as the cube-on-edge, or Goss texture, (011)[100]. The intensities in the pole figures are lower than the values in the legs' pole figures previously presented. However, these values are much higher than for a random distribution and indicate a preferred orientation. Additional scans produced more pole figures that had lower intensity values, but still included concentrations at the same orientations.

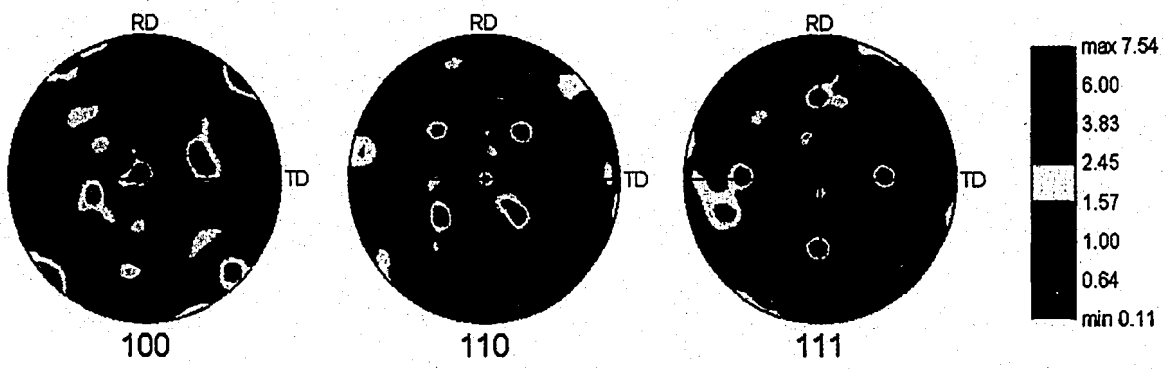

Figure 53: Pole figures for the surface texture of the heavy region.

For this section, pole figures were generated from longitudinal sections as well. The pole figures shown in Figure 54 were from top of the sample (sample D). They are comparable to the results from the sides (C), which were extruded using the same die design (choke bearing land). The same [100] and [-100] poles to the east and west have high intensities, but there are additional preferred orientations near the [011] and [01-1] directions of the same figure. Neither of these textures is as strong as that found in the leg section.

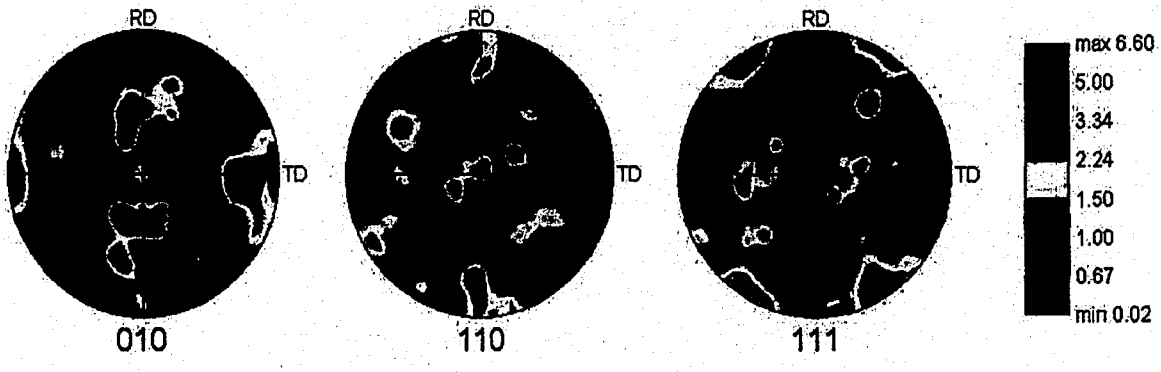

Figure 54: Pole figures for the top (D) of the heavy region measured from a longitudinal section.

To examine the top section (sample D), the sample was studied from the y-direction; therefore, the (010) pole figure is being analyzed. The sample was aligned such that the extrusion direction, [100], is the TD. As shown in Figure 55, the data from the longitudinal sample only needs to be rotated once about the RD by 90° to acquire pole figures consistent with the cross section results. The rotated data from the longitudinal top sample found in Figure 56 compares well with the original data from the cross section (Figure 53). There is good correlation in the 100 pole figures; however, the rotated 110 pole figure lacks the small intensity in the center region that was previously observed.

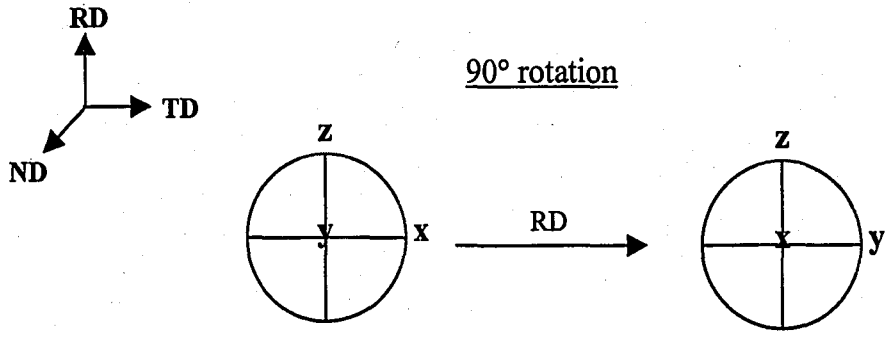

Figure 55: One 90° rotation is needed to return the longitudinal top (D) results to the original coordinate axes.

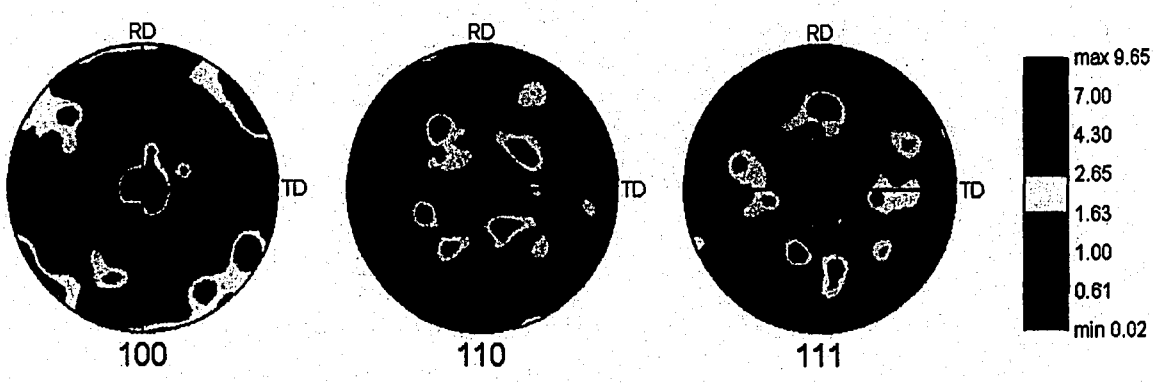

Figure 56: Data from Figure 54 was rotated 90° about RD to compare with Figure 53.

The results of the surface texture analysis are summarized in Table IV. The legs had a very strong cube texture; whereas the heavy section had a weaker Goss texture. The "texture strength" listed in the chart has been quantified by averaging the maximum intensity on the scale from the three pole figures for each region listed in this document. The intensities associated with each pole figure are colored depending on the probability of a particular orientation. The value listed is the number of times that orientation will appear with respect to a completely random texture. For a perfectly random distribution, all orientations will appear with equal likelihood, and the pole figure will have an even intensity of 1.00 with no concentrated areas. The presence of texture multiplies the probability of a grain having a particular orientation.

Table IV: Summary of the results for the surface texture experiments

Fig. #	Region	Bearing Land	S/V	Texture Strength	Texture
48,50,52	legs	parallel	high	strong (12.89)	Cube (001)[100]
53,54,56	heavy	choke	low	medium (7.93)	Goss (011)[100]

3.2 Experimental Extrusion Weld

3.2.1 LOM Investigation

The macroetched rectangular extrudate containing the longitudinal weld seam is shown in Figure 57. The weld is clearly visible in the center of the part. Once again, more information is obtained by examining the part after etching it in 5% HF, which was done for microstructural analysis. After etching samples 9-12, the weld region can be easily identified. Figure 58 presents a macro image of sample 9, the cross section of the experimental extrudate containing the weld. Many large grains can be visually inspected with the naked eye. For some vertical distances, very large grains exist in the vicinity of the weld, while for other heights no grains appear. A bright line is present at the vertical centerline for some locations.

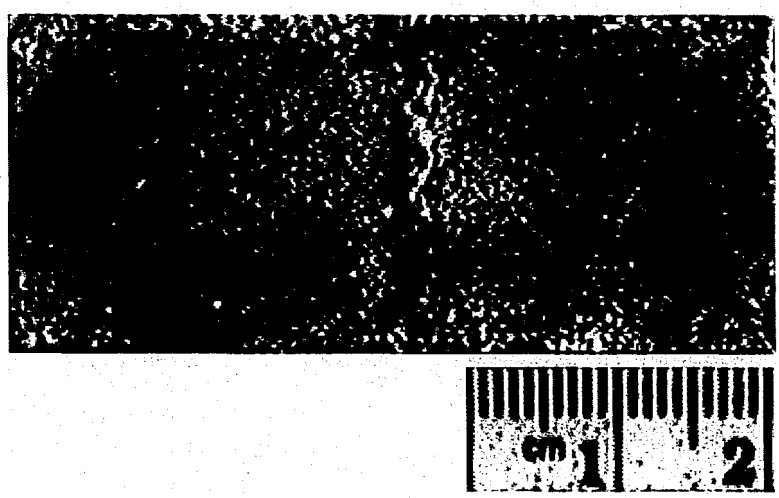

Figure 57: Macroetched rectangular welded extrudate.

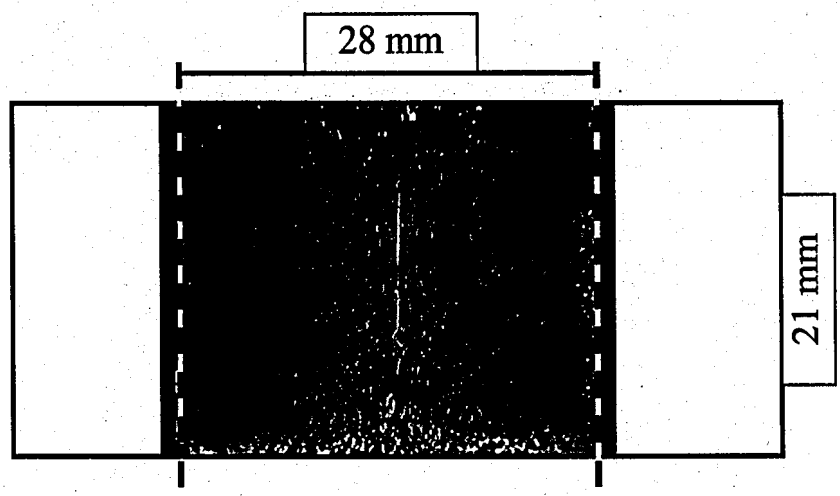

Figure 58: Sample 9, cut from the cross section of the welded sample. The dark rectangle indicates the full with of the extruded profile.

Longitudinal sections provide additional information. Figure 59, from sample 12, the vertical midpoint, displays very large grains at the weld interface. However, Figure 60, sectioned approximately one-quarter distance (6 mm) from the top surface, exhibits a lack of grain structure at the center. In general, there is a bright thin strip of material through the center and a darker undefined region on either side that is surrounded by large grains.

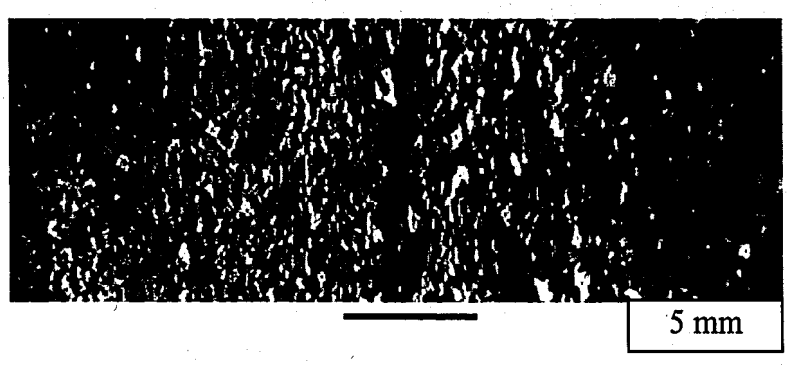

Figure 59: Weld region of sample 12 showing very large grains at the weld interface.

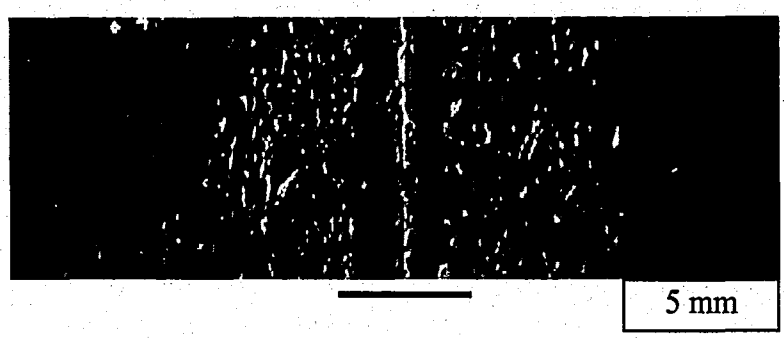

Figure 60: Weld region of sample 11 shows a lack of grain structure at the weld interface.

Figure 61, taken from sample 9, displays the typical microstructure at distances far away from the weld. Grains vary in size from 50 to 400 μm in diameter and are near-equiaxed. Figure 62 is a micrograph taken from sample 9 at the weld. This image reveals few large grains, and areas with fine grains intermixed with an "unstructured" region that does not display any grain boundaries. Since extrusion welds undergo subsequent deformation after they are formed, the metal streams blend together. There is no definitive weld line at the center, which is typical of traditionally welded microstructures.

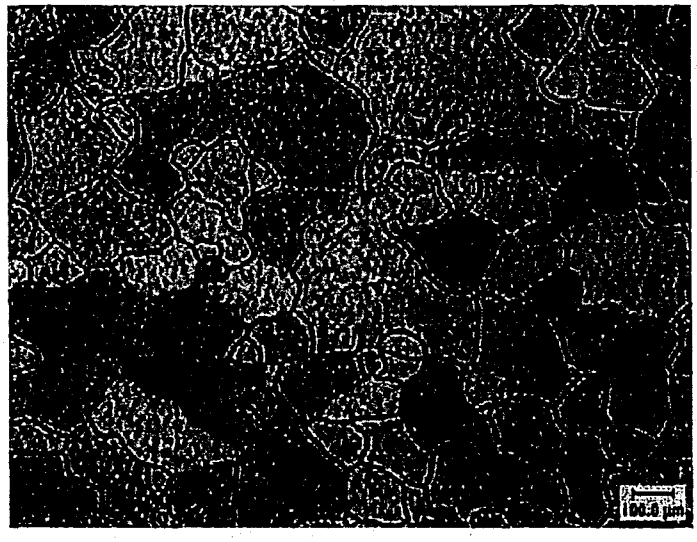

Figure 61: Grain structure of the parent metal (at distances far from the weld).

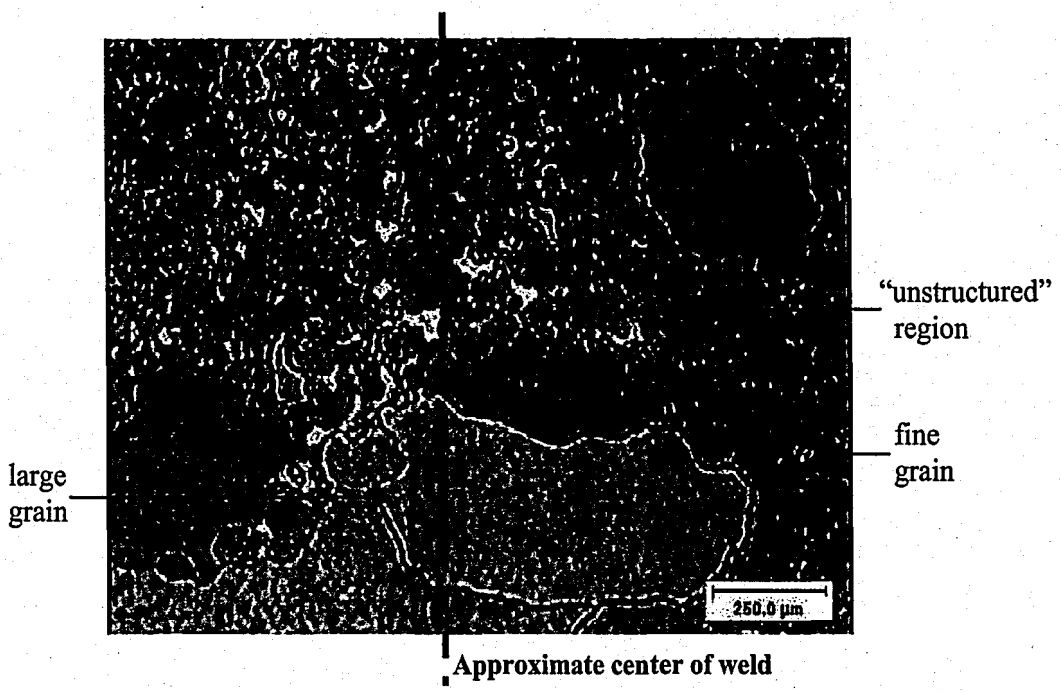

Figure 62: Center of the profile showing characteristics of the weld region.

Figures 63-65 are composite images that span the entire weld region and accurately reflect what was depicted in the macro photographs (Figures 58-60). Figure 63, taken from sample 9, shows the typical microstructural features of the weldment, pressure affected zone (PAZ), and the parent metal. Because of the nature of longitudinal extrusion welds formed with porthole dies, the materials surrounding the weld is known as the PAZ because the weld does not involve the traditional local melting of material that leads to the normal heat affected zone (HAZ).

The weld microstructure of sample 9 is bounded by very large grains and consists of an area possessing both fine grains and an unstructured region. The vertical bright line at the weld in Figure 58 corresponds to the area containing small grains, at the center of the weld. Adjacent to these grains is the unstructured region that does not contain any boundaries. The PAZ consists of large grains that diminish in size to that of the parent material.

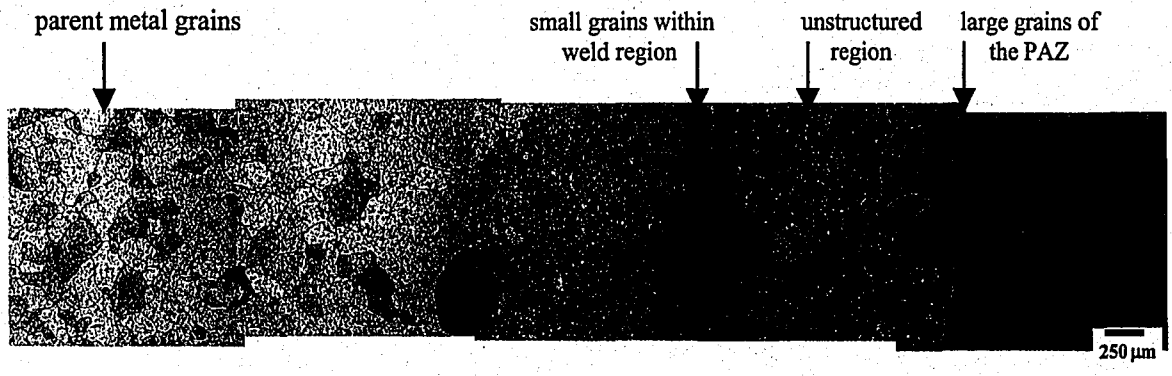

Figure 63: Extrusion weld and the surrounding areas from sample 9.

The images presented in Figure 64 and 65 are pictures from samples 12 and 11, respectively. The microstructure of sample 12 is dominated by very large grains and has a very small, if any, area consisting of both fine grains and an unstructured region. This is consistent with the macro image of Figure 59. Figure 64 is taken from sample 11, a longitudinal area 6 mm from the top surface. The weldment at this location spans a much larger area than for sample 12. The center of the specimen that appears bright in the macro photograph (Figure 60) correlates to an area containing small grains, which exists at the center of the weld. On either side is an unstructured region that does not contain any grain boundaries. The large grains that appear are typical for a PAZ. Once again, they decrease in size at distances further from the weld.

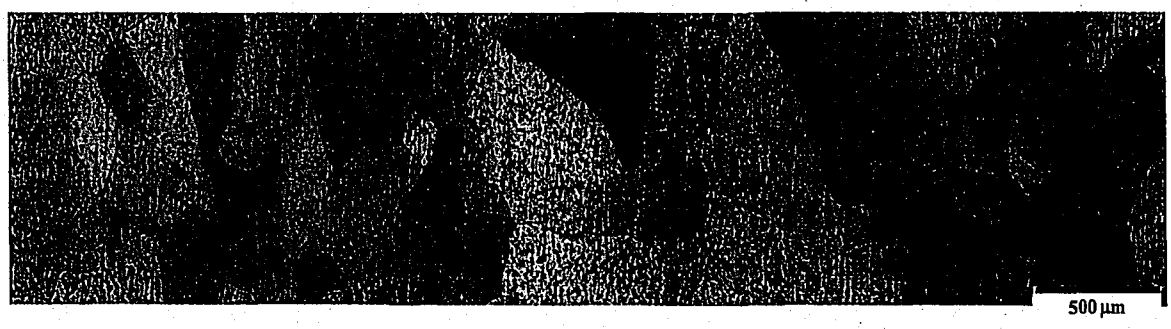

Figure 64: Extrusion weld and the surrounding areas from sample 12.

Figure 65: Extrusion weld and the surrounding areas from sample 11.

3.2.2 Microhardness Measurements

Microhardness measurements were tested for the welded sample to comment on the integrity of weld. The average microhardness for the parent metal was taken far away from the weld to avoid any effects of the weld and PAZ. Four measurements were taken for each sample and are plotted in Figure 66 along with the average value of 22.9 HK.

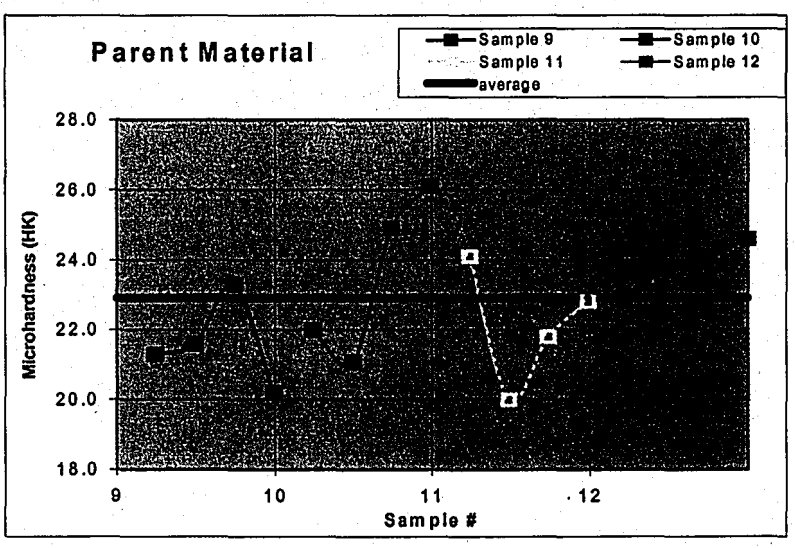

Figure 66: Measurements of the microhardness for grains located far from the weld interface.

For each sample, several microhardness passes were taken across the weld region. The average measurements are shown on the graphs (see Figures 67-69). Figure 67 shows a microhardness traverse across the weld for sample 9 (cross section) and

Figure 68 displays results from measurements of sample 11. Although the graphs appear different, both are reasonable when comparing the data to the microstructures. Next to the weld both samples have low microhardness due to the very large grains of the PAZ. For sample 9, the hardness rises when the measurement is recorded on an area that is lacking a grain structure. The particular horizontal testing paths were performed across a region that was "unstructured" at the weld interface. For sample 11, as shown in Figure 65, there is a large unstructured region, but in the center of the weld small and some medium-sized grains are present. These will have a higher hardness than the material in the PAZ, but lower than the unstructured metal it is adjacent to. Hence there is a local minimum at the weld interface where a fine/medium grain structure exists. Figure 69 was tested from Sample 12. The weld region at this height consists solely of large grains and is therefore the weakest area of the extrudate.

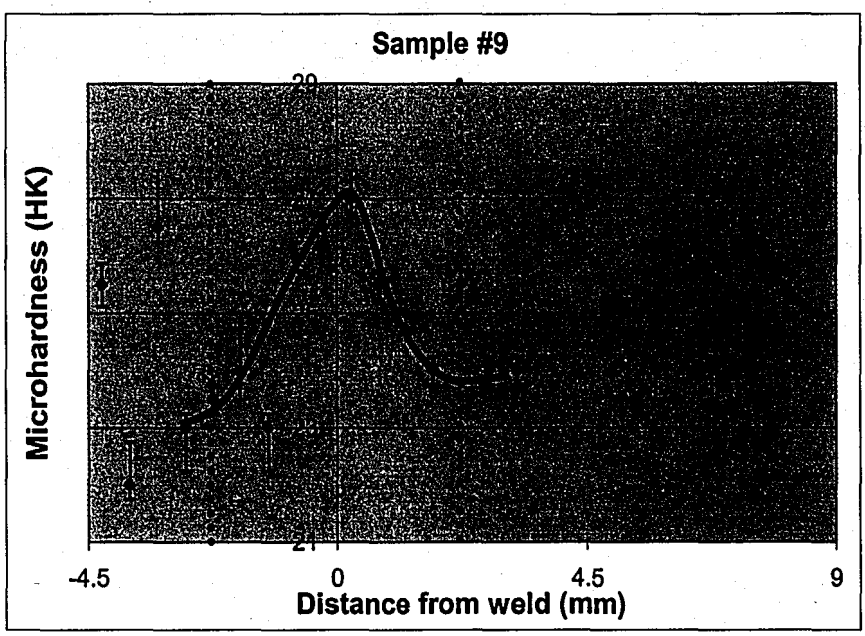

Figure 67: Microhardness from weld region of sample 9.

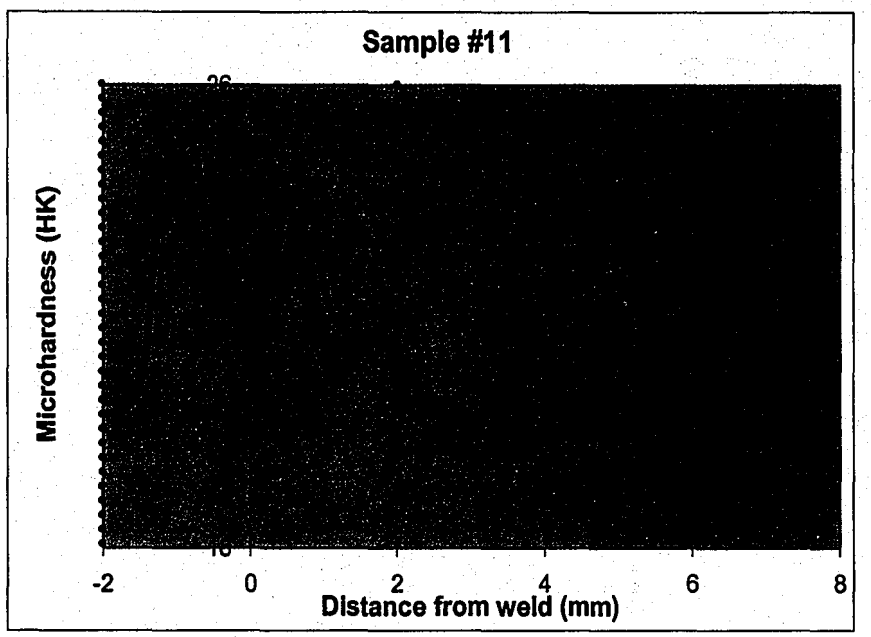

Figure 68: Microhardness from weld region of sample 11.

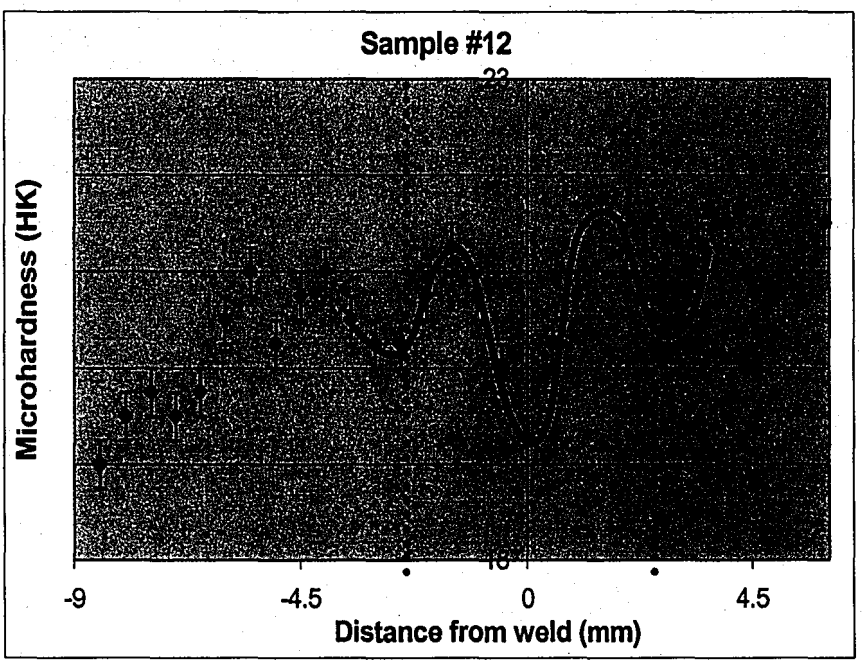

Figure 69: Microhardness from weld region of sample 12.

3.2.3 EBSD Analysis

The EBSD results for the experimental die weld sample are illustrated by the pole figures in Figure 70. The grain map in Figure 71 explains the initial results, which display two distinct textures. There are two large areas on either side of the weld possessing a Goss texture, (011)[100]; in fact, these are simply very large grains. A medium-sized grain within the weld zone has a <111> orientation. The "unstructured" region (as it was previously described) is actually comprised of small grains that were not observable in the LOM images with the etching time and solution used. Upon initial inspection, it appears these grains had a mixed orientation. Further investigation of these small grains recorded at higher magnification revealed a propensity for these grains to develop a cube-on-edge texture shown in Figures 72 and 73. Similar to the previous results, several <111> oriented grains also existed. The miscolored points on Figure 73 are areas where the EBSD software did not correctly index the BKP. Most of these points occur at grain boundaries where the dislocation density is high.

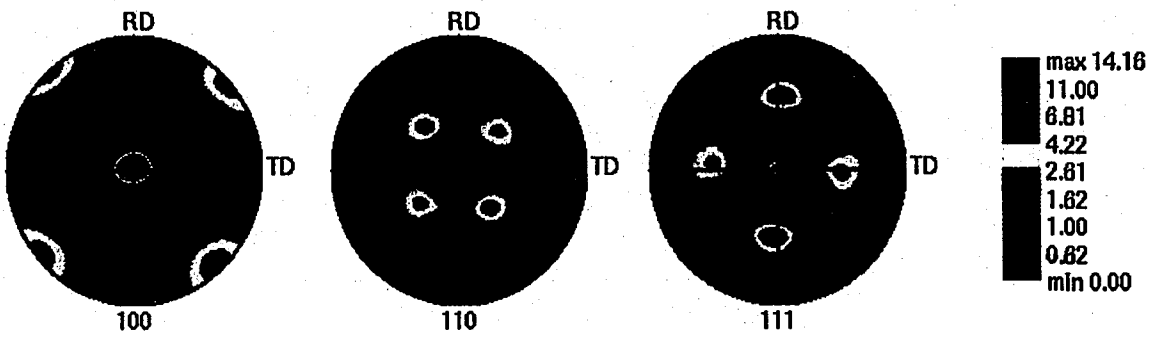

Figure 70: Pole figures for the experimental sample containing the longitudinal weld. Note the two distinct textures, <100> and <111>.

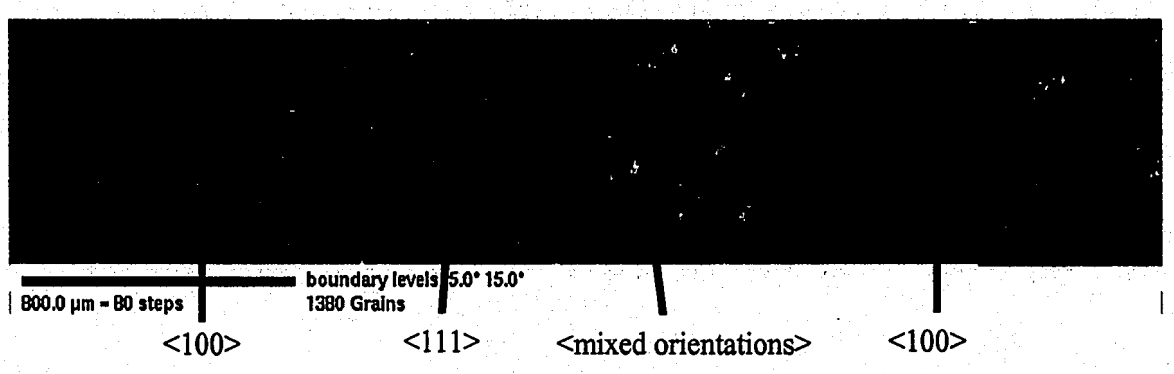

Figure 71: Grain map displaying 2 distinct textures and a mixed orientation distribution.

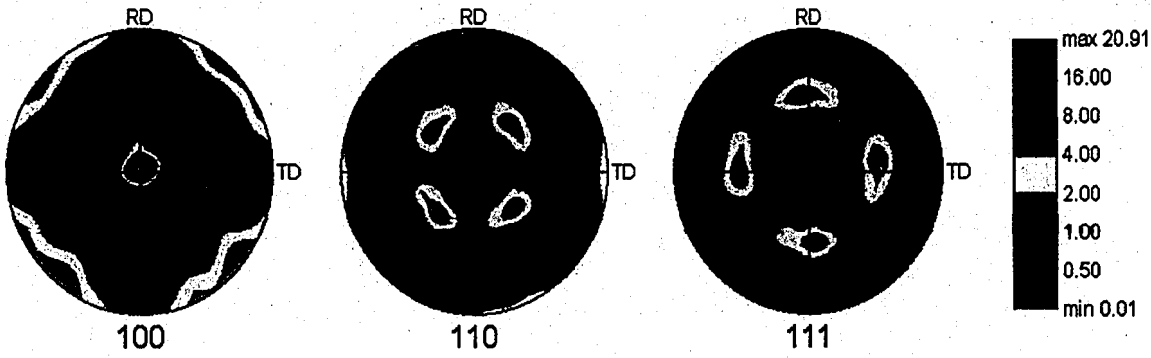

Figure 72: Pole figures for a large EBSD scan found in Figure 73. A rotated (45°) cube texture is preferred.

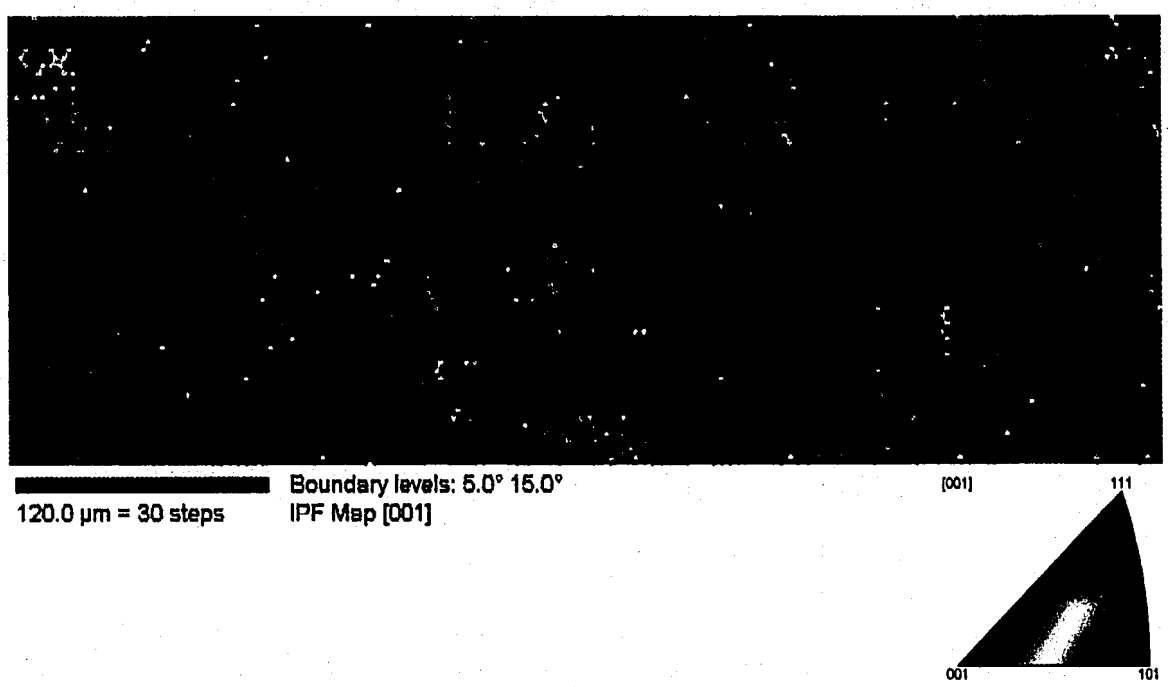

Figure 73: An IPF grain map indicating a strong <100> texture.

3.3 Industrial Extrusion Weld

3.3.1 LOM Investigation

Figure 74 presents the image of the macroetched industrial welded extrudate. This picture is very useful because it shows the grain flow and clearly defines the location of the extrusion weld diagonally from the upper right to the lower left. Figure 75, the sample etched for microanalysis, also presents the weld very clearly. Large grains exist at the center of the weld. The grain size decreases when moving away from the center of the piece towards the edges, where deformation is highest due to localized deformation.

Figure 74: Photograph of the macroetched industrial welded sample.

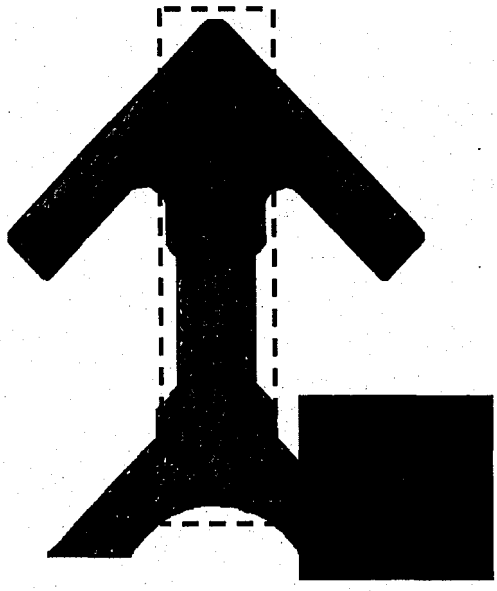

Figure 75: Image of the weld cross section after it has been etched for microstructural analysis.

This sample was studied primarily for the orientation information. However, LOM images were acquired to gain an initial understanding of the range of grain sizes. Composite LOM images halfway across the top (near the corner), middle (M), and bottom (near the hole) of the welded region are shown in Figures 76-78. In addition, the images across the longitudinal microstructure at M are shown in Figure 79. Microhardness tests, shown in Figure 80, were performed across the longitudinal sample to see the difference in mechanical properties between the grains of this sample vs. the experimental welded piece. The industrial sample's grains have a high hardness relative to the experimental profile previously studied. There is little variation across the weld. Most measurements varied only slightly from the average of 130 HK.

Figure 76: Composite LOM images that span half the weld region; taken from the top corner of the piece.

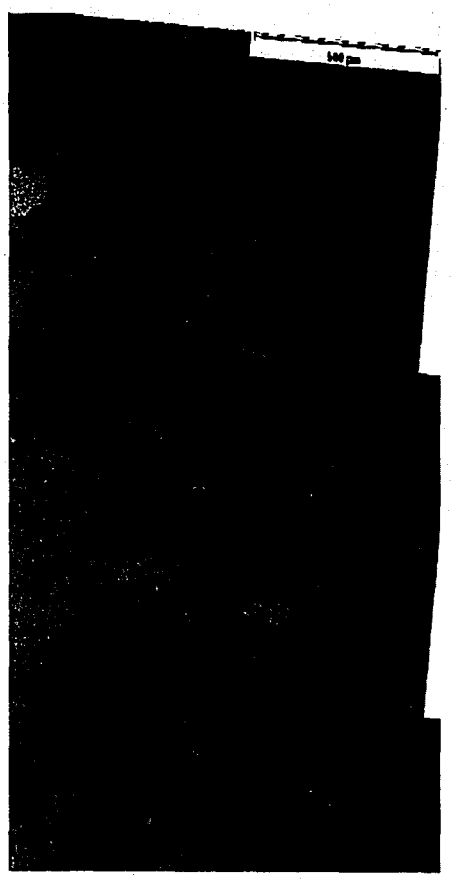

Figure 77: Composite LOM images that span half the weld region; taken at the mid-section of the welded region.

Figure 78: Composite LOM images that span half the weld region; taken from the bottom of the weld near the hole.

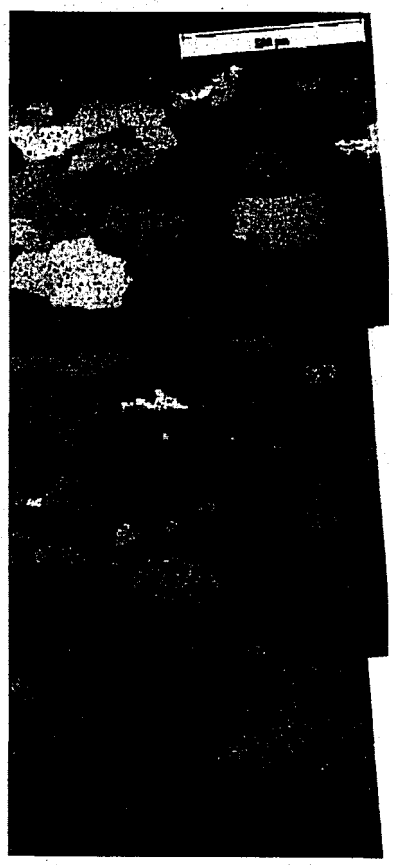

Figure 79: Composite LOM images that span half the weld region, taken from a longitudinal specimen at the mid-section of the weld.

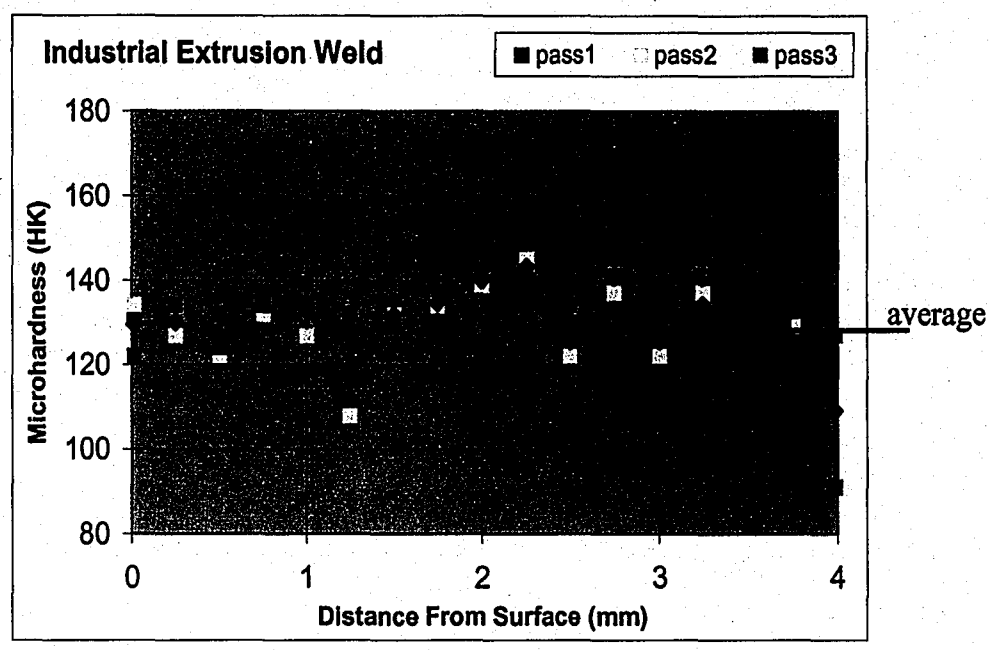

Figure 80: Microhardness measurements taken across the industrial weld sample.

3.3.2 EBSD Analysis

The EBSD analysis is shown in Figures 81 and 82. The pole figures in Figure 81 indicate a strong cube texture, (001)[100]. The inverse pole figure grain map shown in Figure 82 indicates that this <100> texture exists on either side of the weld as well as within the weld. The larger grains observed in the weld region possess the same texture as the surrounding material. Figure 82 was "cleaned" by editing the mislabeled points. The points that were incorrectly indexed were re-colored with the average color of the four surrounding points (up, down, left, and right).

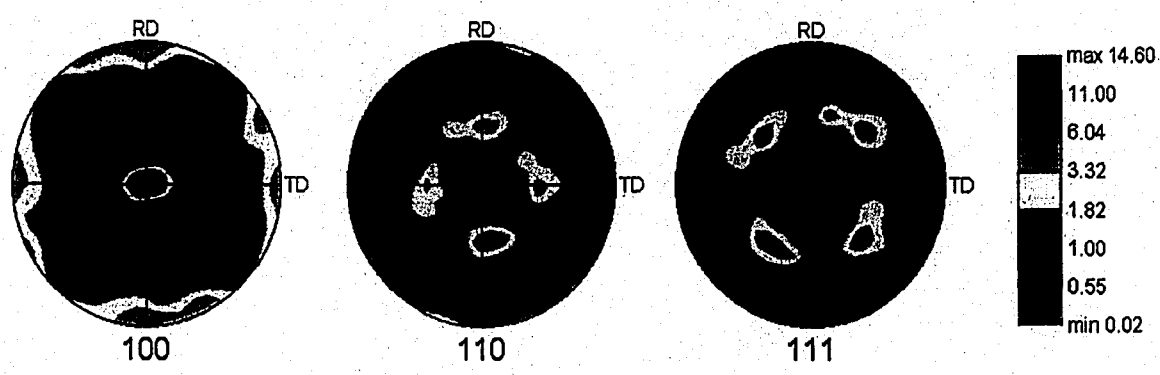

Figure 81: Pole figures for EBSD scan across the middle of the weld.

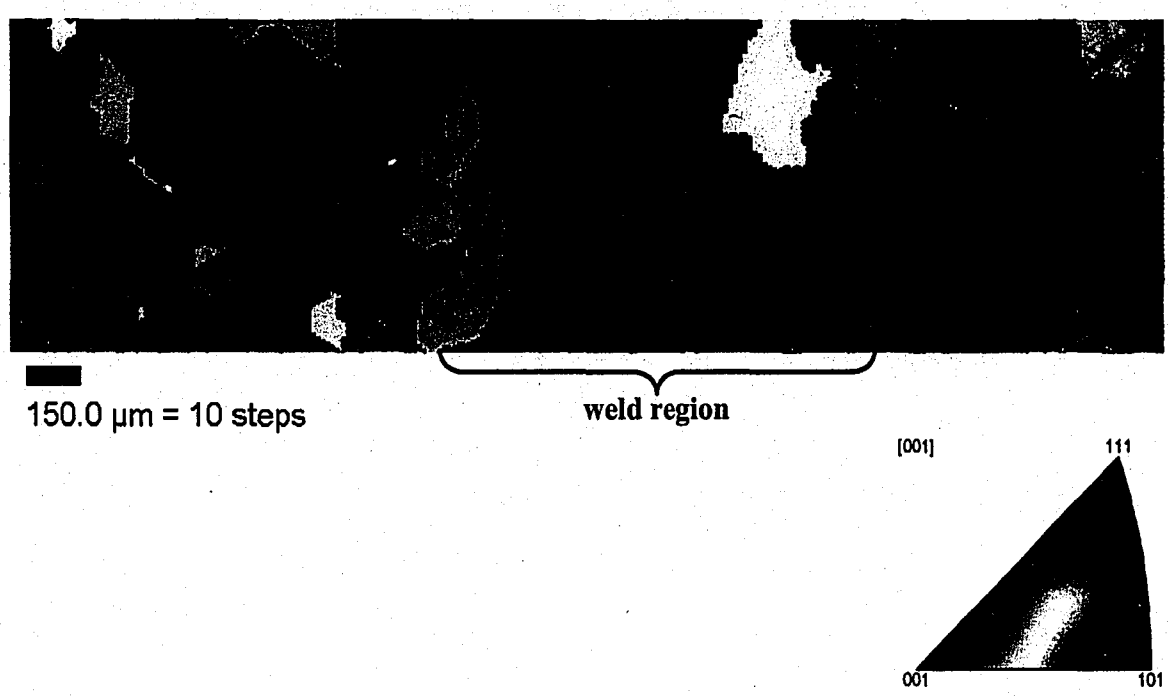

Figure 82: IPF grain map displaying larger grains in the weld region and a consistent <100> texture.

4.0 DISCUSSION

4.1 Solid Extrudate

4.1.1 Microstructural Gradients

Localized deformation due to geometrical factors causes structural differences to appear across the profile of a finished product having a complex shape. The distribution of grain size, shape, and texture in the material layers depends on strain. Strain varies as a function of position and increases as the distance from the center of the part increases. Thus, the localized deformation is highest at the surface for thick extrudates.

After microetching, 5 different zones appeared in the heavy region of the solid extrudate. These zones have differences in the size and shape of the grains. The brightness also varies, which is a product of how the etchant functions. Those grains that appear darker would have been attacked more by the etchant meaning they have higher energy, most likely due to the deformation or high dislocation density.

Microhardness tests were only taken across half of the samples because the shape was vertically symmetric. It should be noted that the local maximum of the microhardness results from sample 2 was only about 89 ± 2 whereas the local minimum for sample 7 was 106 ± 2. These two numbers should coincide since this is approximately where the horizontal and vertical passes would intersect. Because the microhardness tests were taken from different directions the orientations of the grains influence the mechanical properties and may lead to this discrepancy. Additional comments on the absolute determination of microhardness measurements appear later.

Microhardness tests were performed across sample 3 as well. The graph shape is analogous to that of sample 2. However, all values are approximately 10 HK higher. Using the deviation in the microhardness from vertical paths as a guide, sample 2 was likely sectioned at the minimum position, while sample 3, which is from further away from the top surface, and has higher strength. The shape of the plots for samples 2 and 3 is comparable because the variations from the side surfaces are similar. The 10 HK difference in values accounts for the influence on hardness from the top surface.

Sufficient microhardness measurements were taken in this research to confidently establish general trends for the strength of the grains as a function of distance from the surface. However, inadequate measurements were recorded to be certain of the accuracy of the absolute microhardness values. To improve the smoothness and increase the confidence and statistical accuracy of the results, more measurements should be taken for each distance and the data averaged. Multiple samples would give an increased number of measurements; however, it would be difficult to confirm that the samples were taken from the exact same locations.

The microhardness plots appear jagged at times because measurements were recorded for macro-distances, i.e. the x-axis scale was plotted in mm. Therefore, the size of the grains are very small relative to the distance between sampling points. Many grains exist between the plotted points, and were not tested. An increased number of measurements at intermediate distances would smooth the shape of the curves.

The microhardness results should be used as a qualitative analysis to determine relative variations while a smaller significance should be placed on the absolute quantitative values. There are many variables associated with hot deformed samples as

well as the Knoop microhardness test itself. Complex thermal and mechanical processing conditions are necessary to form the metal into the final product's shape. Microstructures can vary significantly on a local level even if microhardness tests are taken at similar locations on the same part. The number and spatial distribution of strengthening precipitates and their orientation have the largest influence on microhardness results. These properties may vary even for grains in close proximity. Microhardness discrepancies are also present due to changes in the *grain* size, shape, and orientation. The locations of the hardness indents relative to the grain boundaries affect results. This consideration becomes increasingly important as the grain size decreases.

The Knoop microhardness indenter requires accurate measurement of the elongated axis only. Imprecise measurements are possible, especially with the poor resolution camera linked to the computer measurement system that was used. In addition, the usually sharp indent corners may be poorly defined when it coincides with a precipitate or other inclusion. Both of these factors limit the accuracy of the Knoop microhardness test. A Vickers square indenter requires all four corners of the diamond indent to the measured and is thus more accurate, but also more time consuming. It was assumed these variations due to testing were consistent for all measurements, and thus the same relative trend is preserved.

In order to understand what the microhardness values signify, it is necessary to correlate these results to the microstructural features provided by the LOM images. This is done in Figure 83. Microhardness measurements across the sample are compared to a macro photograph taken with the stereomicroscope. The combined microhardness and microstructure are used to characterize and describe the metallurgical states of the grains.

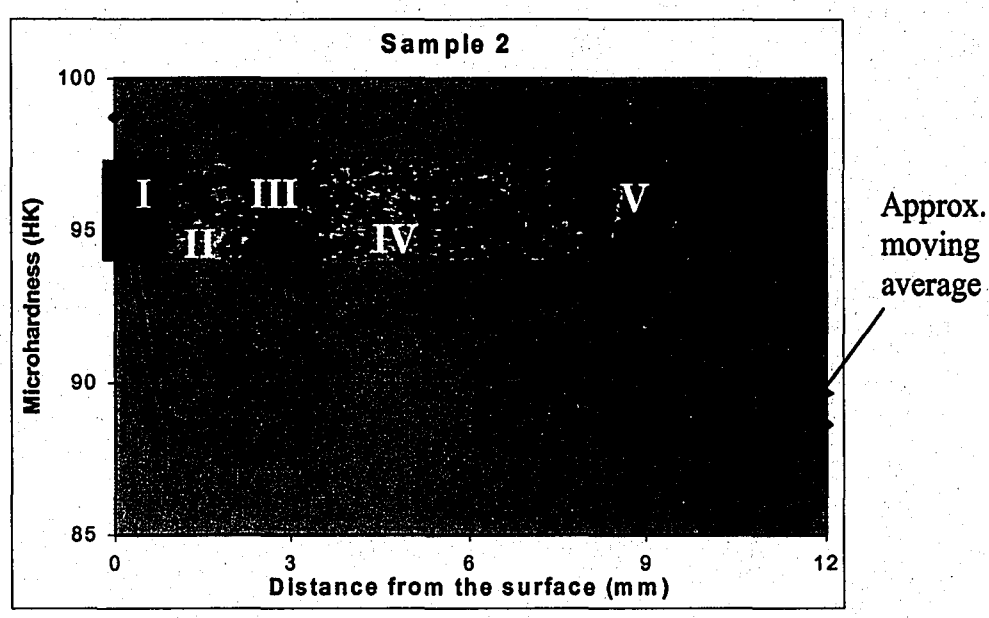

Figure 83: Correlation between the microhardness and microstructure of sample 2.

The high hardness at the surface is due to the small, heavily deformed grains (zone I). This high strain originates from the surface material's interaction with the die bearing lands and the long path the material travels from the highly strained intensive shear zone in the billet. These grains need to accommodate the misfit between the grains below the surface and are in the shape needed to produce the exact dimensions/geometry of the part. The low microhardness measurements that follow are associated with the large grains that appear below the surface (II). Due to their size and low hardness values it is a reasonable assumption to conclude that these grains have recrystallized and have gone through significant grain growth. Recrystallization and grain growth occur due to the large increase in temperature during the extrusion process. Because of the high deformation of the exterior grains, the temperature increase will be the highest closer to the surface. Zone III grains have been recrystallized but have higher hardness values than II because of their smaller grains size.

Zone IV are also small grains, but appear darker in the macro images and have a higher microhardness. The higher strain energy results in a darker appearance because they have been attacked more by the etchant. These grains have been deformed, but did not recrystallize. There is a gradient in the amount of recovery the grains undergo. The grains increase in size and decrease in hardness closer to the center of the profile, where they achieve their maximum size (zone V). These grains are similar in shape to those of the cast structure. The innermost grains undergo much lower deformation and strain than those further away from the center.

The moving average curve of the microhardness measurements was modified slightly to remove the rough, jagged points, and produce the smooth shape that is expected. The curve should be continuous because there is no strict delineation between the microstructural regions II-V, but a subtle change from one grain structure to another. However there is a sharp transition between I, the deformed surface grains, and II, the large grain growth region. This shift occurs at about 100 μm (thickness of about 2 layers of surface grains) from the edge.

The microstructure of the legs was fairly consistent. The average microhardness was around 123 HK. These grains are smaller than those of the heavy section and did not undergo any grain growth. In addition, the leg underwent significantly more deformation. To form these sections, due to their shape, heavy redundant deformation was induced creating an increase in temperature resulting in recrystallization and a strong texture.

4.1.2 Recrystallization Behavior

The heavy section showed considerable variation in grain size and hardness due to the tendency for the outer grains to recover and recrystallize, whereas the inner grains were as deformed. The heat generated by local deformation near the surface could not be dissipated. However, questionably, the material at the very surface did not recrystallize. There are several reasons that may explain this. First, these grains may have initially recrystallized but were subsequently deformed to have the misfit shape between the inner grains and the product dimensions.

It is also probable that the material forming the very surface did not come from the high-energy intensive shear zone but instead was a small amount of material that originated from the dead metal zone (DMZ) and slowly "leaked" out. This is demonstrated by the visioplasticity modeling shown previously in Figure 14. In this picture, there is a thin layer of light colored material at the surface that may have originated from the DMZ. The DMZ material has low strain and does not provide the necessary driving force for recrystallization.

A third reason is associated with the specific alloy itself. 6xxx alloys are highly quench sensitive. It is possible that the extrudate had been incompletely quenched, the outside surface was cooled properly, but for only a short time so that the cooling penetration was low. Perhaps this was the desired condition for the product, similar to case hardened steels which have a high surface hardness. No information was given by the company about the cooling conditions for this extrudate.

4.1.3 Texture Formation

It is important to understand which die characteristics influence the metal flow and the resulting texture. There are other means for correction such as die layout (extrudate placement with relationship to center position), changing the length of the bearing lands, or adding feeder plates, in order to manipulate the amount of work done by friction. The avoidance of significant microstructural gradients in the extrudate contributes to achieving optimum mechanical properties.

Strain localization modifies the microstructure and contributes to the development of the material anisotropy caused by texture formation.[48] When a polycrystalline metal plastically deforms, the crystallites are rotated with the crystal slip, and their crystallographic orientation tends to be partially aligned depending on the flow geometry and magnitude. This partial alignment is called preferred orientation or texture.[49]

The grains of the highly deformed leg have recrystallized but did not grow. They are equiaxed in shape and possess a cube texture, (001)[100]. The surface of the heavy section possesses the Goss texture component (011)[100]. The deformed, unrecrystallized surface grains have undergone significant shear and compression forces.

Material that is formed by a choke bearing land continues to undergo deformation while passing through the die orifice. It was incorrectly believed that the heavy section would have a stronger surface texture; however, this was not the case. Therefore, it is necessary to consider other factors that may influence the metal flow characteristics and grain alignment since the cause of texture cannot be solely linked to the die bearing angle. The legs, because of their high S/V, experience high strain localization, which

results in a stronger texture. The fact that this section undergoes a greater reduction in cross section from the billet is captured by the localized extrusion ratio.

The localized extrusion ratio is illustrated in Figure 84. The localized extrusion ratio is the extrusion ratio, R, that exists if only a particular segment of the extrudate is considered.[50] The heavy section (II), which is formed by a choke bearing land to slow the metal flow, is closer in size to the billet than the legs (III). The localized extrusion ratio for the heavy section is therefore much lower than the ratio for the leg section. The material forming the leg undergoes heavy localized deformation and thus has a strong texture. The localized extrusion ratio describes the amount of deformation that a particular segment of an extrudate will receive. A large localized extrusion ratio indicates high deformation, and predicts a strong texture for the particular extrudate section.

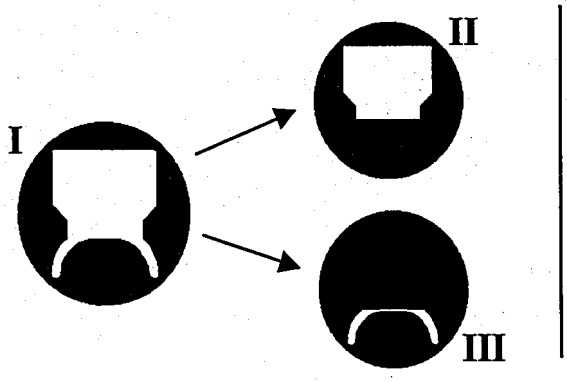

$$R_i = \frac{\text{billet area}}{\text{area of piece}} = \frac{\text{white + gray}}{\text{white}}$$

$$R_{III} > R_{II} > R_I$$

Figure 84: Demonstration of the localized extrusion ratio.[50]

The cause of texture is partially due to the non-uniform deformation (measured by the redundant work) that exists in the extrusion process. At high plastic strain, heterogeneous deformation exists and is accompanied by the development of shear bands. Strong texture will exist at the surface where redundant deformation is the highest.[51-52]

Grains' structure and orientation may change from the inside of the extrudate radially outwards towards the surface. The center of the extrudate may not be deformed at all in some cases of low extrusion ratios.[32]

4.2 Experimental Extrusion Weld

4.2.1 Microstructural Gradients

It is important to compare the microhardness results to the microstructures of the areas where the measurements were recorded. Surrounding the weld, all the samples studied possessed low microhardness due to the very large grains of the PAZ. The hardness then rises when the test was performed on an area that is "unstructured". The particular horizontal traverse taken across the weld interface of sample 9 was tested across such an "unstructured" region. Therefore, there is one maximum at the center of the weld. For sample 11, as shown in Figure 65, there is a large unstructured region surrounding some medium-sized grains present at the center of the weld. These grains have a higher hardness than the material in the PAZ but lower than the unstructured metal it is adjacent to. Hence, there is a local minimum at the center, where a structure exists, between two local maximums on either side of the weld for the unstructured regions. For sample 12, the weld consists solely of large grains; thus it is the weakest area of the extrudate. The microhardness plots display a minimum at the center of the weld.

It was discovered later using the SEM and EBSD that the "unstructured" region, which appeared using LOM, was actually composed of fine-sized grains. This area has a high relative microhardness because the indents span across several grain boundaries.

These boundaries, which did not appear using LOM, were unavoidable. The grains are too small to accommodate the size of the Knoop indenter for the given load.

The hardness values ranged from 18 to 28 HK, which is extremely soft. This can be attributed to two factors: recrystallization and low deformation. Because hollow profiles are essentially extruded twice (as described according to Akeret[21]), it is expected that a fine, highly-deformed grain structure would be present at the weld. The deformed outside grains of the initial extrusion (through the ports of the die that divide the metal streams) form the weld. These fine grains have high energy and are easily recrystallized. Hence, at the center height of the weld, fine grains exist. Further to the top and bottom of the extrudate, the weld consists of large grains. These grains originate from the corners of the initial extrusion and possess even more energy (greater localized deformation) and hence large grain growth occurs.

For this profile, the grains at the weld interface have recrystallized and are not highly deformed. The extremely low reduction ratio (9.2) for this experimental profile implies that this piece lacks the large deformation of typical extrusion processes.

4.2.2 Texture Analysis

In a porthole die, the metal streams follow a comparable path; thus, the microstructure on either side of the weld should have similar orientations. Dissimilar microtextures may indicate problems with the die design or process conditions. This investigative practice indicates EBSD's performance as a quality control device. Dies that have not been designed properly fail to provide for the ideal metal flow patterns, which would result in an inferior weld with sub-standard mechanical properties and poor

surface quality. An uneven buildup of material within the die will cause a disparity in the velocity of the metal streams; different textures result, indicating that the die requires cleaning. After extended use, a die that has worn preferentially at particular sections will also alter local orientations.

The EBSD results for the experimental weld extrudate are found in Figures 70-73. The pole figures found in Figure 70 display two distinct textures present. A strong Goss texture exists and there is a weaker population of <111> orientations. The grain map in Figure 71 explains this. Both sides of the weld show the <100> crystal alignment. Grains on either side of the extrusion weld have comparable paths through the porthole die and are formed by the same die characteristics; therefore, they should have similar textures and properties. Inside the weld area, a separate <111> fraction appears. Next to this area, the very small grains, which appear as an unstructured region in the LOM images, also have a dominant Goss texture with a smaller <111> fraction as well. The extrusion ratio for this extrudate was very low (R = 9.2) and only small strains are present in the grains. The grains may have recrystallized and subsequently deformed to acquire the cube-on-edge texture.

Characteristics of the material flow are substantially influenced by the area reduction. Lower reductions, as seen in the solid test shape, may allow material streams with different velocities to enter the die orifice before completely welding. This leads to poor mechanical properties, evident in the low microhardness results. Industrial applications implement greater reductions, which allow the streams to flow together and join in time to weld properly.

4.3 Industrial Extrusion Weld

4.3.1 Microstructural Gradients

The LOM images of the industrial welded sample reveal small microstructural gradients present in the size of the grains. The exterior grains are smallest due to the high localized deformation. The center of the weld possesses the largest grains; this was consistent for the entire length of the weld. Typical average microhardness measurements for the tested points were about 130 HK with small percentage variations. These values are much higher than the experimental weld. The sizeable difference is due to the large discrepancy in overall deformation. Industrial practices typically have large extrusion ratios, using very high strain to form the part into the desired shape. The complexity of the shape will also compound the already high localized deformation.

A good adhesive bond is achieved by increasing the reduction to a certain minimum value where metallurgical bonding takes place on the atomic scale. In principle, a fraction as large as possible of the total strain from billet to shape should take place after the streams of metal have encountered each other in the weld chambers. This increases deformation and produces a uniform microstructure beneficial for improved mechanical properties. The complex profile produced under industrial extrusion process conditions had a continuous cube texture across the seam weld.

4.4 Electron Backscatter Diffraction

4.4.1 Accuracy of EBSD Technique

EBSD is a proven technique; the automated crystallographic orientation microscopy (ACOM) is an appropriate tool for texture analysis and stereographic evaluation. Figure 85 compares the secondary electron image from the SEM to the computer generated grain map from the EBSD data. There is a strong correlation between these two images, the outline of the grains accurately match as well as the multiple scratches on the surface. The scratches are areas of high deformation and thus the computer is unable to properly index the pattern due to the low image quality of the EBSD pattern. Because of the high local concentration of dislocations, the grain boundaries also appear darker than areas within the grains. There are a few points within the grains that are darker than the surrounding material. It is believed that there are large precipitates or inclusions.

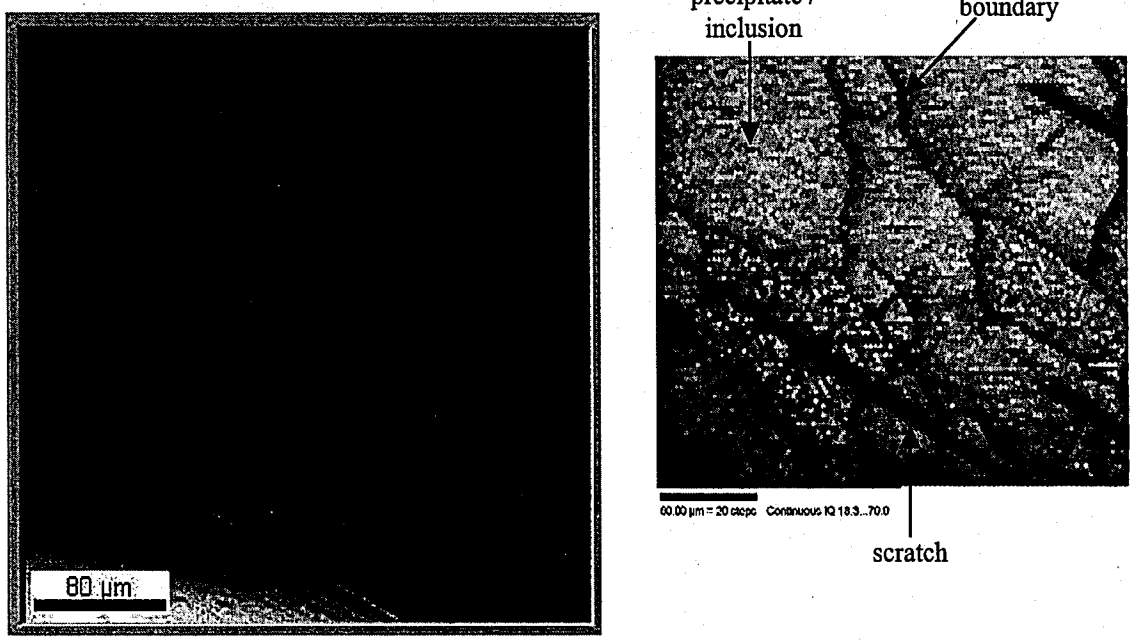

Figure 85: Secondary electron image and the corresponding EBSD grain map.

Figure 86 presents another grain map microstructure constructed by the EBSD system. This area depicts the large grains just beneath the surface from the heavy section of the solid extrudate; these grains have undergone grain growth. The surface of the part appears to the right and is darker in grayscale indicating higher deformation. Again, the computer-generated picture closely resembles images from the SEM or LOM.

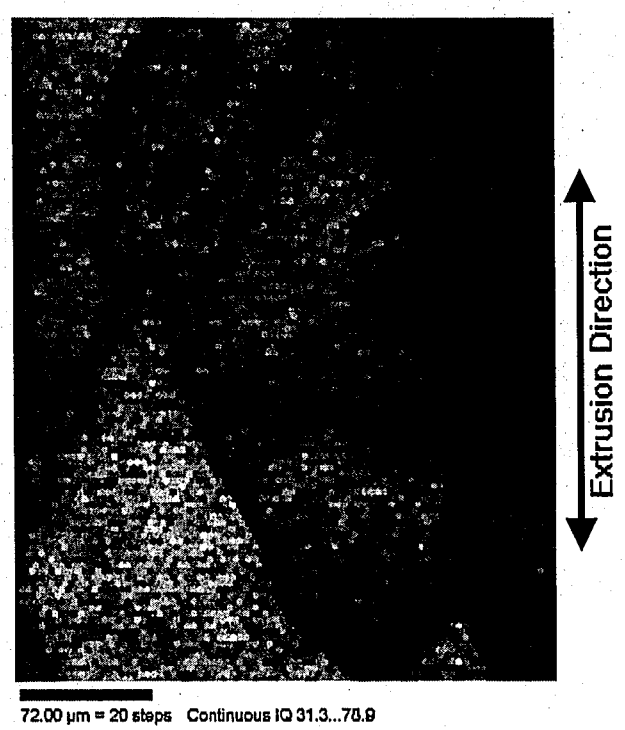

Figure 86: EBSD grain map of the large grains beneath the surface of the heavy section from the solid extrudate.

4.5 Future Work

4.5.1 Microtexture Gradients

This thesis presents the microstructural gradients that occur due to localized deformation. The variations due to geometrical differences were evaluated on the basis of grain size, shape, and microhardness. The microtexture was only evaluated at the

surface to determine the influence of different die bearing lands. Using EBSD, several area scans could be set up such that the orientation of the grains is completely reported as a function of distance from the side and top surface.

In addition, it was stated that the center grains in the heavy section of the solid extrudate would resemble those of the cast microstructure because they are not as heavily worked as the surface material. An orientation investigation could be done on a cast billet slice before it is extruded to compare the orientations before and after the deformation process. The EBSD results are also capable of simultaneously reporting statistics on the size and shape of the cast grains.

4.5.2 Comparison of Deformation Percentages

Both welded samples reveal a recrystallized microstructure, however the test sample is very soft due to its low extrusion ratio. The analysis presented in this research could be expanded to both welded and non-welded samples of similar shape, but possessing different reduction ratios. This would isolate the deformation percentage variable. Thus, the microstructure can be directly related to extrusion ratio.

5.0 CONCLUSIONS

This research examined the response of 6xxx aluminum alloys to the extrusion process. Localized deformation is a natural outcome of large strain plasticity and will cause variation in metal flow leading to microstructural gradients, especially in the production of complex shapes. This study encompasses the examination of localized deformation as a result of geometrical differences and also microstructural variation due to longitudinal extrusion welds. Three samples were studied: a solid extrudate with two different regions of diverse surface area to volume ratios, a simple rectangular test sample containing a longitudinal weld, and a complex industrial extrudate, also with a weld. The characterization of the microstructure is very important to understand the deformation mechanics of the extrusion process. LOM, microhardness tests, and EBSD were used to measure the gradients in grain size, shape, mechanical properties, and microtexture. Based upon the performed research, the results of this investigation can be summarized by the following conclusions:

- The heavy region of the solid extrudate displays significant variation in both grain size and microhardness from the exterior of the part to the center. The localized strain is highest at the surface. These small exterior grains are highly deformed and have high hardness. Beneath this layer, the grains have recrystallized, undergone grain growth, and have a much lower microhardness. The hardness increases as the grains decrease in size and as the percentage of recrystallized material diminishes. A local microhardness maximum is achieved. Closer to the center of the part, the

grain size increases along with a corresponding decrease in the microhardness. The surface grains of the heavy region possess a Goss texture, (011)[100].

- The legs of the solid extrudate are heavily deformed and have completely recrystallized. The grains are equiaxed and possess nearly uniform microhardness. A typical cube recrystallization texture results, (001)[100]. The surface texture is influenced greater by the high amount of deformation rather than by the type of bearing land used. This concept is described by the localized extrusion ratio.
- The simple rectangular extrudate that contains a longitudinal weld was extruded under controlled test conditions and had a very low extrusion ratio. Localized deformation existed due to the presence of the extrusion weld. The microstructure and strength of the weld varied greatly depending upon the vertical position examined. The large grains, typical of the PAZ, possess the lowest relative microhardness. The medium-sized grains at the center of the weld have a higher hardness than the PAZ grains and those of the parent material (regions unaffected by the weld). The fine grains, which appear as an unstructured region in the LOM micrographs, possess the highest microhardness. The Goss texture dominated the pole figures; however, a smaller fraction of <111> orientations also appeared for some grains within the weld region.
- The complex welded sample underwent heavy deformation and had uniform high microhardness values relative to the experimental rectangular extrudate. LOM images show some variation in grain size across the piece. The microstructure was composed of small grains towards the exterior with larger grains at the center of the weld. The cube texture was a consistent across the part.

- EBSD is an extremely important tool for the characterization of deformed microstructures. Although there are some limitations, once these are understood the technique may be successfully applied. The small differences in crystallographic orientations among individual grains can be accurately determined.
- The amount of localized deformation greatly influences the formation of microstructural gradients. The history of the deformation process determines the microstructure of the final extrudate. There is a complex interaction between the thermal and mechanical processes occurring during the hot extrusion of 6xxx aluminum alloys.

6.0 REFERENCES

1. L. Edwards and M. Endean, ed., Manufacturing With Materials, Butterworth-Heinemann Ltd., 1995, p. 148-150.

2. W.J. Callister Jr., Materials Science and Engineering An Introduction, John Wiley & Sons, Inc., 1997, p. 345-346.

3. G.E. Dieter, Mechanical Metallurgy, McGraw-Hill, 1986, p. 616-617, 620-621, 631-632.

4. W.F. Smith, Principles of Materials Science and Engineering, McGraw-Hill, 1996, p. 257.

5. H.E. Boyer and T.L.Gall, ed., Metals Handbook Desk Edition, American Society for Metals, 1985, p. 1•15-16, 26•49.

6. K. Laue and H. Stenger, Extrusion, American Society for Metals, 1981, p. 1, 74-75, 113, 130-136.

7. M. Conserva, G. Donzelli, and R. Trippodo, Aluminum and its Applications, Edimet Spa, 1992, p. 46-49.

8. I.J. Polmear, Light Alloys Metallurgy of the Light Metals, Edward Arnold Ltd and American Society for Metals, 1981, p. 58-63, 82-83.

9. P.K. Saha, Aluminum Extrusion Technology, ASM International, 2000, p. 87-109, 149, 165-168.

10. J.E. Hatch, ed., Aluminum: Properties and Physical Metallurgy, American Society for Metals, 1984, p. 50-51.

11. H. Baker, ed., ASM Handbook Volume 3: Alloy Phase Diagrams, ASM International, 1992, p. 3•18.

12. R.J. Anderson, The Metallurgy of Aluminum and Aluminum Alloys, Henry Carey Baird & Co., Inc., 1925, p. 682, 722-725.

13. M. Van Lancker, Metallurgy of Aluminum Alloys, John Wiley & Sons Inc., 1967, p. 132-144.

14. F. King, Aluminum and its Alloy, Ellis Horwood Limited, 1987, p. 112-117.

15. The Aluminum Association, Aluminum Standards and Data, March 1997, p. 6-6.

16. W.J. Mason Sr., "Die Correction Practices", 1987 Aluminum Extruders Council Die Workshops, Working Solutions for Production Personnel, Newport Beach, April 7-8, Baltimore, April 28-29, Chicago, May 12-13, 1987.

17. J. Zasadzinski and W. Misiolek, "Estimating Optimal Speed/Temperature Parameters to Maximize Hot Extrusion Exit Speed", Proceedings of the 4th International Aluminum Extrusion Technology Seminar ET'88, Chicago, IL, April 11-14, 1996, vol. II, p. 241-246.

18. A.E. Prats and W.Z. Misiolek, "Analysis of Metal Flow in Weld Pocket Dies", Proceedings of the 6th International Aluminum Extrusion Technology Seminar ET'96, Chicago, IL, May 14-17, 1996, vol. II, p 75-78.

19. L. Ingraldi, V. Giacomelli, and M. Pedersoli, "Design and Correction of Hollow Dies in Europe", Proceedings of the 5th International Aluminum Extrusion Technology Seminar ET'92, Chicago, IL, May 19-22, 1992, vol. I, p. 369-383.

20. J. Zasadzinski, J. Richert, and W.Z. Misiolek, "Weld Quality in Extruded Aluminum Hollow Sections", *Light Metal Age*, vol. 50, no. 7-8, 1992, p. 60-64.

21. R. Akeret, "Extrusion Weld—Quality Aspects are Now Center Stage", Proceedings of the 5th International Aluminum Extrusion Technology Seminar ET'92, Chicago, IL, May 19-22, 1992, vol. I, p. 319-336.

22. U. Chakkingal and W.Z. Misiolek, "Welding Phenomena in Extruded Aluminum Hollow Profiles", Automotive Alloys, Proceedings of the Symposium presented at the 1998 TMS Annual Meeting, San Antonio, Texas, February 16-19, 1998, p. 195-205.

23. P.K. Balasubramanian, "Extrusion of Al-Zn-Mg-Cu-Zr Alloys", *Materials Science and Technology*, vol. 1, 1995, p. 470-474.

24. A. Huot, R.A. Schwarzer, and J.H. Driver, "Texture of Shear Bands in Al-Mg 3% (AA5182) Measured by BKD", *Materials Science Forum*, vols. 273-275, 1998, p. 319-326.

25. H. Valberg and A. Groenseth, "Metal Flow in Direct, Indirect and Porthole Die Extrusion", Proceedings of the 5th International Aluminum Extrusion Technology Seminar ET'92, Chicago, IL, May 19-22, 1992, vol. I, p. 337-357.

26. S.R. Claves, W.Z. Misiolek, and D.B. Williams, "Modeling and Characterization of Localized Strain in Aluminum Alloys", Proceedings from Materials Solutions Conference, Indianapolis, IN, November 5-8, 2001, p. 282-289

27. S. Claves, "Microstructural Evaluation of Heavy Aluminum Extrudates", 2001 Extrusion Drawing & Tube Reducing Conference, New Orleans, LA, April 23-25, 2001, section G.

28. J.A. Trogolo, R.M. Kelly, and W.Z. Misiolek, "Use of EBSD Technique for Microstructure Characterization of the Deformation Zone in Aluminum Extrusion", Proceedings of the 6th International Aluminum Extrusion Technology Seminar ET'96, Chicago, IL, May 14-17, 1996, vol. I, p. 217-221.

29. T. Chanda, J. Zhou, and J. Duszczyk, "FEM Analysis of Aluminum Extrusion Through Square and Round Dies", *Materials and Design*, vol. 41, no. 4, 2000, p. 323-335.

30. T.J. Ward and J.F. Heffron, "The Effects of Nitrogen and Liquid and Gaseous—On Aluminum Extrusion Productivity", Proceedings of the Third International Aluminum Extrusion Technology Seminar ET'84, Atlanta, GA, April 24-26, 1984, vol I, p. 211-219.

31. T. Aukrust, O. Lohne, H.E. Vatne, T. Furu, and S. Tjotta, "Texture and Surface Grain Structure in Aluminum Sections", Proceedings of the 6th International Aluminum Extrusion Technology Seminar ET'96, Chicago, IL, May 14-17, 1996, vol. I, p. 171-177.

32. T. Furu, O. Sodahl, E. Nes, L. Hanssen, and O. Lohne, "The Influence of the Extrusion Speed on the Texture in the Surface Layer of Aluminum Profiles Investigated by the EBSP Technique", *Materials Science Forum*, vols. 157-162, 1994, p. 1197-1204.

33. I. Samajdar and R.D. Doherty, "Cube Recrystallization Texture in Warm Deformed Aluminum: Understanding and Prediction, *Acta Materialia,* Volume 46, Issue 9, May 22, 1998, p. 3145-3158.

34. U.F. Kocks, C.N. Tome, and H.R. Wenk, Texture and Anisotropy, Cambridge University Press, 1998, p. 1-11, 222

35. M. Hatherly and F.J. Humphreys, Recrystallization and Related Annealing Phenomena, Pergamon, 1995, p. 43-56.

36. L. Poizat and B. Hutchinson "Simulation of Texture Development During Axisymetric Compression and Tension," Institutet For Metallforskning, Swedish Institute for Metals Research, reproduced by National Technical Information Service, 1997.

37. V. Randle, "Crystallographic Characterization of Planes in the Scanning Electron Microscope", *Materials Characterization*, vol. 34, 1995, p. 29-34.

38. P. Camus, "SEMs Perform Diffraction Analyses", *R&D Magazine*, October, 1998, p. 65.

39. A. Goyal, E.D. Specht, Z.L. Wang, and D.M. Kroeger, "Grain Boundary Studies of High Temperature Superconducting Materials Using Electron Backscatter Kikuchi Diffraction", *Ultramicroscopy*, vol. 67, 1997, p. 35-57.

40. G. Gottstein and L.S. Shvindlerman, Grain Boundary Migration in Metals, CRC Press, Boca Raton, 1999, p. 323-328.

41. TexSem Laboratories, Incorporated, OIM™ For Windows Instruction Manual, TSL, 1997, p. 47-53.

42. B.W. Bennett, and H.W. Pickering, "Effect of Grain Boundary Structure on Sensitization and Corrosion of Stainless Steel", *Metallurgical Transactions A*, vol. 18A, no. 6, 1987, p. 1117- 1124.

43. J.I. Goldstein, D.E. Newbury, P. Echlin, D.C. Joy, A.D. Romig Jr., C.E. Lyman, C. Fiori, and E. Lifshin, Scanning Electron Microscopy and X-ray Microanalysis, Plenum Press, New York, 1992, p. 90-106.

44. J. Van Rijkom, P.H. Bolt, and D. Weeke, "A Review of New Approaches and Technologies in Extrusion Welds Related to the Background of Existing Knowledge", Proceedings of the 7th International Aluminum Extrusion Technology Seminar ET2000," The Aluminum Association and the Aluminum Extruders Council, Chicago, IL, May 16-19, 2000, vol. I, p. 249-260.

45. F. J. Humphreys, "Quantitative Metallography by Electron Backscattered Diffraction", *Journal of Microscopy*, vol. 195, no. 3, 1999, p. 170-185.

46. R.M. Kelly, personal communication, July 7, 1999.

47. W.Z. Misiolek, Extrusion Dies, 1995/1996 Year End Report, internal communication, Rensselaer Polytechnic Institute, Troy, NY, 1996, p. 2-1—2-28.

48. H.E. Deve and R.J. Asaro, "Development of Plastic Failure Modes in Crystalline Materials: Shear Bands in fcc Polycrystals", *Metallurgical Transactions A*, vol. 20A, no. 4, 1989, p. 579-593.

49. M. Hirao and N. Hara, "Ultrasonic Pole Figure for the Texture of an Aluminum Alloy", *Applied Physics Letters*, vol. 50, no. 20, 1987, p. 1411-1412.

50. S.R. Claves, W.Z. Misiolek, R.M. Kelly, D.B. Williams, "The Influence of Die Design on the Surface Texture of an Aluminum Extrudate", *Aluminum Transactions*, in press.

51. C.J. Taylor, T. Zhai, A.J. Wilkinson, and J.W. Martin, "Influence of Grain Orientations on the Initiation of Fatigue Damage in an Al-Li Alloy", *Journal of Microscopy*, vol. 195 no. 3, 1999, p. 239-247.

52. D.N. Lee, Y.H. Chung, and M.C. Shin, "Preferred Orientation in Extruded Aluminum Alloy Rod", *Scripta Metallurgica*, vol. 17, no.6, 1983, p. 339-342.

VITA

Steven was born to Robert and Michaele Claves on November 21, 1977 in Brooklyn, NY. He lived in Staten Island, NY for the first 18 years of his life. After graduating from Monsignor Farrell High School in 1995, Steven began attending Lehigh University in Bethlehem, PA with interests in both engineering and business. He graduated in 1999 with a Bachelors of Science in Materials Science and Engineering with a minor in Economics.

In 1998 Steven spent 3 months working as a student engineer at Boeing Defense and Space Group: Helicopter Division in Philadelphia, PA. He continued his industrial work experience in 2000 when he worked as a visiting research scientist for Alusuisse Technology and Management Center in Chippis, Switzerland. This past summer, Steven worked as a metallurgist for VAW of America in St. Augustine, FL. Steven has been the primary author for 3 journal articles and 5 conference papers, while co-authoring another journal article and 2 more conference papers. He has also given 3 presentations in the areas of localized deformation in extrusion and the characterization of deformed aluminum microstructures.

Presently, Steven is investigating various characterization methods applied to deformed microstructures. He is concentrating on phase identification and texture determination using EBSD on the SEM, and CBED on the TEM. Steven will be continuing this research as he pursues his Ph.D. in Materials Science and Engineering at Lehigh University.

END OF TITLE